AN INVESTIGATION OF THE FLOW AROUND SLENDER DELTA WINGS WITH LEADING EDGE SEPARATION

ANDREW J. BERGESEN
and
JAMES D. PORTER

AN INVESTIGATION OF THE FLOW AROUND SLENDER DELTA WINGS WITH LEADING EDGE SEPARATION

BY

LT. ANDREW J. BERGESEN, USN
and
JAMES D. PORTER

REPORT NO. 510 MAY, 1960

Submitted in partial fulfillment of the requirements for the Degree of Master of Science in Engineering from Princeton University, 1960.

ACKNOWLEDGEMENT

The authors desire to thank the staff of the Subsonic Aerodynamics Laboratory of the Aeronautical Engineering Department at Princeton University for their efforts in behalf of this project. Specifically, Mr. Rudolf F. Lehnert contributed generously of this time and was a constant source of information.

We wish to express our appreciation to Professor David C. Hazen, our faculty advisor, who whetted our interest in the subject of delta wings and infected us with his contagious enthusiasm.

Bibliographical Control Sheet

1. Originating agency and monitoring agency:

   O.A.: Princeton University, Princeton, N. J.
   M.A.: Office of Naval Research, Air Branch (Code 461), Washington 25, D. C.

2. Originating agency report number: Aeronautical Engineering Department Report No. 510

3. Title and classification of title: An Investigation of the Flow Around Slender Delta Wings with Leading Edge Separation

4. Personal author: Bergesen, Lt. Andrew J., USN and Porter, James D.

5. Date of report: May, 1960

6. Pages: 22

7. Illustrative material: 71

8. Prepared for Contract No.: Nonr-1858(14)

9. Prepared for Project No.: NR 212-000

10. Security classification: Unclassified

11. Distribution limitations: Specified by ONR ltr (461:TLW:eew) of March 22, 1960

12. Abstract: A low speed investigation of the flow over aspect ratio one delta wings of varying thickness has been made to better understand the relation between the vortices produced by leading edge separation and the non-linearity of the lift curve. The formation of the leading edge vortices is shown in smoke photographs. The vortex core loci over the wing and downstream are plotted. An empirical expression was developed for the lift curve.

TABLE OF CONTENTS

LIST OF FIGURES

SYMBOLS

a	local semispan
α	angle of attack
AR	aspect ratio
b	wing span
C_{L_ℓ}	lift coefficient predicted by linearized potential theory $\left[C_{L_\ell} = \frac{2\pi AR}{p AR + 2}\alpha\right]$
ΔC_L	additional lift coefficient due to vortices over the wing
c_r	root chord
ϵ	semi-apex angle
Γ	vortex strength
p	$= \dfrac{\text{wing semiperimeter}}{\text{wing span}}$
Re	Reynolds Number
t/c	thickness to chord ratio
T.E.	trailing edge station
V	free stream velocity
x'	chordwise coordinate from point of maximum thickness
x	fractional chordwise location from leading edge
y	spanwise coordinate
z	coordinate normal to wing planform on the body
z'	coordinate normal to the horizontal plane downstream of the trailing edge

SUMMARY

A low speed investigation of the flow over aspect ratio one delta wings of varying thickness has been made to better understand the relation between the vortices produced by leading edge separation and the non-linearity of the lift curve. The formation and the position of the vortex cores were determined by means of smoke flow visualization techniques. Lift curves of the models were obtained from the wind tunnel.

It was found that at the same angle of attack the vortex cores moved outward on the wing as wing thickness increased. Downstream of the trailing edge, the vortex cores followed a helical path which is believed to be related to the "vortex explosion" phenomenon. An empirical equation was developed which predicts the lift curves for sharp leading edged delta wings of various thicknesses and of aspect ratios from one to two.

INTRODUCTION

Traditionally, the influence of viscosity on the flow over a wing was assumed to be confined to a thin boundary layer. Outside the boundary layer, the flow was considered to be inviscid and could be analyzed by linear potential theory. Where the leading edge is sharp on a thin swept wing, the flow may not be considered inviscid, because the boundary layers developed on the lower surface separate at the sharp leading edge. Specifically, for a delta wing, with highly swept, sharp leading edges, at angles of attack greater than zero, the boundary layers on the pressure side separate at the sharp leading edges to form vortices which grow in size and strength toward the trailing edge. The leading edge vortices are the significant characteristic of such wings.

The effect of the vortices is to produce a complex flow field over the wing with associated non-linear aerodynamic characteristics. For such a flow field, deviation from potential wing theory exists which results in a non-linear lift curve.

Following the principle that only when the physical situation is fully understood can the mathematical treatment be applied intelligently, smoke visualization techniques were applied to the flow field. In addition to the qualitative photographs, quantitative results were obtained in the form of vortex core locations with angles of attack for the three aspect ratio one delta wings shown in Fig. 1.

Based on the vortex core locations, an empirical expression for the lift curve was obtained which is applicable to delta wings up to 12 percent thick and of aspect ratio one to two.

BACKGROUND

History

In 1936, Winter[1] first described the conical vortex at the wing leading edge. By means of flow visualization techniques (smoke, tufts, and "soot and petroleum"), he described the flow as "flowing spirally, forming a 'vortex braid' whose position, magnitude and extent are determined by the plan form, aspect ratio and angle of attack."

In 1947, Wilson and Lovell[2] determined by tests of a delta wing and tuft analysis, that "the flow over triangular wings of low aspect ratio is characterized by vortices above the upper surface of the wing, inboard of the tips. These vortices aid in obtaining high maximum lift coefficients and can be produced by using airfoil sections having sharp leading edges."

Örnberg[3] in 1954, identified the secondary vortices produced by the separation of the upper surface boundary layer.

Many have contributed significantly to the understanding of the flow, in the form of wind tunnel tests, flow visualization techniques and mathematical treatment. A partial listing of the papers published on the subject is contained in the references and bibliography section.

Flow Description

As the angle of attack increases from zero, the stagnation point moves from the leading edge to the under surface of the wing. The flow proceeds from this stagnation point to the leading edge due to the favorable pressure gradient in this region. Suction on the upper surface tends to draw the flow around the leading edge. However, for a sharp leading edge, the centrifugal force on a fluid element approaches infinity and the fluid cannot remain attached to the surface of the wing. The separated fluid takes the form of a vortex sheet which grows in strength as it proceeds downstream on the body. Thus, when it rolls up it takes

the form of a conical spiral. The vortex sheets roll up in opposite senses on the wing into cores of rotating fluid which lie above and inboard of the leading edges as seen in Fig. 7. These leading edge vortices are the dominant feature of the flow.

In addition to the strong flow from the lower surface, there is the secondary flow pattern which is produced by the separation of the outflowing air in the boundary layer on the upper surface as it nears the leading edge, as seen in Fig. 2. This separation occurs due to an adverse pressure gradient on the upper surface outboard of the primary vortex cores. The secondary separations give rise to small triangular-shaped viscous regions on the upper surface near the leading edge. Investigation[4] of these viscous regions by means of a pressure probe located the secondary vortex cores below and outboard of the primary cores and confirmed the rotation of the vortices as opposite in sense to the primary vortices. Downstream of the trailing edge, the secondary vortices are well defined, as seen in Fig. 11.

Theoretical Treatment

The flow pattern in quite different from that usually considered in the theory of inviscid fluid motion presented by R. T. Jones.[5] Jones' theory requires the fluid to turn through an angle at a sharp leading edge and so, in the linearized approximation, predicts infinite values of the velocity and pressure along it. It is not these singularities in themselves which render such theories for the slender delta wing inadequate, since they are of the type acceptable elsewhere in the theory of thin airfoils; but rather that the flow pattern found in a real fluid does not resemble that of the potential flow model which predicts them.[6]

Mangler and Smith[6] treat the flow theoretically by constructing a potential flow model, in which the vortex layer is replaced by a vortex sheet of spiral form and the problem is then reduced to a two-dimensional one by the use of slender body theory and the assumption of a conical vorticity field. The shape and the strength of the vortex sheet are determined by utilizing two boundary conditions: the sheet lies in a stream surface of the flow with no difference in the pressure across it and the velocity is assumed to be constant along straight lines through the apex of the delta. This assumption agrees with experiments at supersonic speeds,[7] however, at low speeds, this assumption breaks down near the trailing edge as indicated in Fig. 33. It is noted that recent tests at the National Physical Laboratory (Aero. Div.) have found core velocities in the direction of the core path to be on the order of 1.5 times the free stream velocity.

Brown and Michael[8] considered the actual flow solution to be extremely difficult, hence a flow model more amenable to calculation was adopted. This simplified model replaced the spiral sheet with two concentrated line vortices above the wing and two feeding vortex sheets connecting the source of vorticity (leading edge) and the concentrated line vortices. Here also, conical flow is assumed.

Legendre[9] in 1952 considered the problem as a potential flow and represented the vorticity in the fluid by a pair of isolated vortices lying along streamlines. This introduced a many-valued function for the pressure which placed a pressure discontinuity along the path around either one of the isolated vortices. In 1953, Adams[10] suggested that these discontinuities should be placed on surfaces or sheets joining the vortices to the leading edge. Following Adams' suggestion, Legendre published a revised analysis of the problem in 1953.

Figure 3 shows the predicted inward and upward movement of the primary vortex cores with angle of attack for slender delta wings with leading edge separation. The theoretical curves are derived for supersonic flow with the secondary vortices not considered. Experimental curves from Fink and Taylor[11] and this report are included for comparison. It is noted that the experimental curves are from low speed studies.

Authoritative opinion on the effect of the secondary vortices is quite diverse. Reference 4 states that the real flow was different from that derived by Mangler and Smith due to secondary vortices. Lee[12] suggests that the influence on the main flow by secondary vortices is negligible. Attention is directed to Figs. 9 and 11 which show the secondary vortices downstream to be of comparable size to the primary vortices. This indicates that the size and hence the strength of the secondary vortices on the body may be of appreciable magnitude and hence exercise a large influence on the flow field.

To the authors' knowledge, no mathematical solution exists which will accurately predict the flow field over the delta wing with leading edge separation.

Lift Curve

Figure 4 shows the lift curves of the delta wing models tested to be non-linear. The actual lift coefficients exceed those predicted by slender wing theory. It has been theorized[13,4] that the extra lift produced by a delta wing with leading edge separation is due to the extra entrainment of air by the leading edge vortices. Furthermore, that the non-linear nature of this extra lift is due to the inward and upward movement of the vortex cores and their increase in strength with angle of attack, giving an ever increasing entrainment effect.

Adams[10] and Edwards[14] have derived formulas for predicting the lift curve based on Legendre's theory. Their formulas are applicable only for small angles of attack. Figure 4 shows the results of these formulas as well as comparisons

with slender wing theory and experiments. The predicted lift curves fall short of desired accuracy.

Adams' formula:

$$C_L = \frac{\pi}{2} \mathcal{R} \alpha + \pi \left(1 + \frac{1}{2\sqrt{2}}\right) (4 \mathcal{R})^{\frac{1}{3}} \alpha^{\frac{5}{3}}$$

Edwards' formula:

$$C_L = \frac{\pi}{2} \mathcal{R} \alpha + \pi \left(1 + \frac{1}{2\sqrt{2}}\right) (\mathcal{R})^{\frac{1}{3}} \alpha^{\frac{5}{3}}$$

An empirical lift curve formula has been developed from this investigation which is covered in a subsequent section.

MODELS AND APPARATUS

Models

All models were aspect ratio one delta wings. Model I was a flat plate of 1/8 inch thick sheet metal. A hollow version of model one was also constructed for the smoke flow work. See Fig. 1.

Models II and III were Fiberglas models of thicknesses 12 percent and 6 percent respectively. The root chord sections are parabolic with maximum thickness at the 0.50 root chord location, as shown in Fig. 1.

For smoke flow studies, holes of 1/16 inch diameter were placed at appropriate locations on the upper surfaces.

Smoke Generator

Kerosene is used for producing the smoke. The kerosene is boiled by passing it through an electrically heated tube. The vapor passes through a small orifice and is broken into tiny particles, which produces a dry, dense white smoke.

Wind Tunnels

The Princeton 4 ft. by 5 ft. wind tunnel was used for force measurements and the Princeton 3 ft. by 4 ft. three-dimensional smoke tunnel was used in the smoke flow visualization studies.

PROCEDURE

Force Measurements

The lift force was measured by the beam balance system of the wind tunnel. The tunnel velocity was 115 fps, giving a Reynolds Number based on root chord of approximately 1.5×10^6.

Smoke Flow Visualization

The technique can best be described by a three-dimensional view of the smoke tunnel as shown in Fig. 5. The model is mounted in the test section as shown. For the vortex core pictures in the cross-flow plane, a 1600 mm projector with a 1000 watt bulb was used to project a plane of light normal to the free stream as shown on Fig. 6b. The plane was created by inserting a piece of metal, having a 1/32 inch slit in front of the bulb casing as shown in Fig. 5b. Smoke, under pressure, is forced through a tube into the hollow model and out the holes in the wing. Tunnel velocity was maintained at 11 fps. The photographs of the vortex cores were taken through a hole in the downstream section as shown. By means of this procedure, quantitative data was obtained of the core positions.

The distance from camera to model was approximately twenty feet. The pictures were taken with a 35 mm camera with a 360 mm telephoto lens. With f = 5.5, pictures of the flow on the model were taken at one second exposures and downstream shots were taken with two second exposures.

For the top and bottom views of the flat plate model, a Speed Graflex camera was used. Light was supplied by standard flood lights.

RESULTS AND DISCUSSION

Flow Visualization in the Cross-Flow Plane

Flat Plate Delta

Figures 7 and 8 show the vortices at 0.50 root chord and the trailing edge, respectively, at various angles of attack. The inward and upward movement of the cores as angle of attack is increased is evident.

Figure 9 shows the vortices at 0.25 c_r downstream of the trailing edge. Up to $\alpha = 20^\circ$, the primary and secondary vortices appear to be comparable in size. Above $\alpha = 20^\circ$, the secondary vortices become smaller than the primary vortices. This change in relative size may indicate a reduction in the effect of the secondary vortices on the flow field as angle of attack is increased.

Figure 10 shows a sequence at various chordwise stations on the model at $\alpha = 20^\circ$. The build up of the vortices as the flow moves toward the trailing edge is shown.

The relation between the primary and secondary vortices and the feeding sheet at locations from the trailing edge to 0.50 c_r downstream of the trailing edge for $\alpha = 15^\circ$, is illustrated in Fig. 11. Since the photographs do not show clearly the position of the feeding sheet at the various downstream locations, the sketches have been included. At the trailing edge, the triangular regions outboard and below the primary vortices are the viscous regions in which the secondary vortices have formed. At 0.10 c_r downstream, the wake intersects the sheet between the primary and the secondary cores. This point of intersection is a stagnation point in the cross-flow plane and the flow splits and proceeds toward the primary and the secondary cores. Because this stagnation point occurs on the sheet between the two vortices, it indicates that the effects of the pressure gradients produced by the two vortex systems are almost equal at that point. From this, it appears that the strength of the secondary vortices is significant compared to that of the primary vortices. Figure 27 shows a total head survey[4]

made in the cross-flow plane at 0.67 c_r on a model similar to the flat plate delta tested in this report. The smoke patterns shown in Fig. 11 are quite similar to the contours found by the survey, Figure 11 shows that as the flow proceeds downstream, the feeding sheet moves toward the primary vortex, and the secondary vortices rotate about the primary vortices.

6% Delta

Figure 12 shows a sequence at various chordwise stations on the model at $\alpha = 15^\circ$. Figure 13 shows the vortices at the trailing edge at various angles of attack. Qualitative comparison of the flat plate delta and the 6% delta is difficult. However it does appear, from a comparison of Fig. 8a and Fig. 13a, that at $\alpha = 5^\circ$, the vortices at the trailing edge of the flat plate delta are well defined compared to the vortices on the 6% delta.

Figure 14 shows the cross-flow plane at 0.25 c_r downstream of the trailing edge. The position of the feeding sheet between the primary and secondary vortices is shown clearly in Figs. 14c and 14d. The diameters of the cores and the vortices increase with angle of attack. It appears that the relative size of the secondary and the primary vortex is not as significant for the 6% delta as it was for the flat plate delta. For example: Fig. 9b (flat plate delta, $\alpha = 10^\circ$), shows the secondary vortex to be almost equal in size to the primary vortex and Fig. 14b (6% delta, $\alpha = 10^\circ$), shows the secondary vortex to be approximately one half the size of the primary vortex. It may be speculated that the effect of the secondary vortices on the flow field diminishes with wing thickness.

Flow Visualization on the Surfaces of the Flat Plate Delta

It can be seen in Fig. 15 that at $\alpha = 0^\circ$, there is laminar flow over the wing. At this angle of attack the lift curve slope may be computed from linearized potential theory. This has been done with good accuracy by many investigators.

As α is increased to 2°, it can be seen in Fig. 16 that the flow is beginning to form a vortex along the leading edge on the upper surface. The under surface flow is relatively unaffected.

Turning to Fig. 17 for $\alpha = 4^{\circ}$, the spiral vortex along the leading edge can now be seen more clearly. Very little effect is noted on the under surface, as the tendency to flow toward the leading edge is slight.

In Fig. 18 for $\alpha = 6^{\circ}$, the spiral vortex continues to grow, and as more air is entrained in the vortex it is seen that the region of reattached flow is decreasing. On the under surface, more air is flowing toward and over the leading edge and is entrained in the vortex.

As α increases to 10°, the vortex grows and the reattached region shrinks. On the under surface, the amount of flow that is passing over the leading edge and being entrained is increasing slowly.

In Figs. 20 to 24, the flow on the upper and lower surfaces is shown with increasing angles of attack, up to 35°. It can be seen that more of the upper surface flow continues to roll into the vortex and the reattached region decreases in size, until at $\alpha = 35^{\circ}$ there is essentially no reattachment.

On the under surface, more and more of the flow is passing out and over the leading edge. This effect is very pronounced at the higher angles of attack. It may also be seen in Fig. 25a, which is a view of the flow over the leading edge, and also in Fig. 25b, which is a view from the trailing edge.

Figure 26 shows the vortex cores downstream of the trailing edge as viewed from the top and is an illustration of their tenacity.

Graphical Analysis of Vortex Core Loci on the Body

Flat Plate Delta

Examining Fig. 28 it may be seen that the curves of z/a and y/a fall on one line for the chordwise positions chosen. This chordwise independence is also illustrated in Figs. 31 and 32. The core is seen to be independent of chordwise location until about 0.80 c_r where the core moves inward and upward. This can be attributed to trailing edge effects; that is, the core line is bent toward the direction of the free stream as it nears the trailing edge.

The core positions with respect to z/a and y/a versus α/ϵ are plotted in Figs. 29 and 30. Here it may be seen that z/a is approximately linear with angle of attack for $\alpha > \epsilon$. It is also seen that the core moves inward very rapidly at small angles of attack. At $\alpha = \epsilon$, the core has already moved inboard about 90 percent of its total inward movement. Theoretical curves of Brown and Michael[8] have been included for comparison. Their z/a versus α/ϵ curve shows good agreement with the experimental results.

Figures 33 and 34 show the side view and plan view with the z and y scales amplified to illustrate the core movements.

6% Delta

Now, turning to Fig. 35, it may be seen that z/a versus y/a continues to move inward and upward with increasing angle of attack. Individual movements are seen in Figs. 36 and 37. The movement is no longer independent of chordwise position. The core locus moves inward with increasing chordwise position. These effects are clearly shown in Figs. 38 and 39. Again, amplified scales are used to give the side and plan views of the core in Figs. 40 and 41.

12% Delta

In similar fashion to the flat plate and the 6% delta, the 12% delta exhibits inward and upward movement with increasing α as seen on Figs. 42, 43,

and 44. Since the thickness is a function of chordwise location, the core position is not independent of x. In Fig. 45, it can be seen that z/a decreases with increasing x until the core is swept up by the trailing edge effects. Figure 46 shows that y/a is relatively constant with x. The effect of body shape can also be seen in Fig. 47, where the curvature of the z versus x curves is distinctly related to the increase and decrease of body thickness with x. Figure 48 is a plan view showing y versus x, with an amplified y scale.

Downstream Core Loci

Because of the tenacity of the vortex cores behind the delta wing (Fig. 26), it was possible to obtain core position data as far downstream as 1.5 chord lengths. The cores were observed very clearly as far downstream as eight chord lengths (16 ft.).

Flat Plate Delta

In Fig. 49, the variation of $z'/\frac{b}{2}$ with downstream station is shown. It is immediately observable that at all angles of attack, the z' position varies in a sinusoidal manner as the core proceeds downstream. As the angle of attack increases, the path of a vortex core slopes downward at an increasing angle. It is seen that with all the core paths for the various angles of attack plotted on one figure, the paths cross between 0.25 and 0.50 c_r downstream.

In Fig. 52, the variation of $y/\frac{b}{2}$ with downstream station is also seen to be of a sinusoidal nature. There is a trend toward inward motion of the cores with angle of attack. This is just a continuation of the inward motion of the cores over the body as α increases.

6% Delta

In Fig. 50, the $z'/\frac{b}{2}$ versus % c_r downstream curves possess the same characteristics as the corresponding flat plate curves, however, the sinusoidal

variation is less marked. It can be seen that the paths of one core, for increasing angles of attack, cross between 0.50 and 0.75 c_r downstream.

In Fig. 53, the $y/\frac{b}{2}$ versus % c_r downstream curves show a very pronounced sinusoidal relation. The core loci also show an inward motion with angle of attack.

12% Delta

In Fig. 51, the $z'/\frac{b}{2}$ versus % c_r downstream curves again show the same characteristics as the corresponding flat plate curves. A slight sinusoidal variation is observed. The $y/\frac{b}{2}$ versus % c_r downstream is also sinusoidal, as seen in Fig. 54. The paths of one core, for increasing angles of attack, cross between 0.50 and 0.90 c_r downstream.

Summary of Downstream Effects

The vortex cores are seen to spiral downstream on a helical path as shown in Fig. 55. This accounts for the apparent sinusoidal variation of the $z'/\frac{b}{2}$ and $y/\frac{b}{2}$ coordinates versus downstream location. This spiral is of the same sense as the spiral flow around the core. The spiral nature of this core path is related to the presence of the secondary vortices. The secondary vortex is not negligibly small compared to the primary vortex, and thus the center of gravity of the vortex system is not at the center of the primary core, as seen in Fig. 52b. It is known that the secondary vortex rolls up around the primary core, thus it is possible to explain this motion by assuming both vortices rotate around the center of gravity. This would explain the rolling up of the secondary vortex around the primary and the movement of the primary core on a helical path downstream.

It is also seen that the paths of one core pass through the same downstream vertical position as the wing moves through the angle of attack range. This point appears to move downstream slightly as the wing thickness increases.

Thickness Effects on Core Positions over the Body

The effect of thickness on the vortex core position may be seen in Figs. 56, 57, and 58, which are plots of core positions at 0.50 c_r. It is seen that as thickness increases, the core moves outward in an approximately linear manner. It may also be seen that increases in thickness cause no noticeable trend of movement of the core in the vertical direction.

EMPIRICAL APPROACH TO THE LIFT CURVE FOR LOW ASPECT RATIO DELTA WINGS

It is well known that the C_L versus α curve for low aspect ratio delta wings has the shape shown in Fig. 59. That is, the C_L exceeds that predicted by linearized potential theory due to the vortices formed by leading edge separation.

First, let us assume that the lift curve is composed of a linear component and a ΔC_L due to the vortices as shown in Fig. 60.

$$(1) \quad C_L = C_{L_\ell} + \Delta C_L$$

where

$$C_{L_\ell} = \frac{2\pi AR}{PAR+2}\alpha$$ (R. T. Jones' expression for low aspect ratio delta wings)

and

$$\Delta C_L = f\ (\text{vortex position, vortex strength})$$

that is:

$$C_L = f\ (y/a,\ z/a, \Gamma)$$

Expressing in total differential form and linearizing:

$$(2) \quad d\Delta C_L = \frac{\partial \Delta C_L}{\partial\, y/a}\, d\, y/a + \frac{\partial \Delta C_L}{\partial\, z/a}\, d\, z/a + \frac{\partial \Delta C_L}{\partial \Gamma}\, d\Gamma$$

Curves of ΔC_L versus z/a and y/a have been plotted in Figs. 61 and 62. To evaluate the partial derivatives, one must obtain

$$\left(\frac{\partial \Delta C_L}{\partial\, y/a}\right)_{z/a,\ \Gamma = \text{Const.}}, \quad \left(\frac{\partial \Delta C_L}{\partial\, z/a}\right)_{y/a,\ \Gamma = \text{Const.}}, \quad \left(\frac{\partial \Delta C_L}{\partial \Gamma}\right)_{y/a,\ z/a = \text{Const.}}$$

To do this, assume $\frac{\partial \Gamma}{\partial \alpha}$ = constant. This approximation is based on the theoretical calculations of Γ versus α in Ref. 8. Now, any non-linearity in the Γ versus α curve is a second order effect and will be neglected.

With this assumption, it is possible to evaluate the first two derivatives in equation (2) by holding α = constant instead of Γ = constant.

Examining Figs. 61 and 62, it can be seen for a typical case:

$$\alpha = 18^\circ: \ z/a = 0.30 \quad (\text{Fig. 61}) \ ; \quad \frac{\partial \Delta C_L}{\partial\, y/a} \doteq \frac{0.070}{0.104} = 0.673 \quad (\text{Fig 62})$$

$$\alpha = 18^\circ: \; Y/a = 0.716 \; (\text{Fig. } 62); \; \frac{\partial \Delta C_L}{\partial Z/a} \doteq \frac{0.058}{0.035} = 1.66 \quad (\text{Fig. } 61)$$

These partial derivatives differ by a factor of 2.5, so, as a first approximation it will be assumed that $\frac{\partial \Delta C_L}{\partial Z/a} \gg \frac{\partial \Delta C_L}{\partial Y/a}$, and thus $\frac{\partial \Delta C_L}{\partial Y/a}$ will be neglected.

The derivative $\frac{\partial \Delta C_L}{\partial \Gamma}$ must now be evaluated. In Ref. 15, it is stated that the distance between the vortex cores, "$2Y$", is a measure of the vortex strength.

$$(3) \quad 2Y = \frac{L}{\rho V \Gamma}$$

It is readily seen that by differentiating equation (3) and using

$$(4) \quad \frac{\partial \Delta C_L}{\partial \Gamma} = \frac{\partial \Delta C_L}{\partial Y/a} \frac{\partial Y/a}{\partial \Gamma}$$

that

$$\frac{\partial \Delta C_L}{\partial \Gamma} = \frac{\partial \Delta C_L}{\partial Y/a} \left(\frac{-Y}{a\Gamma} \right)$$

Since it has been assumed that $\frac{\partial \Delta C_L}{\partial Y/a} \ll \frac{\partial \Delta C_L}{\partial Z/a}$, unless $\frac{Y}{a\Gamma} \gg 1$, the term $\frac{\partial \Delta C_L}{\partial \Gamma}$ will be neglected. It is known that y/a is always less than one and from Ref. 9 that $\Gamma \gg 1$. Therefore,

$$\frac{\partial \Delta C_L}{\partial \Gamma} \ll \frac{\partial \Delta C_L}{\partial Z/a}$$

and will be neglected.

In view of the above, Eq. (2) may be reduced to:

$$d\Delta C_L = \frac{\partial \Delta C_L}{\partial Z/a} \, d\, Z/a$$

where $\frac{\partial \Delta C_L}{\partial Z/a}$ is obtained from Fig. 61.

The equation will first be evaluated for the flat plate case.

The relation of ΔC_L versus z/a was obtained by Lagrange's polynomial formula.

$$(5) \quad \Delta C_L = 4 \left(Z/a \right)^2 - 0.8 \left(Z/a \right) + 0.06$$

and $$\frac{\partial \Delta C_L}{\partial Z/a} = 8\, Z/a - 0.80$$

$$(6)\quad z/a = 0.616\,\alpha + 0.088$$

Substituting, the equation becomes:

$$(7)\quad \Delta C_L = 1.52\,\alpha^2 - 0.0594\,\alpha$$

and the total expression becomes, for $AR = 1$, $t/c = 0$:

$$(8)\quad C_L = 1.48\,\alpha + 1.52\,\alpha^2$$

Having an expression for C_L for $AR = 1$ and $t/c = 0$, it is possible to expand this to other thicknesses and aspect ratios.

For aspect ratios other than 1, with $t/c = 0$:

$$(9)\quad \Delta C_L = 0.0925\left(\alpha/\epsilon\right)^2 - 0.0146\,\alpha/\epsilon$$

or

$$(9a)\quad \Delta C_L = 0.0925\left(\frac{\alpha}{\tan^{-1}\frac{AR}{4}}\right)^2 - 0.0146\,\frac{\alpha}{\tan^{-1}\frac{AR}{4}}$$

Using the experimental data for the thickness effect it can be derived from Fig. 63 that:

$$(10)\quad \Delta C_{L\,t/c} = \left(0.529\,\alpha - 0.034\right)\sqrt{t/c}$$

Combining the expressions, an equation is obtained which should be applicable over a range of small AR's and t/c's.

$$(11)\quad C_L = \frac{2\pi AR}{pAR+2}\,\alpha + 0.0925\left(\frac{\alpha}{\tan^{-1}\frac{AR}{4}}\right)^2 - 0.0146\left(\frac{\alpha}{\tan^{-1}\frac{AR}{4}}\right) - \left(0.529\,\alpha - 0.034\right)\sqrt{t/c}$$

These equations were then applied to delta wings of aspect ratios of one to two and t/c from 0 to 12 percent.

The results are shown in Figs. 64, 65, 66 and 67. It is seen that the equation gives very good results. From this it can be concluded that the additional lift due to the vortices is due primarily to the vertical height of the vortex cores above the plane of the wing.

To simplify calculations, equation (1) can be expressed as:

$$C_L = A + B - C - D \text{ where}$$

$$A = \frac{2\pi AR}{pAR+2}\,\alpha\ ;\quad B = \frac{0.0925\,\alpha^2}{\left(\tan^{-1}\frac{AR}{4}\right)^2}\ ;\quad C = 0.0146\,\frac{\alpha}{\tan^{-1}\frac{AR}{4}}\ ;\quad D = \left(0.529\,\alpha - 0.034\right)\sqrt{t/c}$$

A, B, C and D are plotted on Figs. 68, 69, 70 and 71 for convenience in evaluating a particular case.

CONCLUSIONS

Smoke flow visualization techniques can be a powerful tool in the investigation of flow over a delta wing.

The path of the vortex cores downstream of the trailing edge is a helix. This helical motion is caused by the rotation of the secondary vortices about the primary vortices.

The strength of the secondary vortices relative to that of the primary vortices is not negligible. Hence, no mathematical treatment which fails to include the effects of the secondary vortices on the flow field can accurately predict the lift curve.

The lift may be considered to consist of a linear component, which can be predicted by potential theory, and an additional lift due to leading edge vortices. An empirical expression has been developed for this additional lift, which relates it to the height of the primary vortex cores above the wing. This expression predicts the lift curves accurately for sharp leading edged delta wings of various thicknesses and of aspect ratios from one to two.

REFERENCES AND BIBLIOGRAPHY

1. Winter, H.: Flow Phenomena on Plates and Airfoils of Short Span. NACA Rep. 798, 1936.

2. Wilson, H. A. Jr. and Lovell, J. C.: Full-Scale Investigation of the Maximum Lift and Flow Characteristics of an Airplane Having Approximately Triangular Plan Form. NACA RM No. L6K20, 1947.

3. Örnberg, T.: A Note on the Flow Around Delta Wings. KTH AERO TN 38, 1954.

4. Marsden, D. J., Simpson, R. W. and Rainbird, W. J.: The Flow Over Delta Wings at Low Speeds with Leading Edge Separation. College of Aeronautics, Cranfield, Rep. No. 114, 1957.

5. Jones, R. T.: Properties of Low-Aspect-Ratio Pointed Wings at Speeds Below and Above the Speed of Sound. NACA Rep. 835, 1946.

6. Mangler, K. W. and Smith, J. H. B.: A Theory on the Flow Past a Slender Delta Wing with Leading Edge Separation. Proc. of the Roy. Soc., No. 1265, 26 May 1959, Vol. 251.

7. Michael, W. H. Jr.: Flow Studies on Flat-Plate Delta Wings at Supersonic Speeds. NACA TN 3472, 1955.

8. Brown, C. E., and Michael, W. H. Jr.: On Slender Delta Wings with Leading-Edge Separation. NACA TN 3430, 1955.

9. Legendre, R.: Écoulement au Voisinage De La Pointe Avant D'une Aile A Forte Flèche Aux Incidences Moyennes. La Researche Aéronautique (ONERA), No. 30, 1952 and No. 35, 1953.

10. Adams, M. C.: Leading-Edge Separation From Delta Wings at Supersonic Speeds. Jour. Aero. Sci. (Readers' Forum), vol. 20, no. 6, June, 1953.

11. Fink, P. T. and Taylor, J.: Some Low Speed Experiments with 20% Delta Wings. A.R.C. 17854, 1955.

12. Lee, G. H.: Note on the Flow Around Delta Wings with Sharp Leading Edges. A.R.C. R&M 3070, 1958.

13. Weber, J.: Some Effects of Flow Separation on Slender Delta Wings. R.A.E. TN 2425, 1955.

14. Edwards, R. H.: Leading-Edge Separation from Delta Wings. Jour. Aero. Sci. (Readers' Forum), vol. 21, no. 2, Feb., 1954.

15. Spreiter, J. R. and Sacks, A. H.: The Rolling Up of the Trailing Vortex Sheet and Its Effect on the Downwash Behind Wings. Jour. Aero. Sci., vol. 18, no. 1, January, 1953.

16. Lomax, H. and Sluder, L.: Chordwise and Compressibility Corrections to Slender-Wing Theory. NACA Rep. 1105, 1952.

Pocock, P. J. and Laundry, W. E.: Some Aerodynamic Characteristics of Delta Wings at Low Speeds. Second Canadian Symposium on Aerodynamics, Institute of Aerophysics, Univ. of Toronto, 25-26 Feb., 1954.

Peckham, D. H.: Low Speed Wind Tunnel Tests on a Series of Uncambered Slender Pointed Wings with Sharp Edges. R.A.E. Rep. No. AERO 2613, 1958.

Küchemann, D.: Types of Flow on Swept Wings with Special Reference to Free Boundaries and Vortex Sheets. Jour. Roy. Aero. Soc., vol. 57, no. 515, November, 1953.

Rose, R. G.: A Note on the Estimation of Some Low Speed Characteristics of Delta Wings. College of Aero., Cranfield, Rep. No. 68, 1953.

Pappas, C. E. and Kunen, A. E.: An Investigation of the Aerodynamics of Sharp Leading-Edge Swept Wings at Low Speeds. Jour. Aero. Sci., vol. 21, no. 10, October, 1954.

Relf, E. J.: Note on the Lift Slope, and Some other Properties of Delta and Swept-Back Wings. A.R.C., R&M No. 3111, 1952.

Crabtree, L. F.: Effects of Leading-Edge Separation on Thin Wings in Two-Dimensional Incompressible Flow. Jour. Aero. Sci., vol. 24, no. 8, Aug., 1957.

Maskell, E. C.: Flow Separation in Three-Dimensions. R.A.E. Report No. Aero. 2565, Nov., 1955.

MODELS OF AR=1

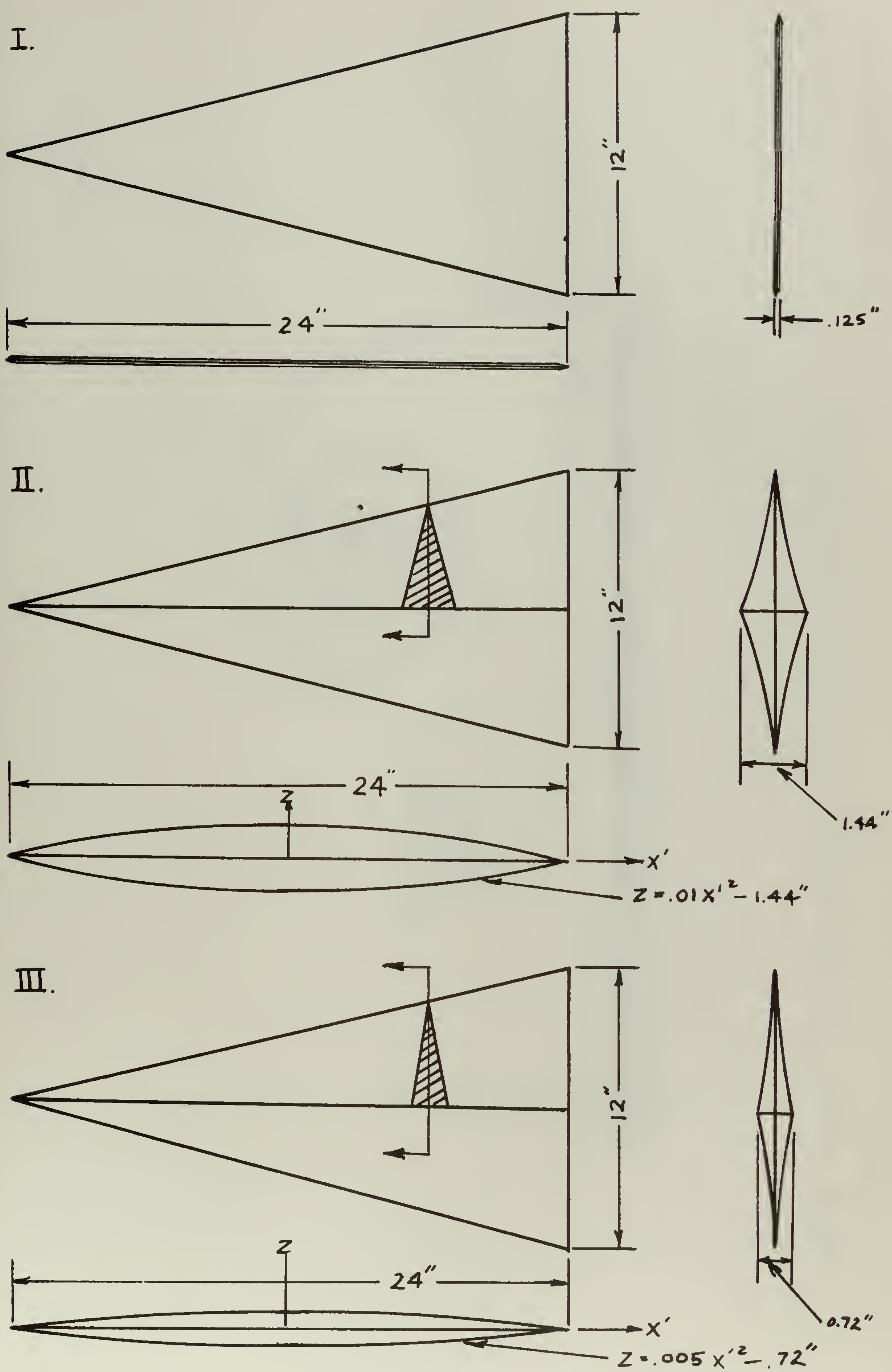

Fig. 1

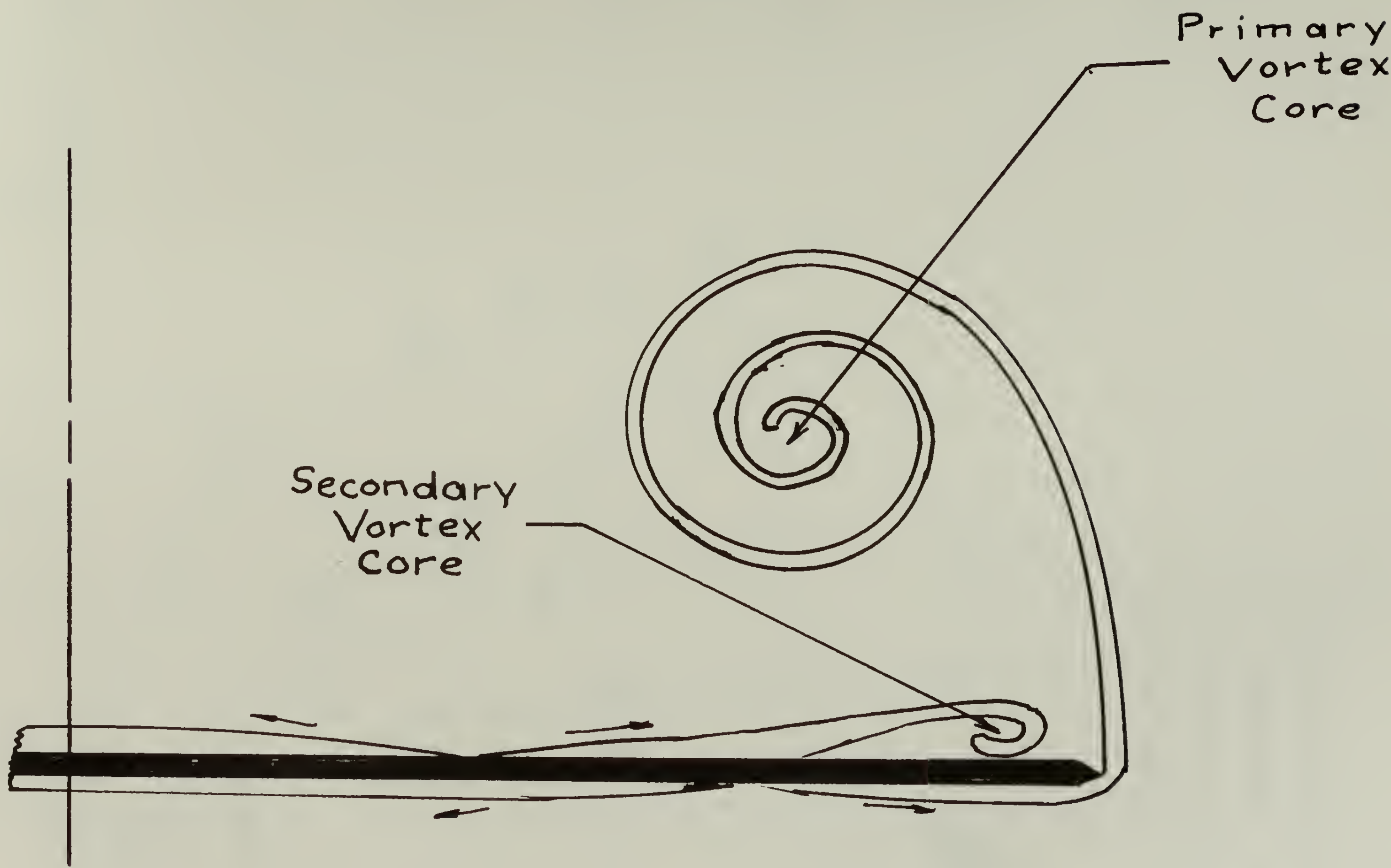

Fig. 2 Flow Characteristics in Cross-Flow Plane

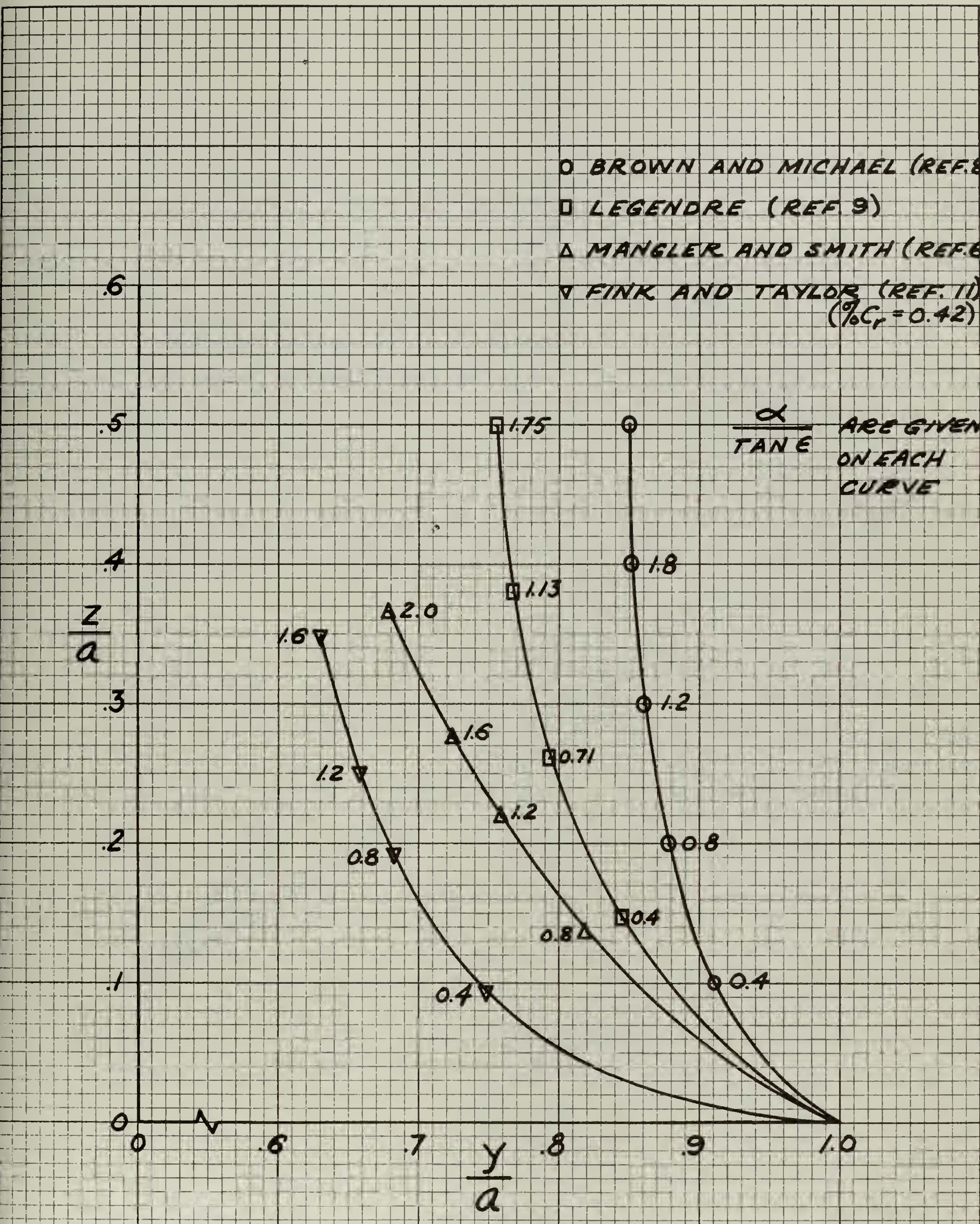

VORTEX CORE POSITIONS
(FIG. 19 IN REF. 4)

FIG. 3

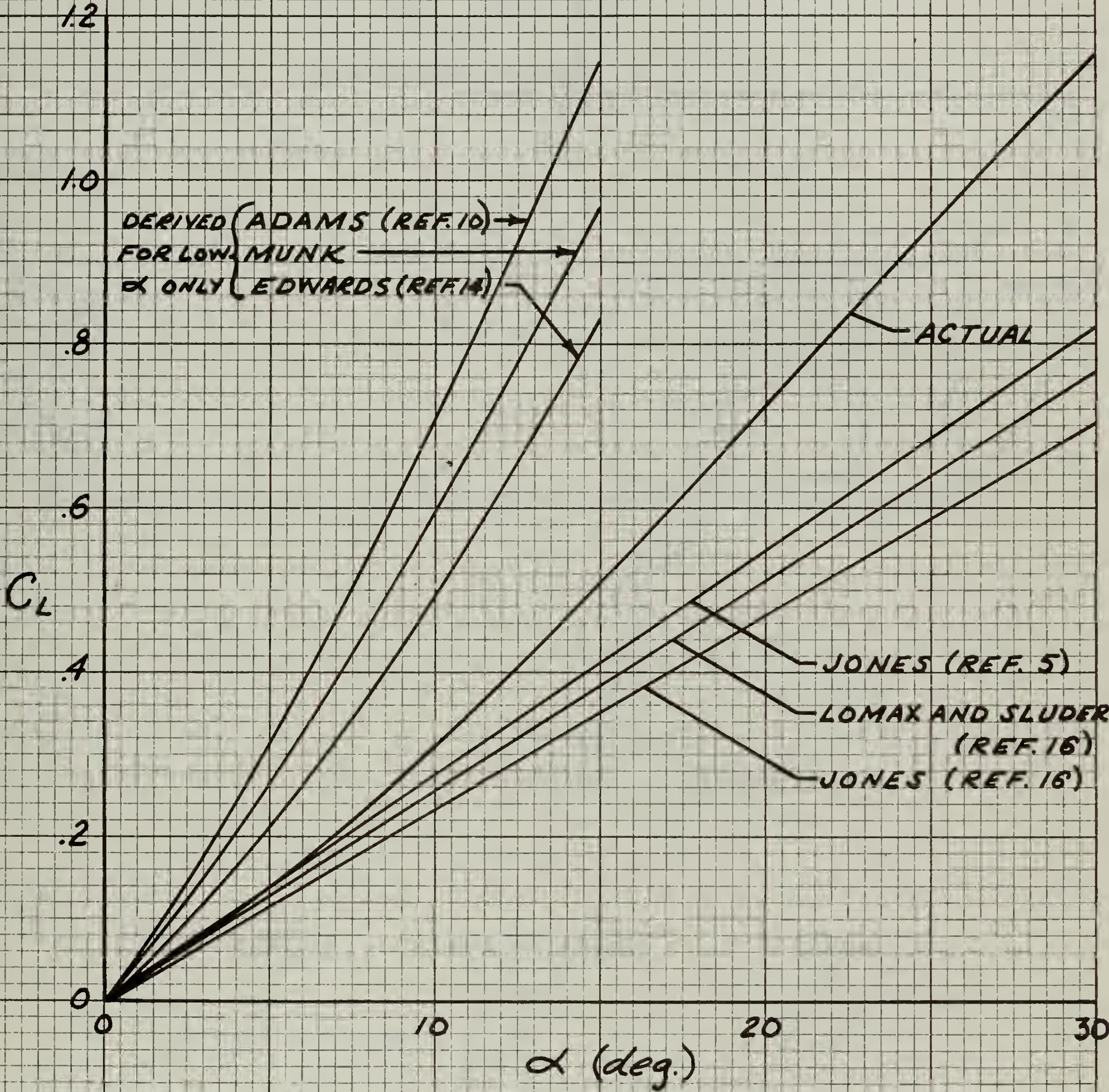

LIFT CURVE OF FLAT PLATE DELTA OF ASPECT RATIO ONE COMPARED WITH PREDICTED CURVES

FIG. 4

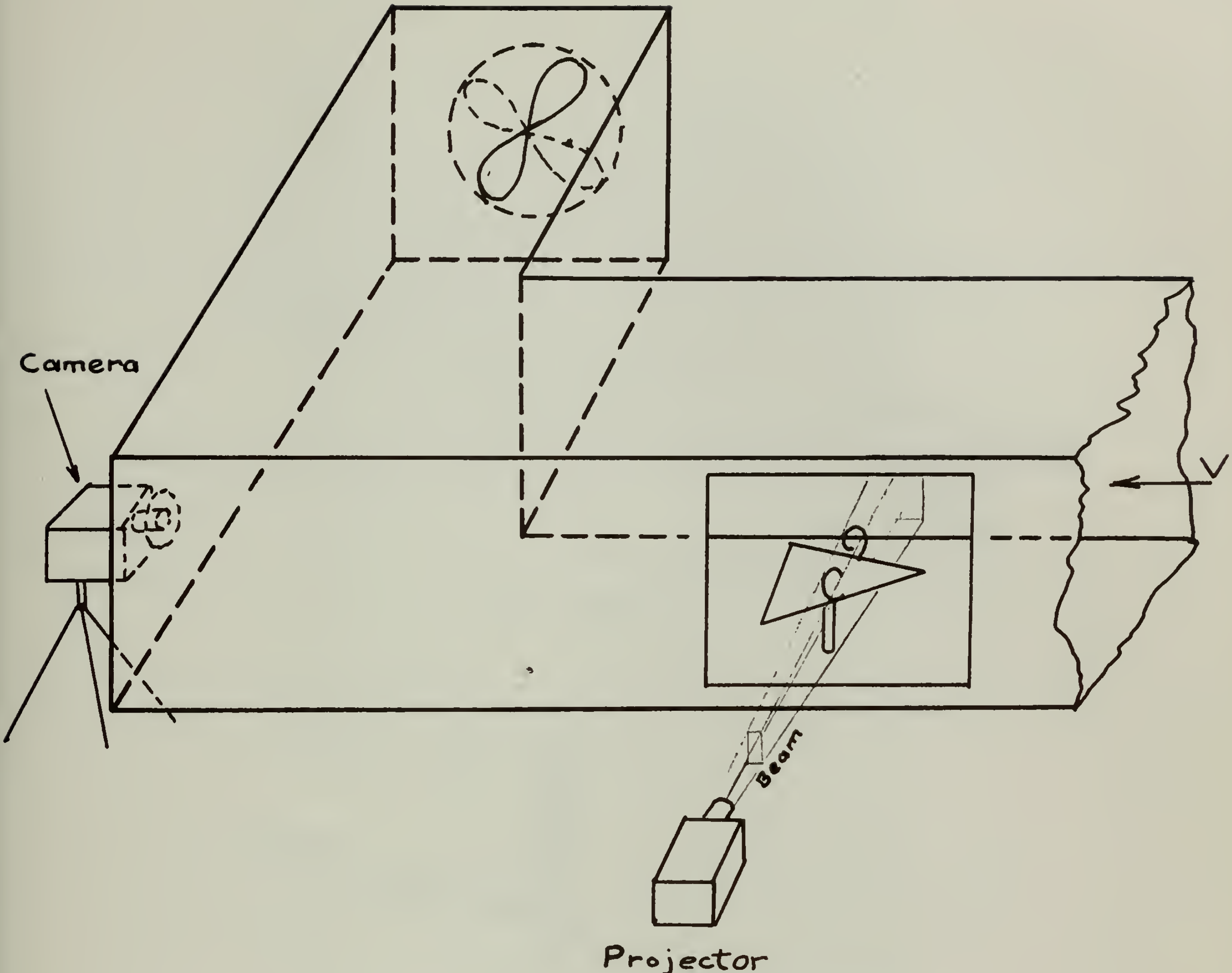

(a) 3D SMOKE TUNNEL

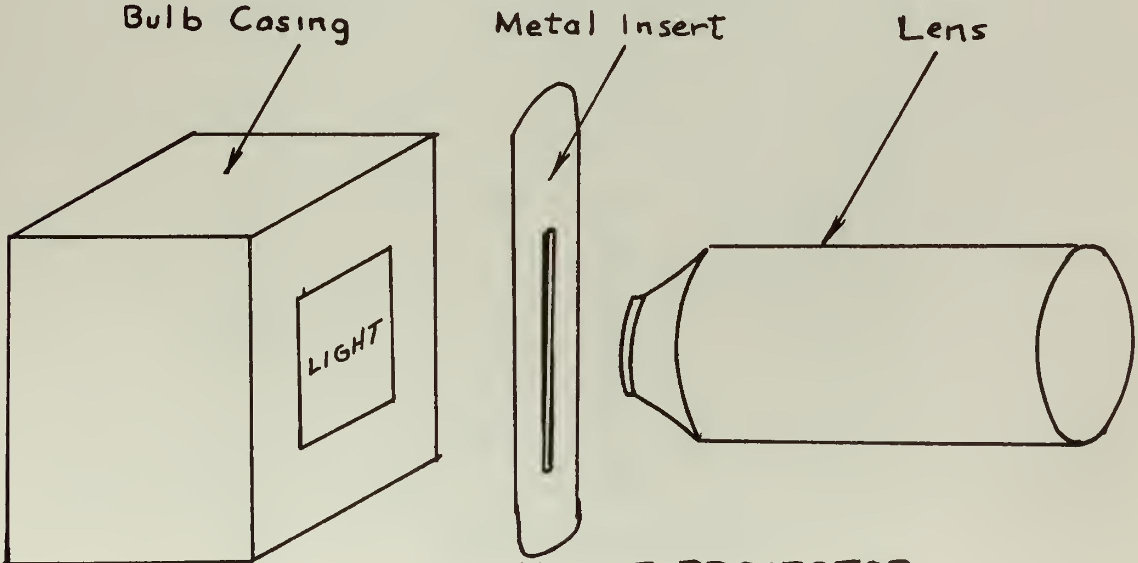

(b). DETAIL OF PROJECTOR

Fig. 5

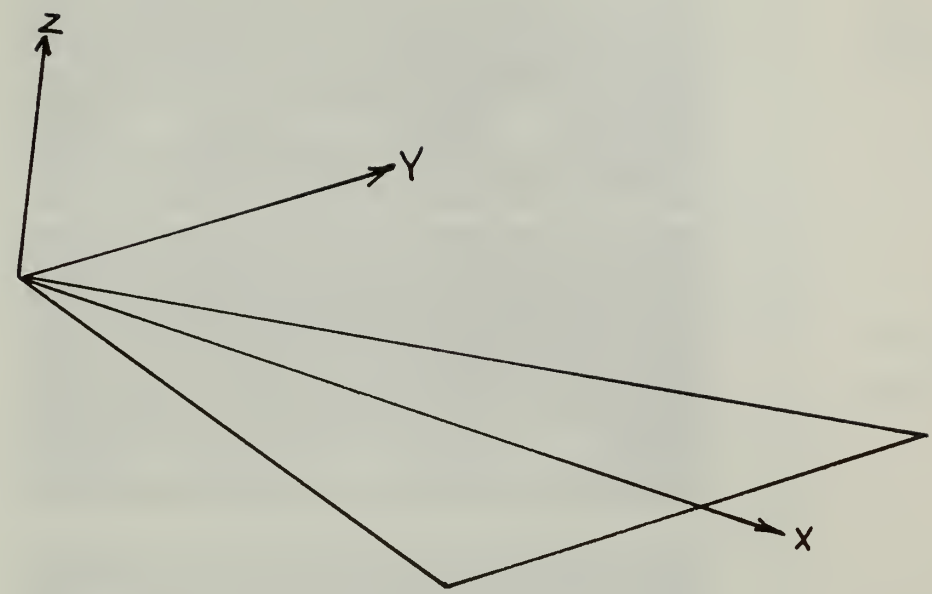

(a) Body

Side View

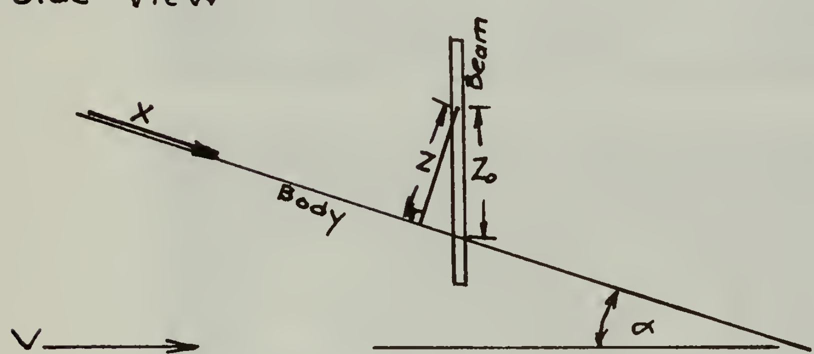

(b) Body

Side View

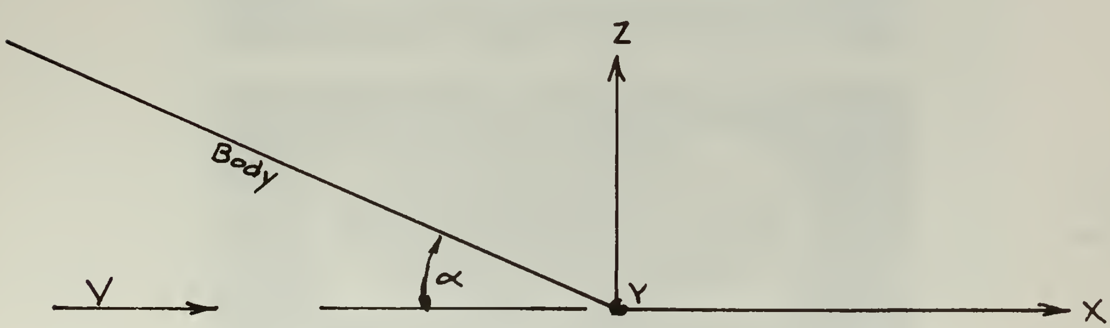

(c) Downstream

Fig. 6 COORDINATES

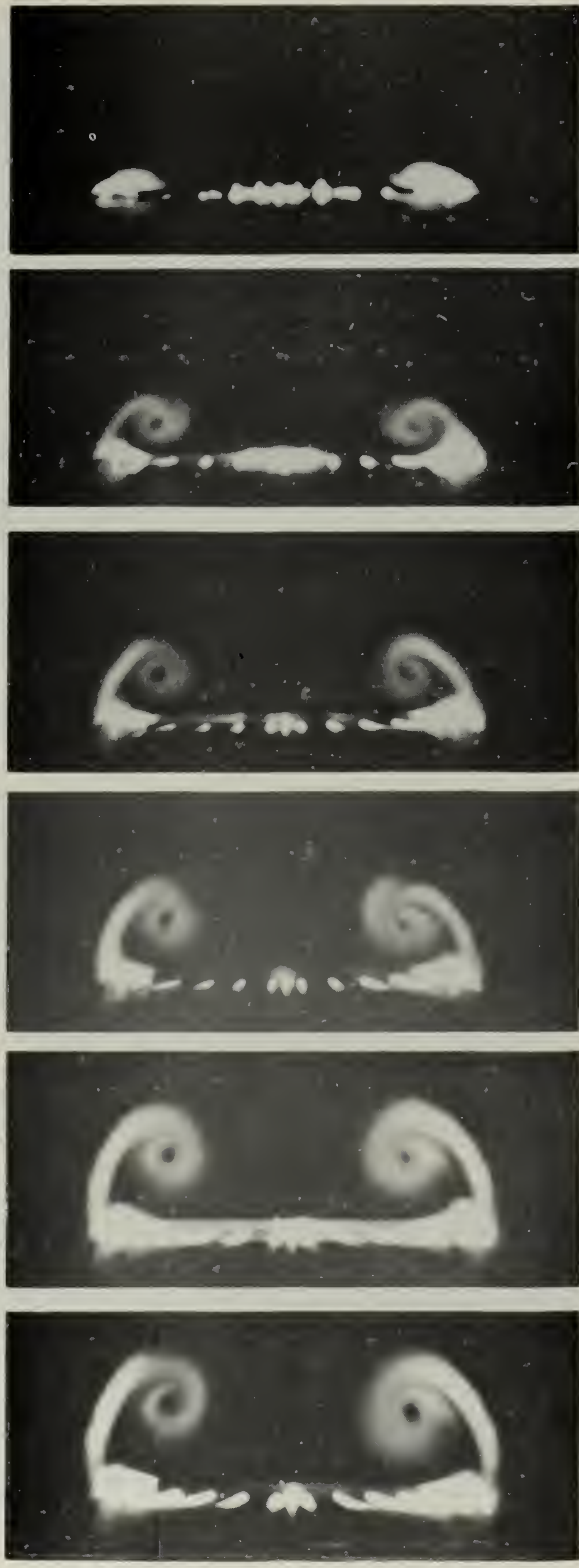

(a). $\alpha = 5°$

(b). $\alpha = 10°$

(c). $\alpha = 15°$

(d). $\alpha = 20°$

(e) $\alpha = 25°$

(f) $\alpha = 30°$

Fig. 7 Flat Plate Delta : Vortices at 0.50 C_r

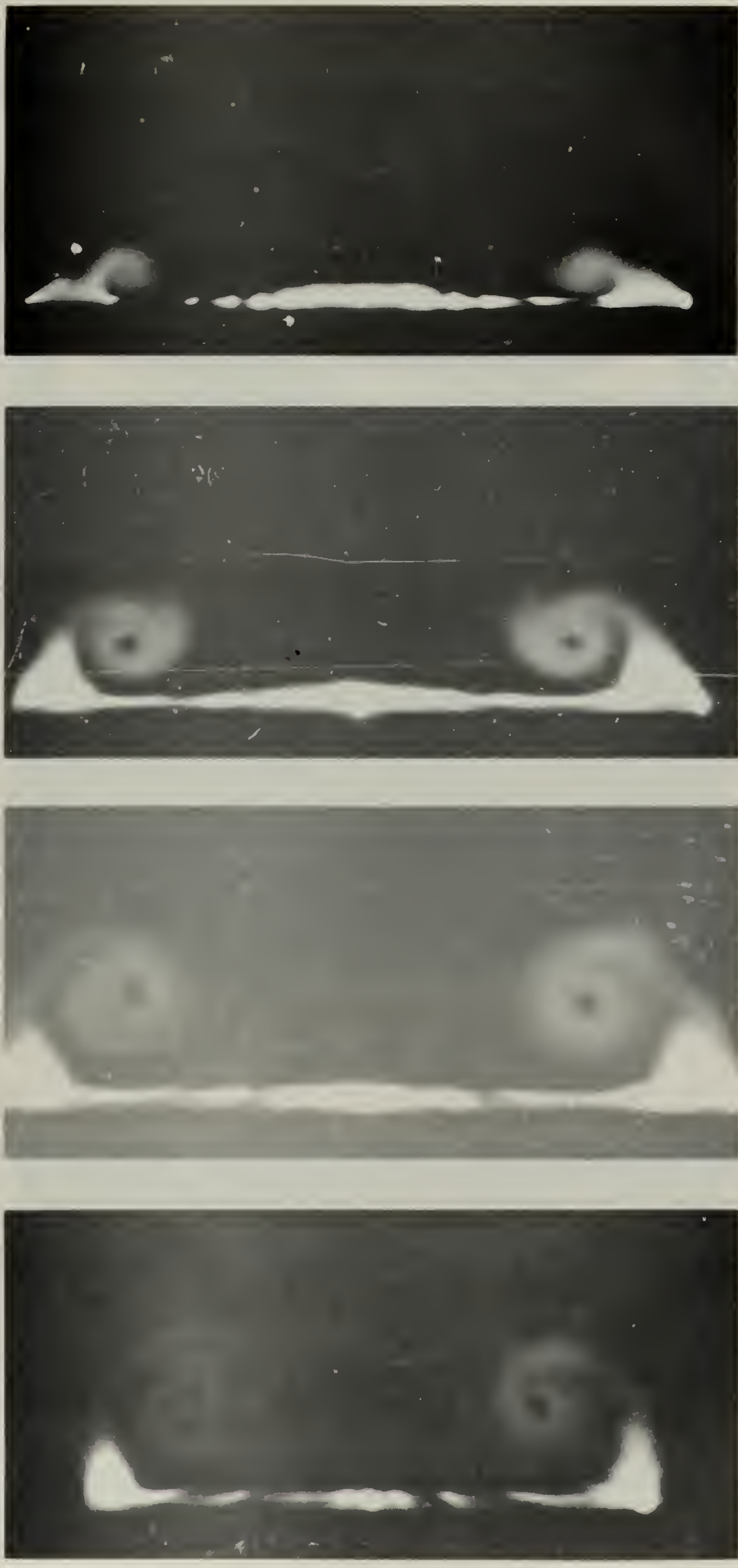

(a). $\alpha = 5^\circ$

(b). $\alpha = 10^\circ$

(c). $\alpha = 15^\circ$

(d). $\alpha = 20^\circ$

Fig. 8 Flat Plate Delta : Vortices at the Trailing Edge

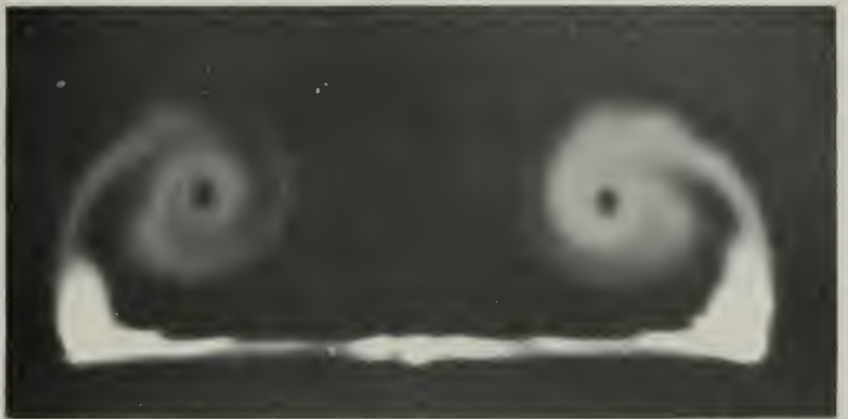

(e).
$\alpha = 25°$

(f).
$\alpha = 30°$

(g).
$\alpha = 35°$

Fig. 8 (Con't)

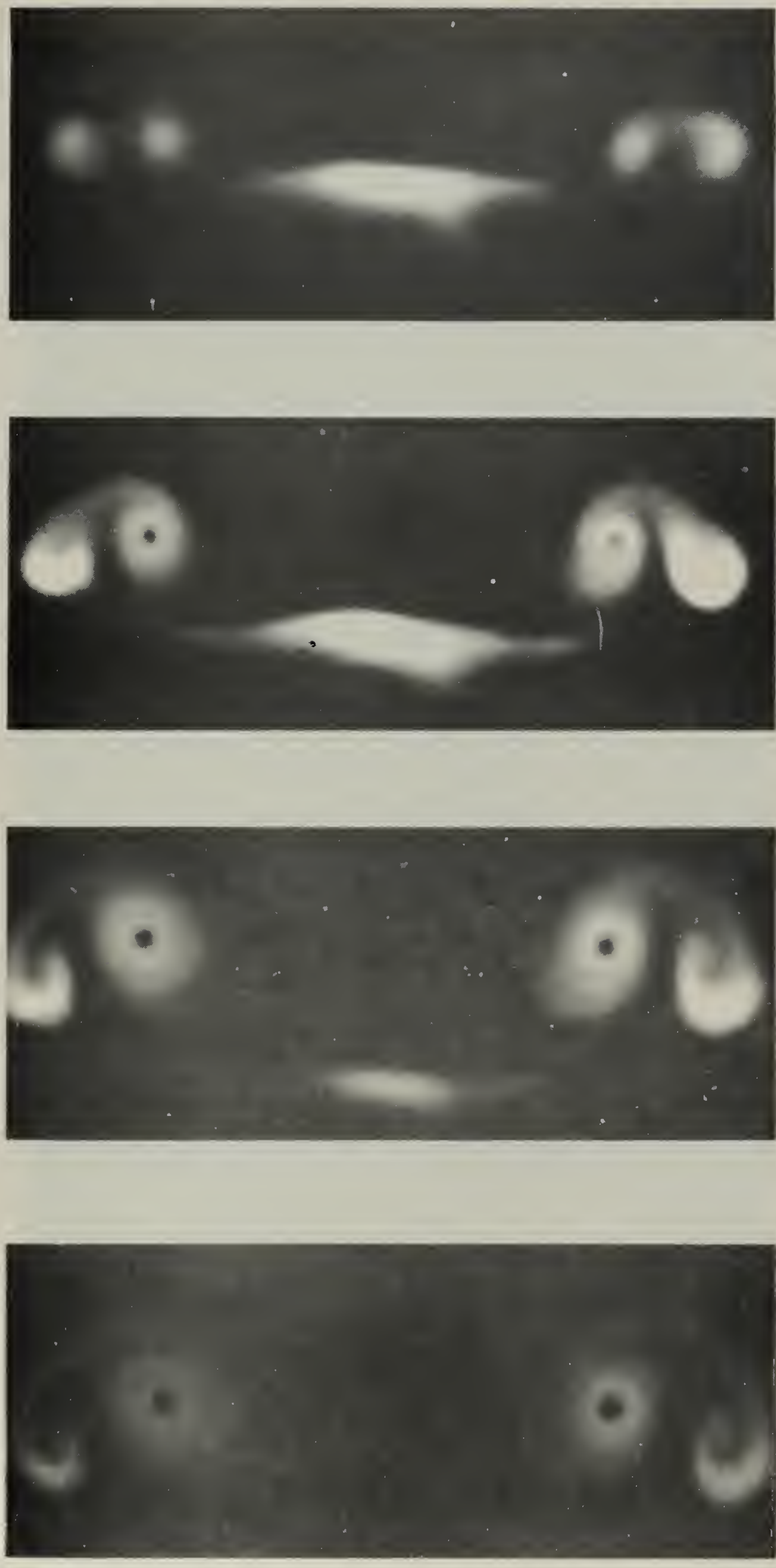

(a). $\alpha = 5^\circ$

(b) $\alpha = 10^\circ$

(c) $\alpha = 15^\circ$

(d) $\alpha = 20^\circ$

Fig. 9 Flat Plate Delta : Vortices at 0.25 C_r Downstream of T.E.

(e).
$\alpha = 25^\circ$

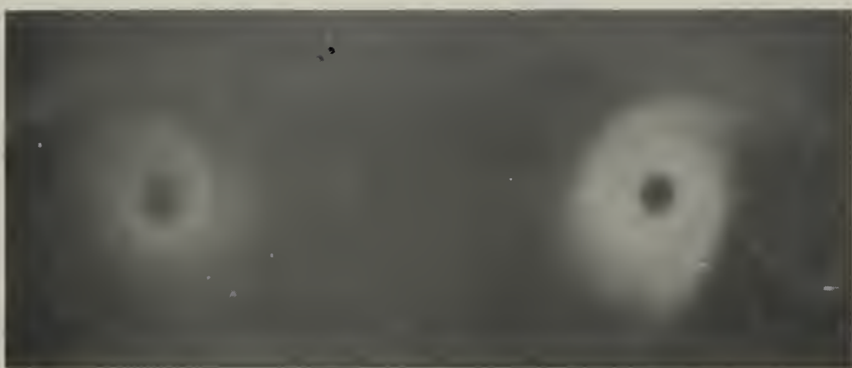

(f).
$\alpha = 30^\circ$

(g).
$\alpha = 35^\circ$

Fig. 9 (Con't)

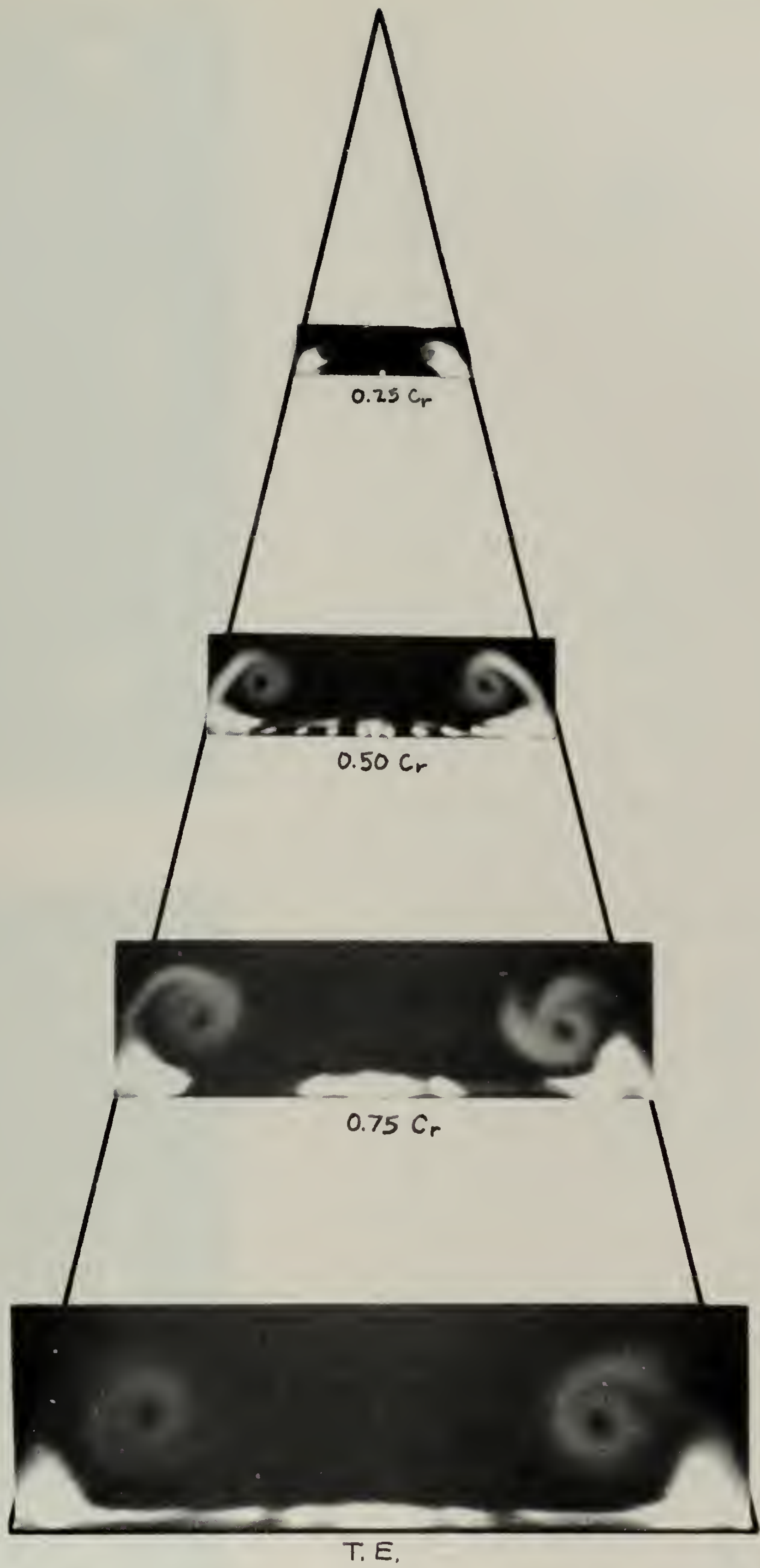

Fig. 10 Flat Plate Delta: Vortices from 0.25 Cr to T.E. at $\alpha = 20°$

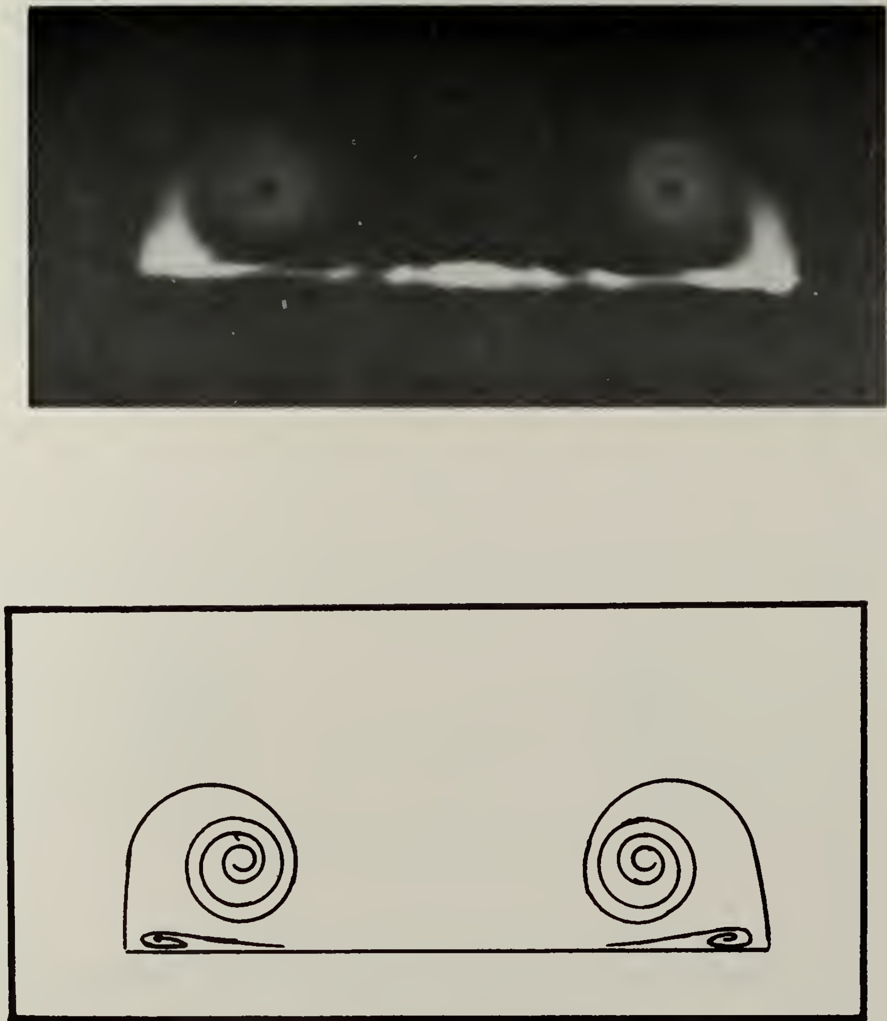

(a). T.E.

(b). 0.10 C_r Downstream

Fig. 11 Flat Plate Delta : Vortices from T.E. to 0.50 C_r Downstream of T.E.

(c) 0.20 C_r Downstream

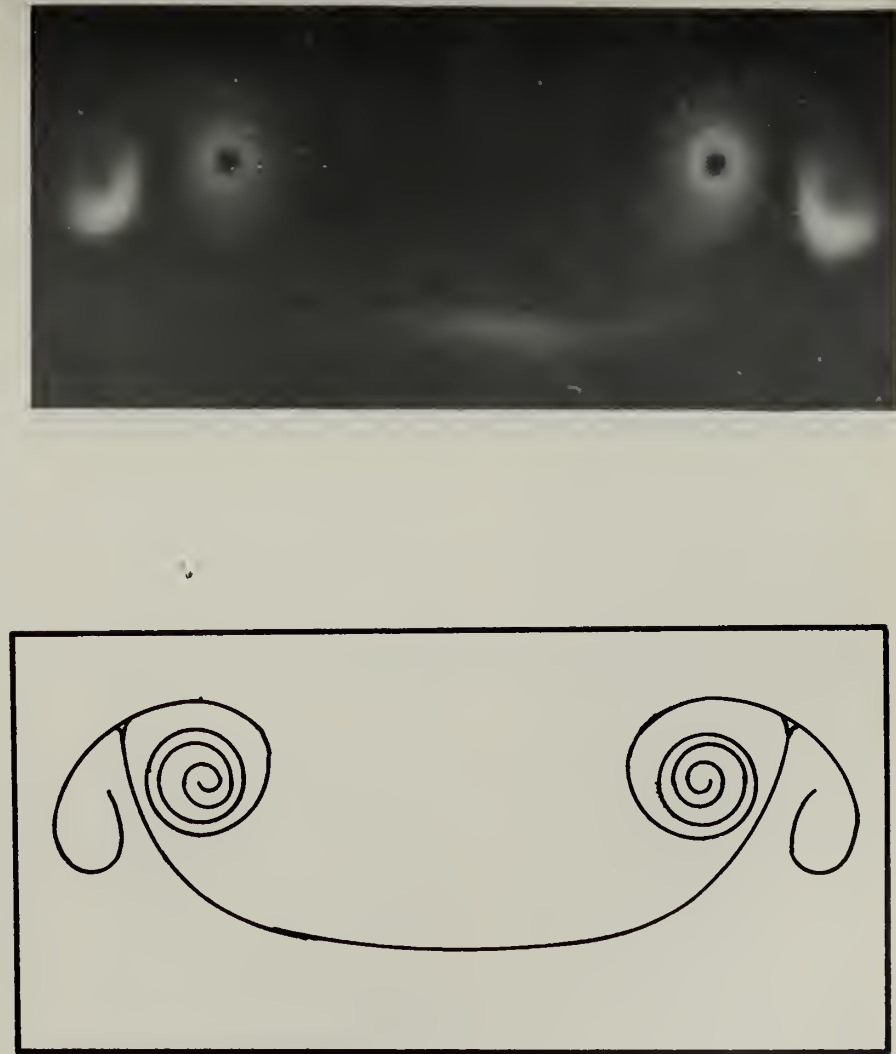

(d) 0.30 C_r Downstream

Fig. 11 (Con't)

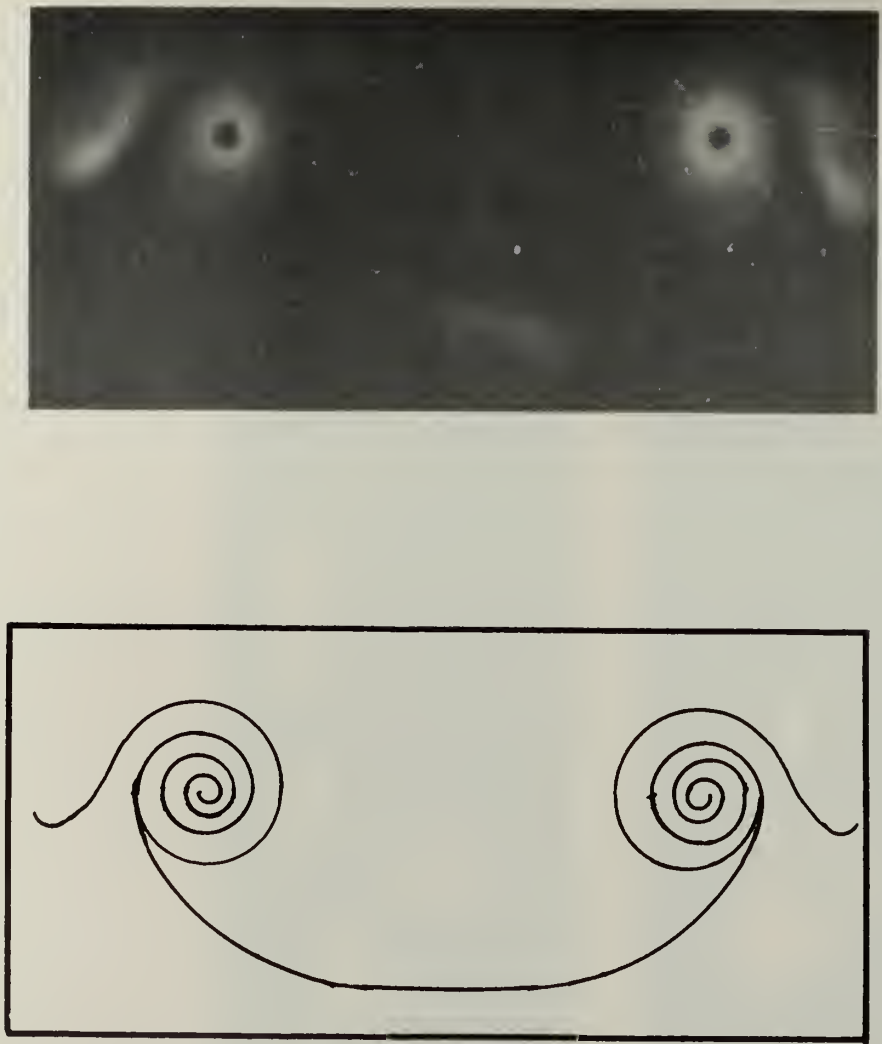

(e) 0.40 C_r Downstream

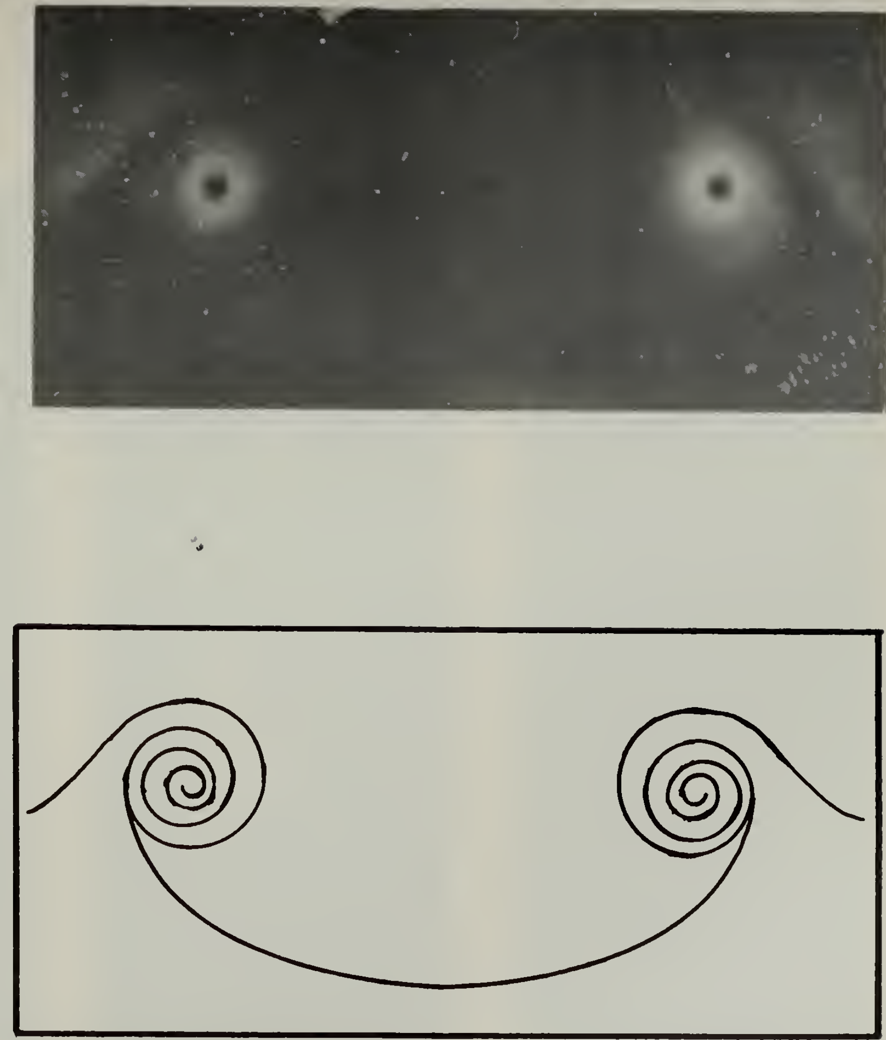

(f) 0.50 C_r Downstream

Fig. 11 (Con't)

(a). $0.25 C_r$

(b). $0.50 C_r$

(c). $0.75 C_r$

(d). T.E.

Fig. 12 6% Delta: Vortices from $0.25\ C_r$ to the T.E. at $\alpha = 15°$

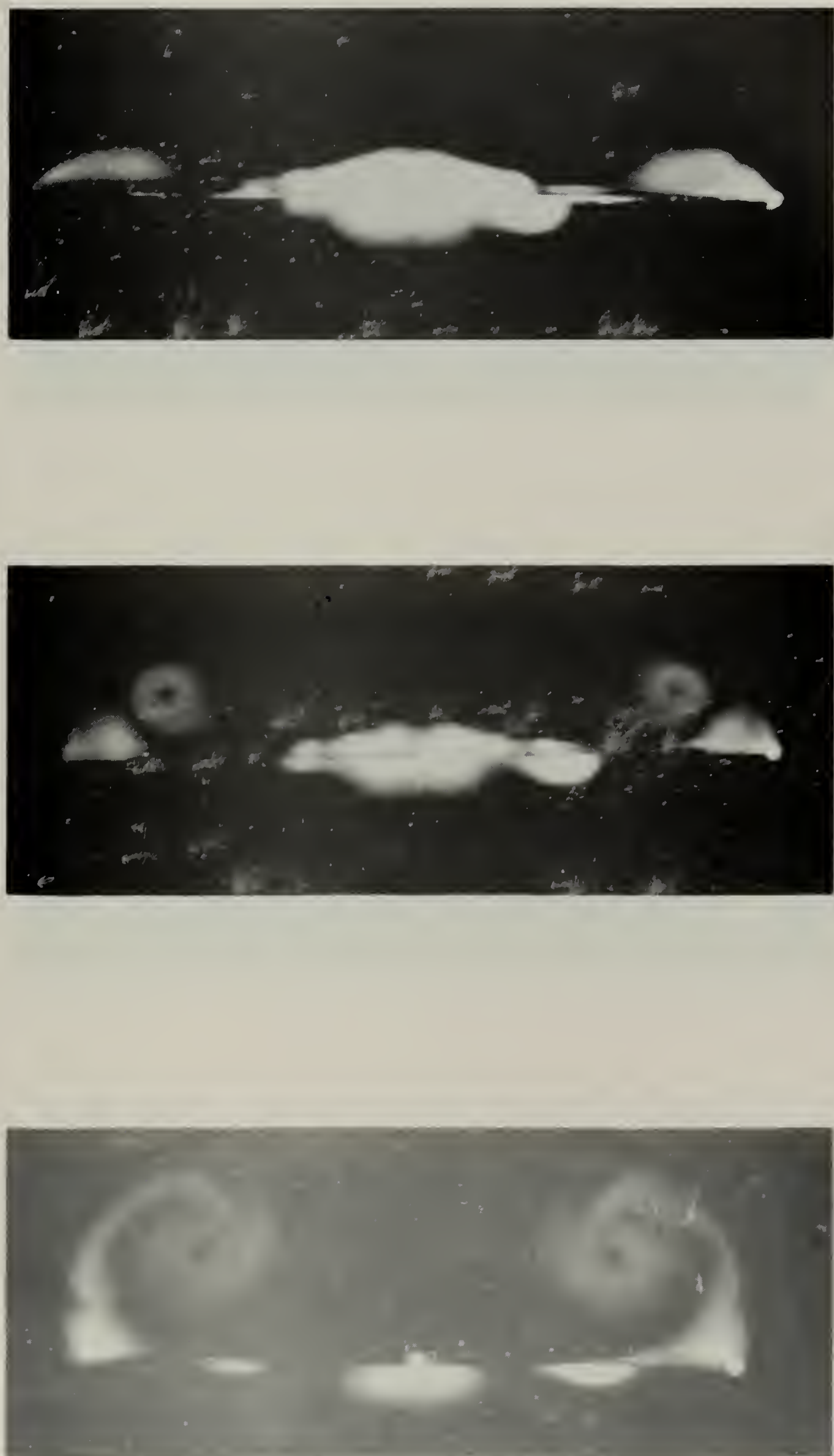

(a). $\alpha = 5°$

(b). $\alpha = 10°$

(c). $\alpha = 20°$

Fig. 13 6% Delta: Vortices at the Trailing Edge

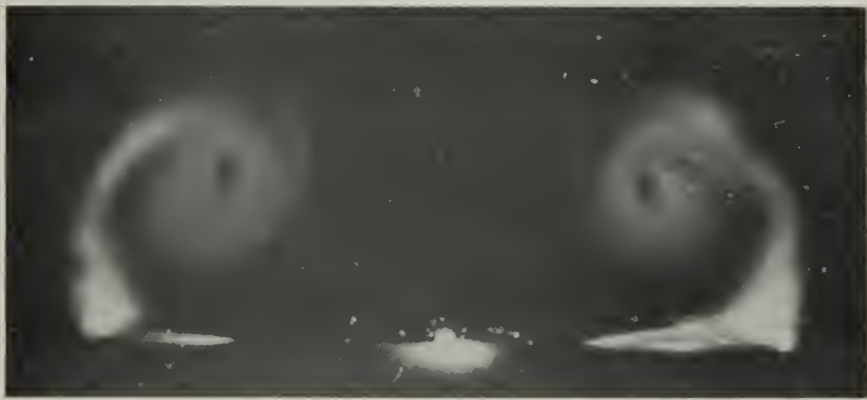

(d).
$\alpha = 25^\circ$

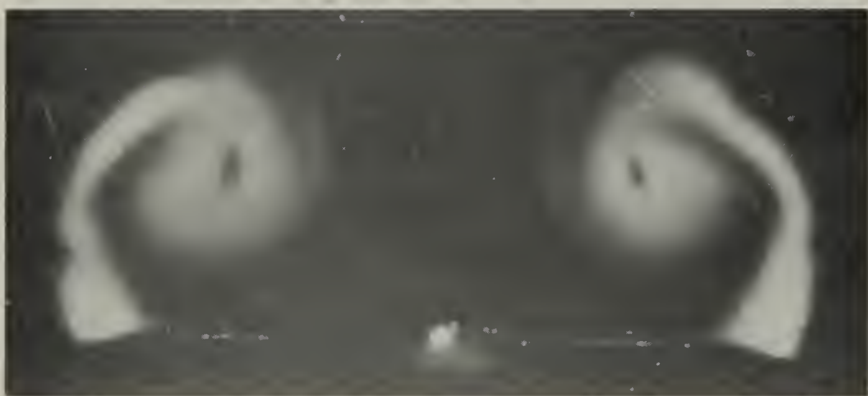

(e).
$\alpha = 30^\circ$

(f).
$\alpha = 35^\circ$

Fig. 13 (Con't.)

(a). $\alpha = 5^\circ$

(b). $\alpha = 10^\circ$

(c). $\alpha = 15^\circ$

Fig. 14 6% Delta : Vortices at 0.25 C_r Downstream of T.E.

(d).
$\alpha = 20°$

(e)
$\alpha = 25°$

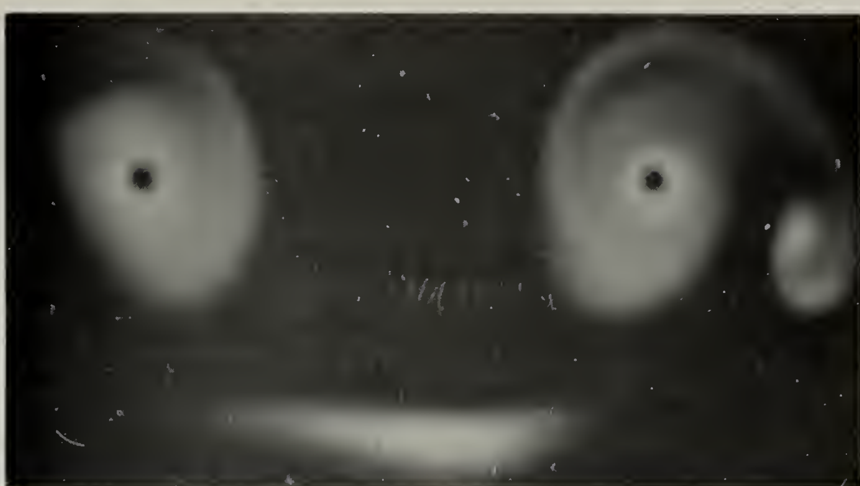

(f)
$\alpha = 30°$

Fig. 14 (Con't.)

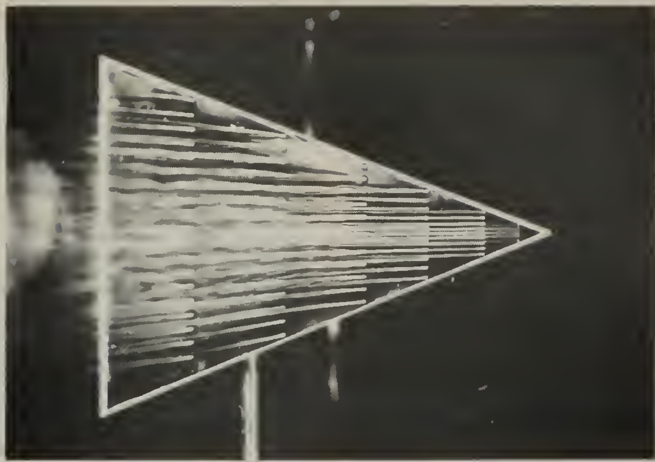

Upper and Lower
Fig. 15, $\alpha = 0°$

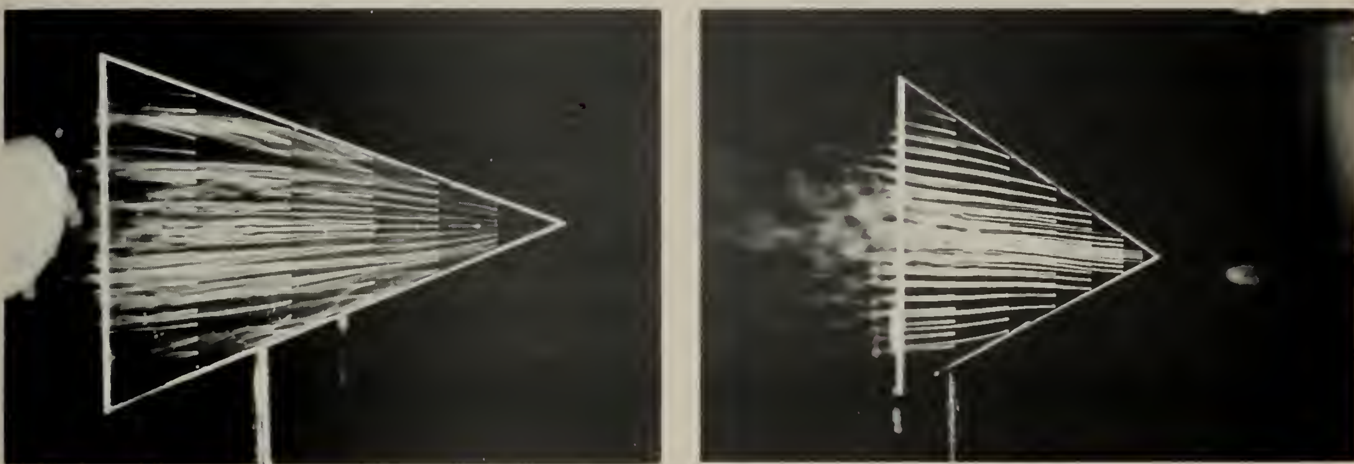

Upper | Lower

Fig. 16, $\alpha = 2°$

Upper | Lower

Fig. 17, $\alpha = 4°$

Flow Over Upper and Lower Surfaces of Flat Plate Delta

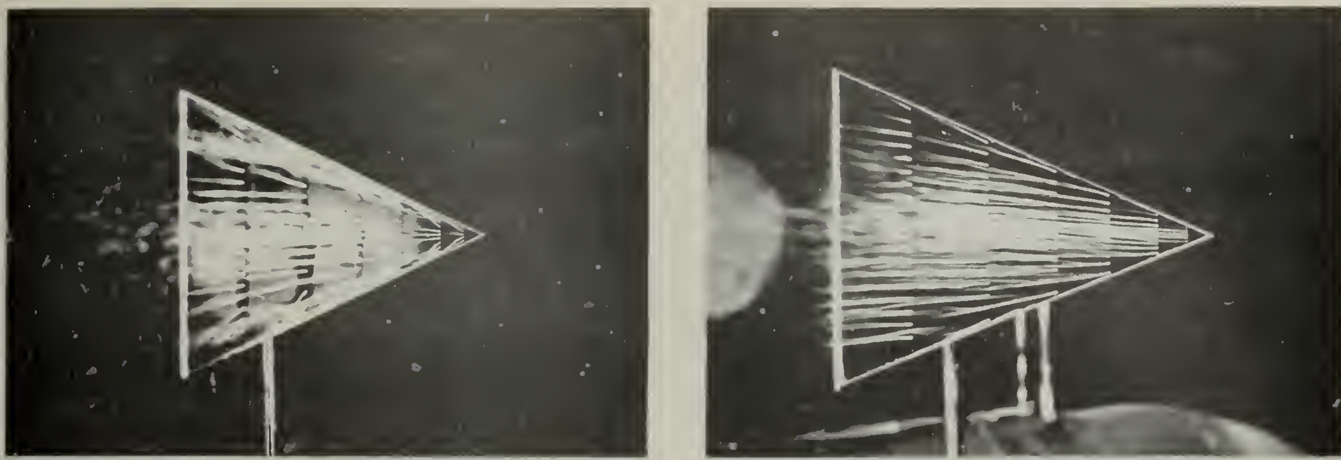

Upper Lower

Fig. 18, $\alpha = 6^\circ$

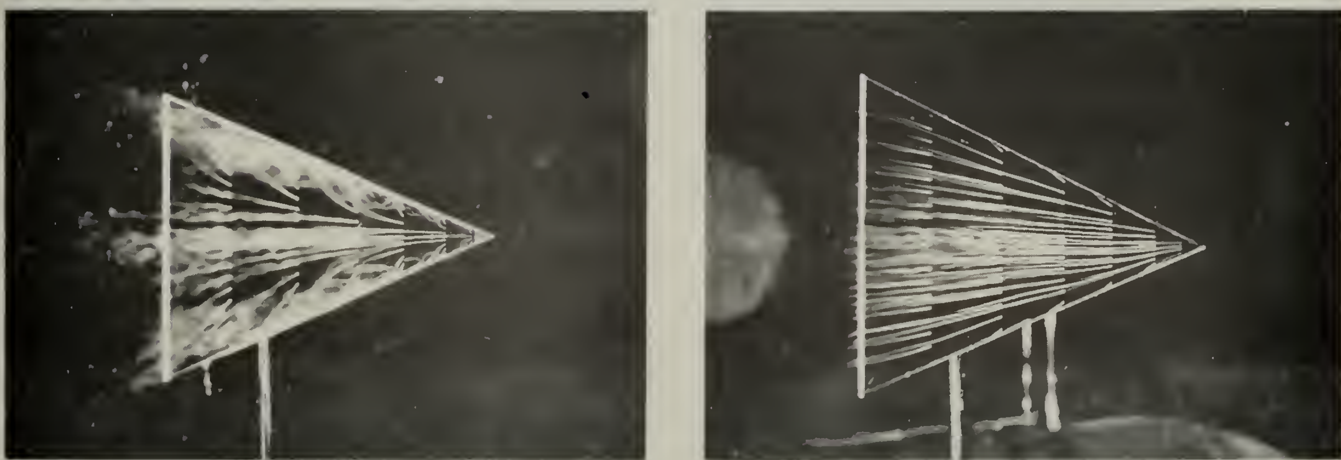

Upper Lower

Fig. 19, $\alpha = 10^\circ$

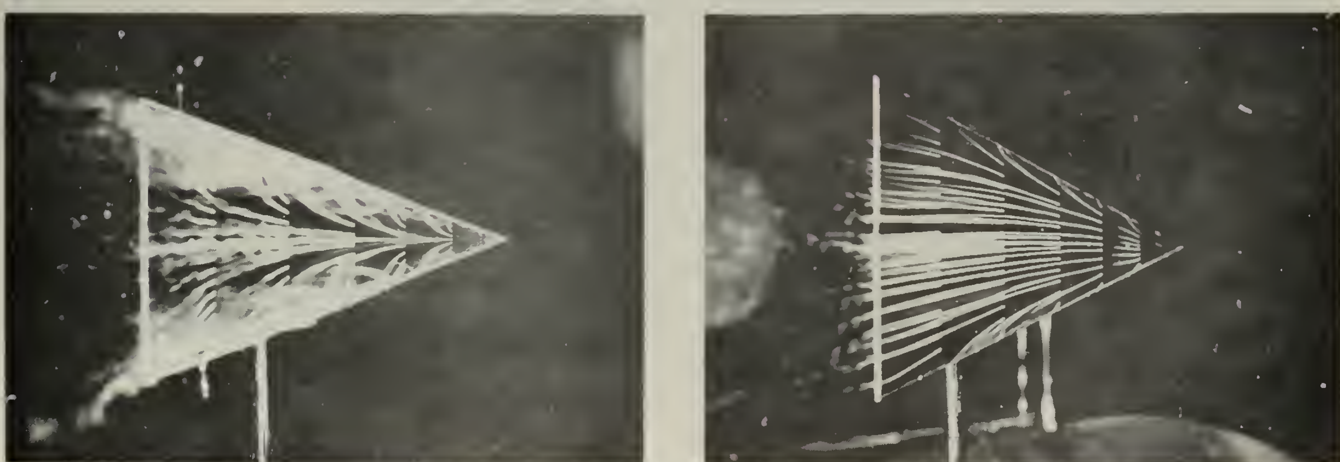

Upper Lower

Fig. 20, $\alpha = 15^\circ$

Flow Over Upper and Lower Surfaces of Flat Plate Delta

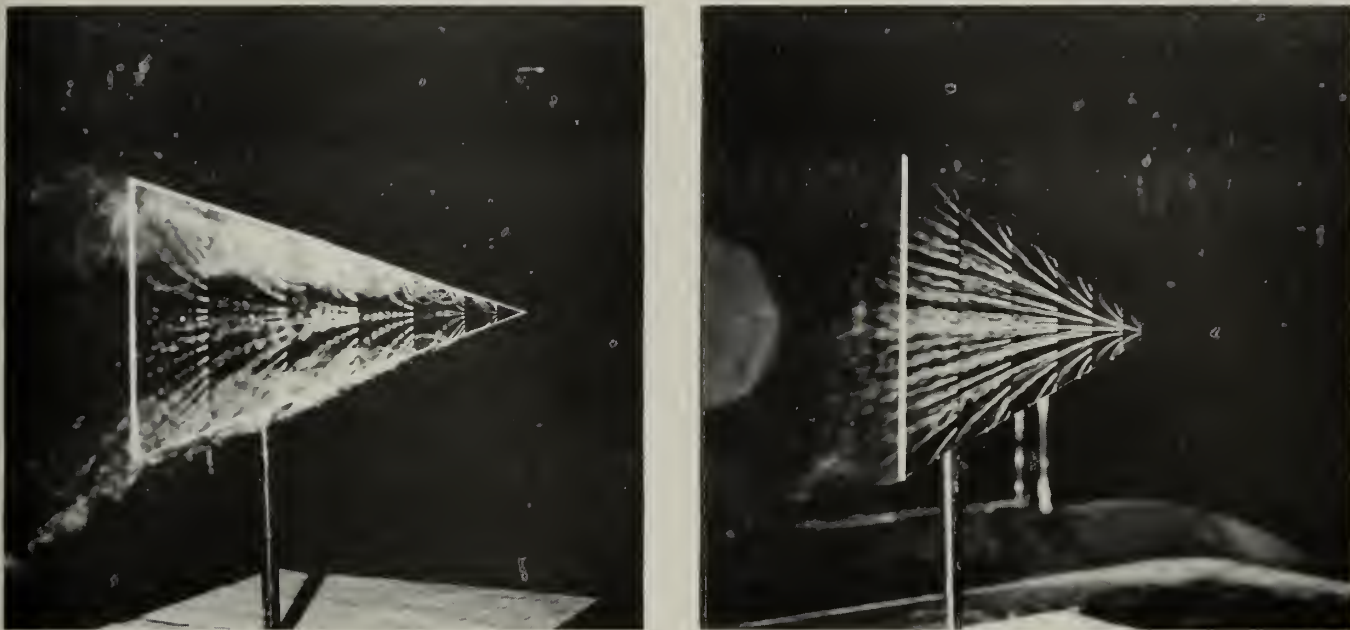

Upper Lower

Fig. 21, $\alpha = 20°$

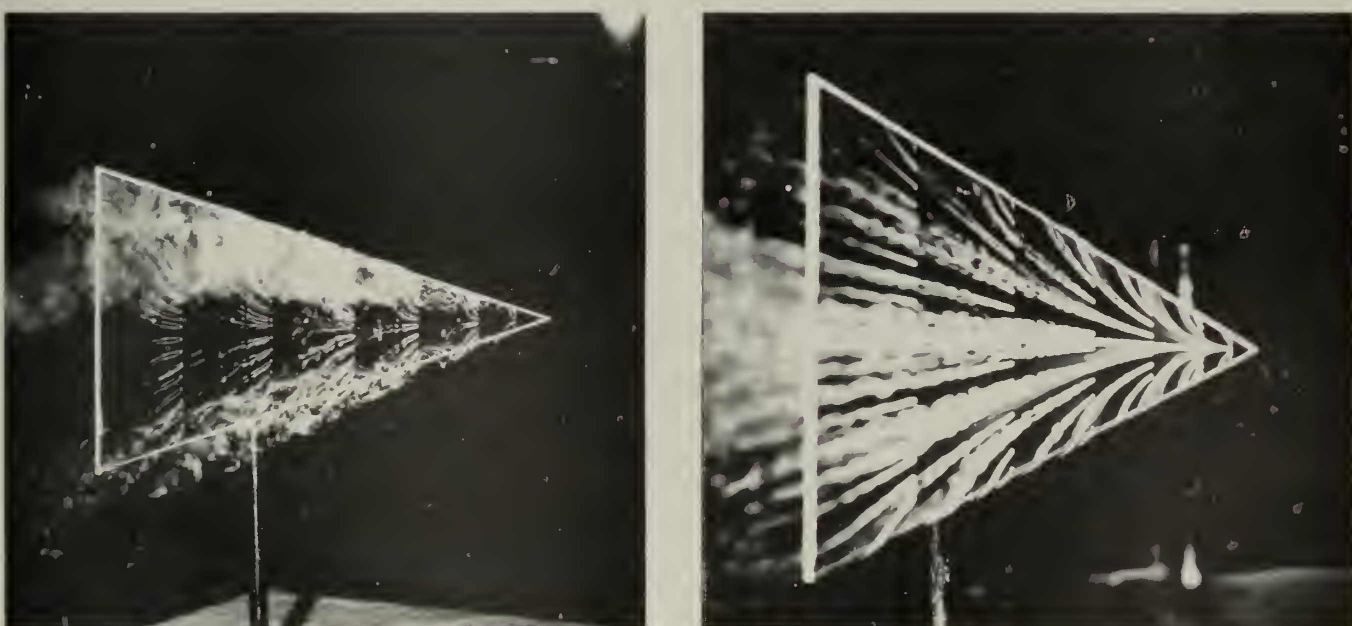

Upper Lower

Fig. 22, $\alpha = 25°$

Flow Over Upper and Lower Surfaces of Flat Plate Delta

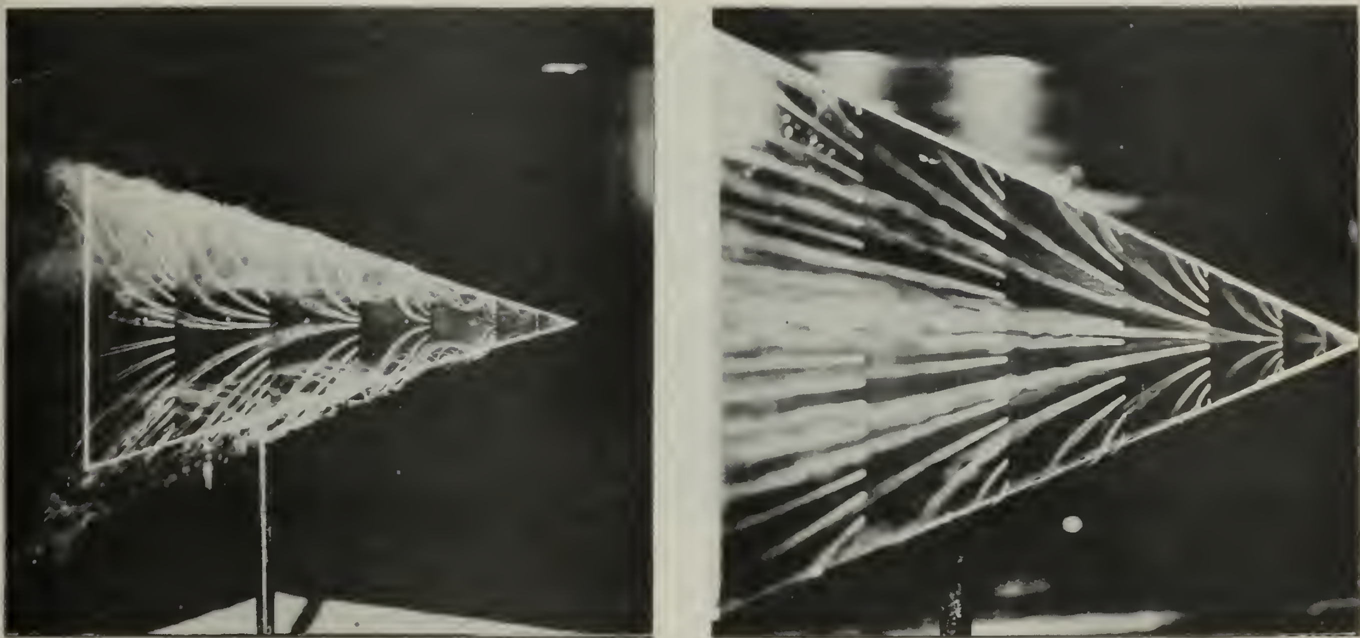

Upper Lower

Fig. 23, $\alpha = 30°$

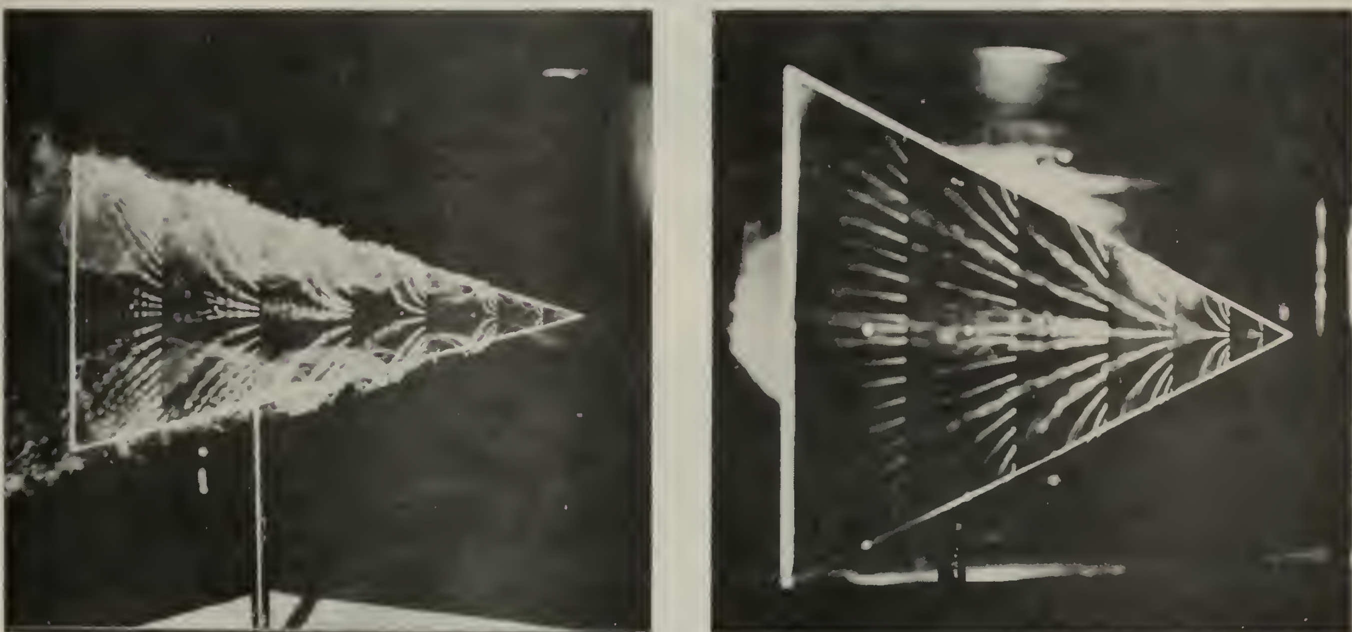

Upper Lower

Fig. 24, $\alpha = 35°$

Flow Over Upper and Lower Surfaces of Flat Plate Delta

Fig. 25 Flat Plate Delta (a) View of Flow Over the Leading Edge

(b) View from the Trailing Edge

Fig. 26 Flat Plate Delta: Vortex Cores Downstream of T.E. Viewed from Above.

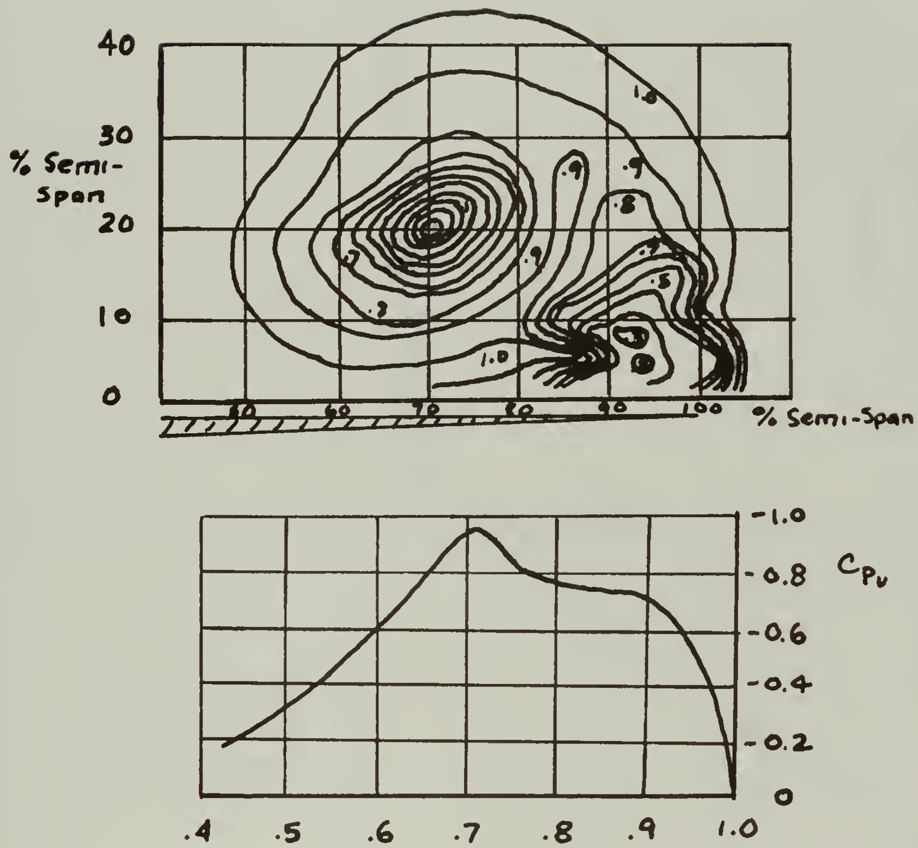

Fig. 27 Total Head Survey at 0.67 Cr on Flat Plate Delta of Æ = 1.46 at α = 14°, and Pressure Distribution (Fig. 23 of Ref. 4)

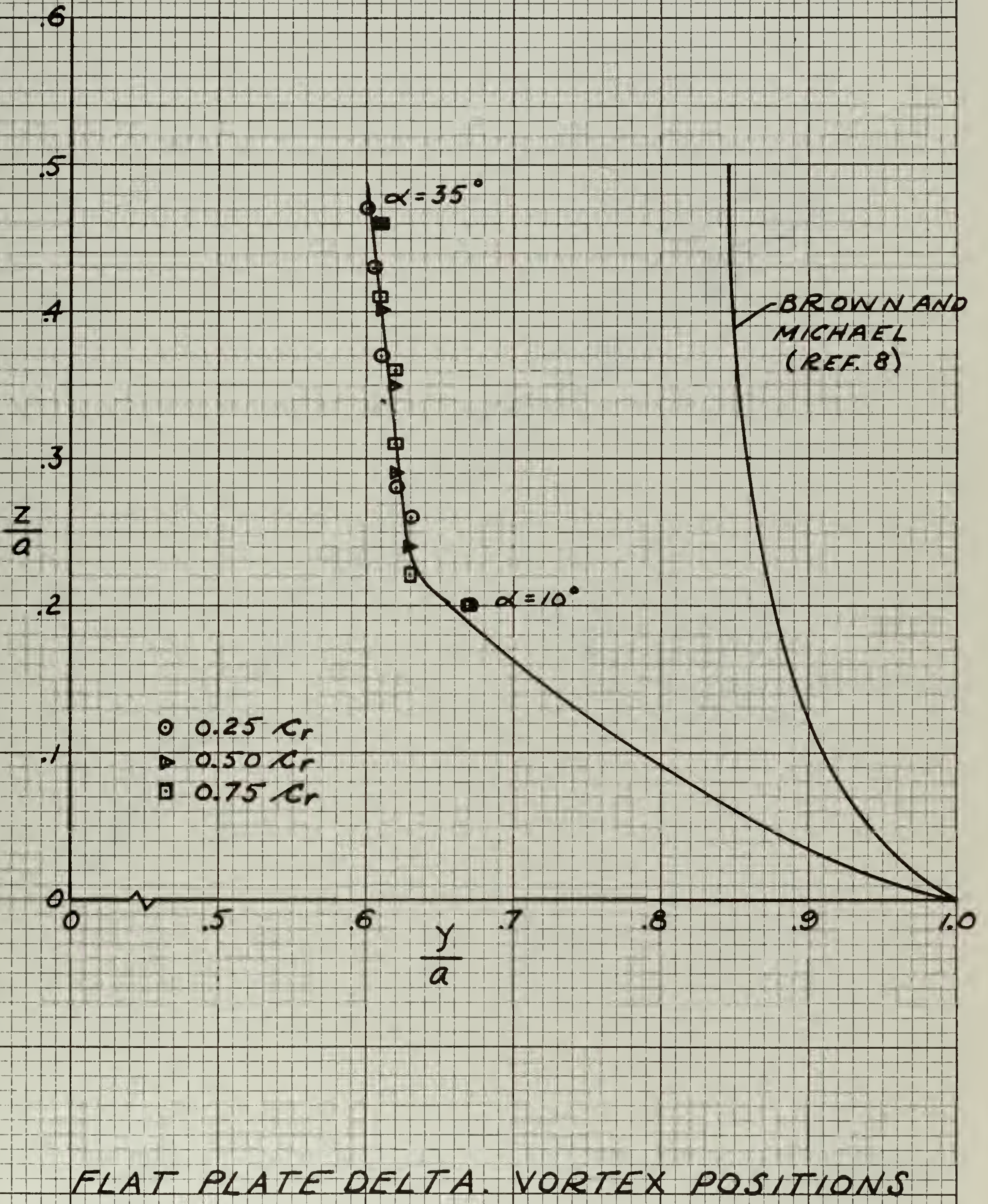

FLAT PLATE DELTA. VORTEX POSITIONS

FIG. 28

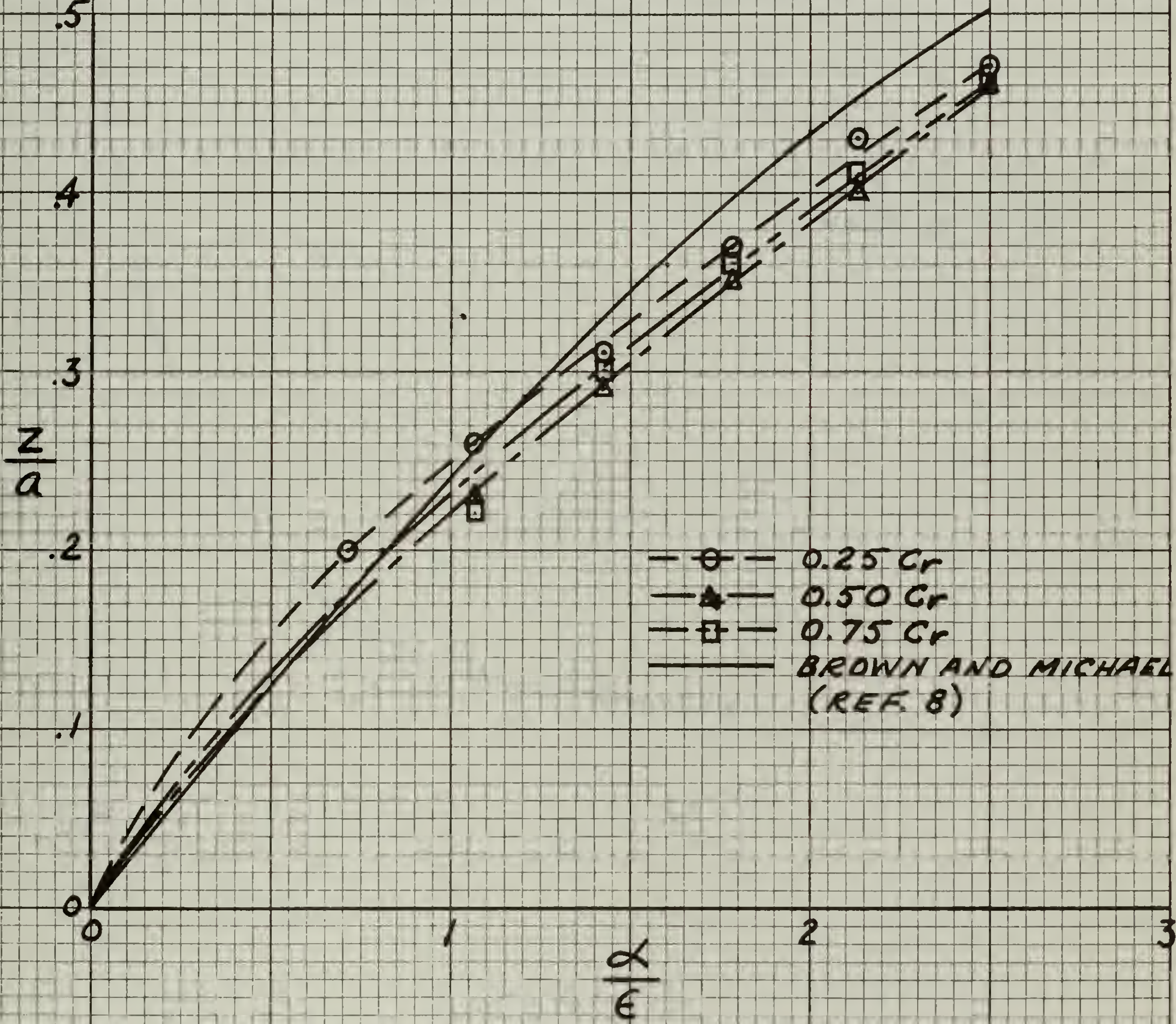

FLAT PLATE DELTA. VORTEX CORE HEIGHT VERSUS α / ϵ

FIG. 29

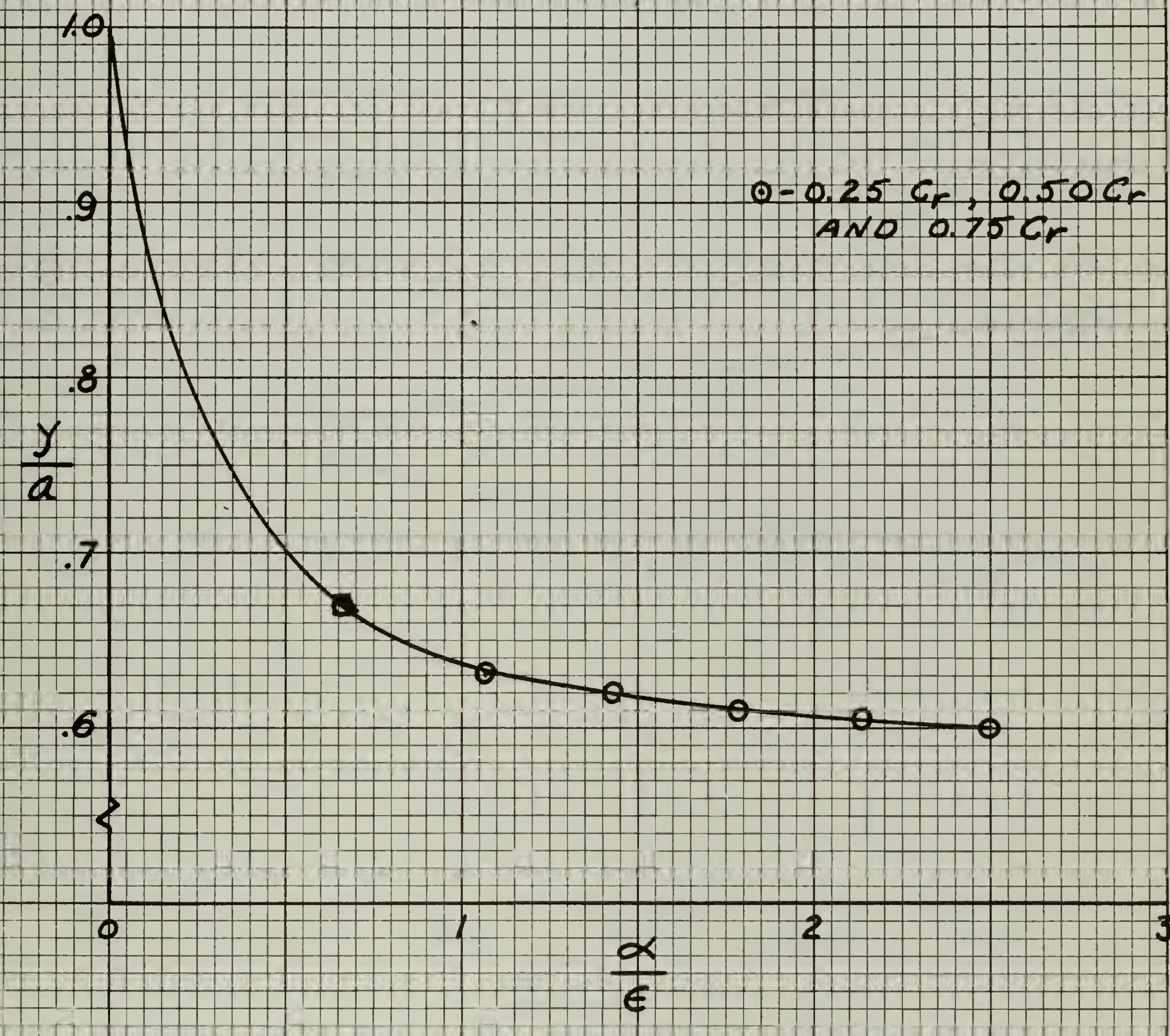

FLAT PLATE DELTA. SPANWISE POSITION OF VORTEX CORE VERSUS α/ϵ

FIG. 30

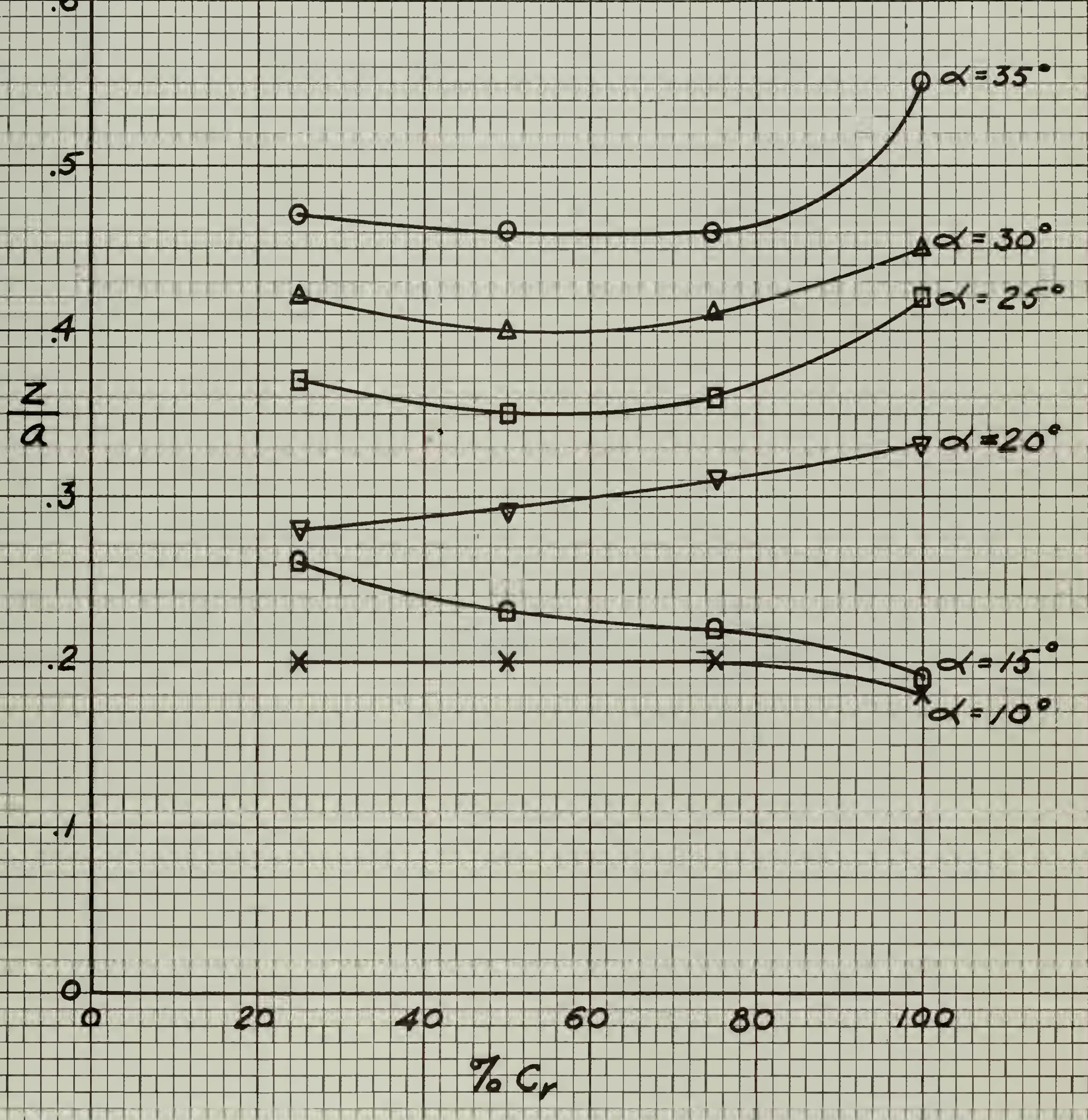

FLAT PLATE DELTA. VORTEX CORE HEIGHT VERSUS % C_r

FIG. 31

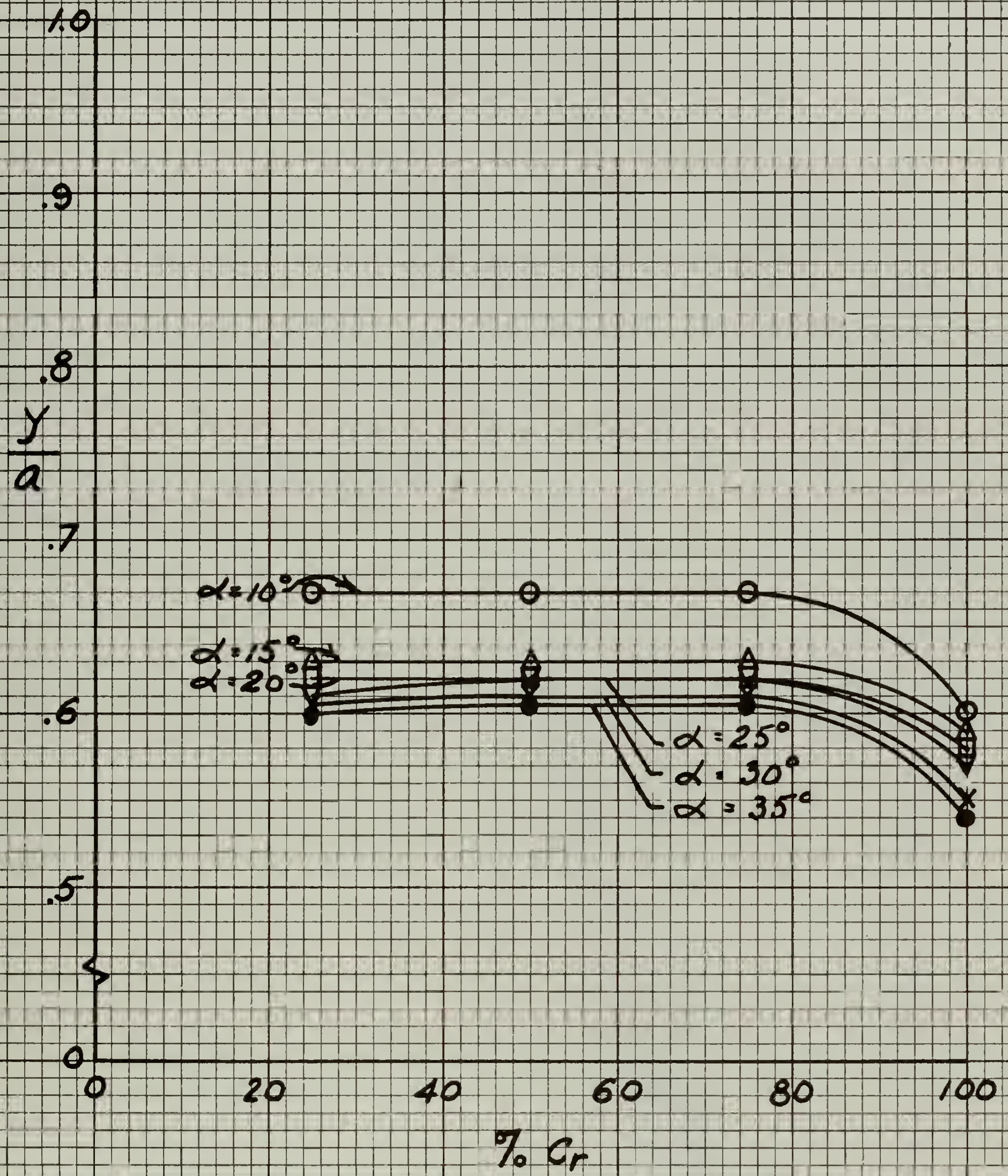

FLAT PLATE DELTA. SPANWISE POSITION OF VORTEX CORE VERSUS % C_r

FIG. 32

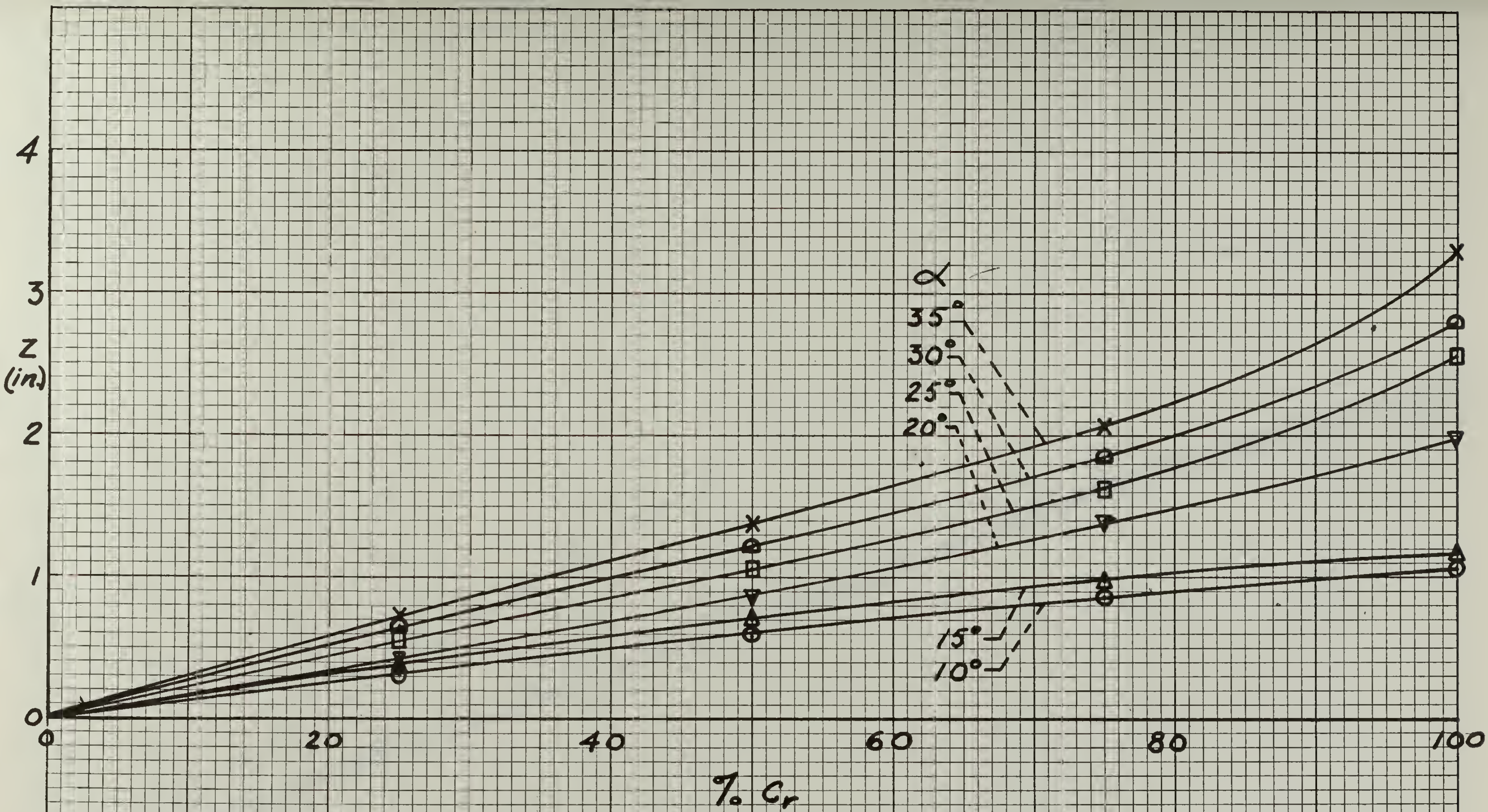

FLAT PLATE DELTA. VORTEX CORE HEIGHT
VERSUS % C_r

FIG. 33

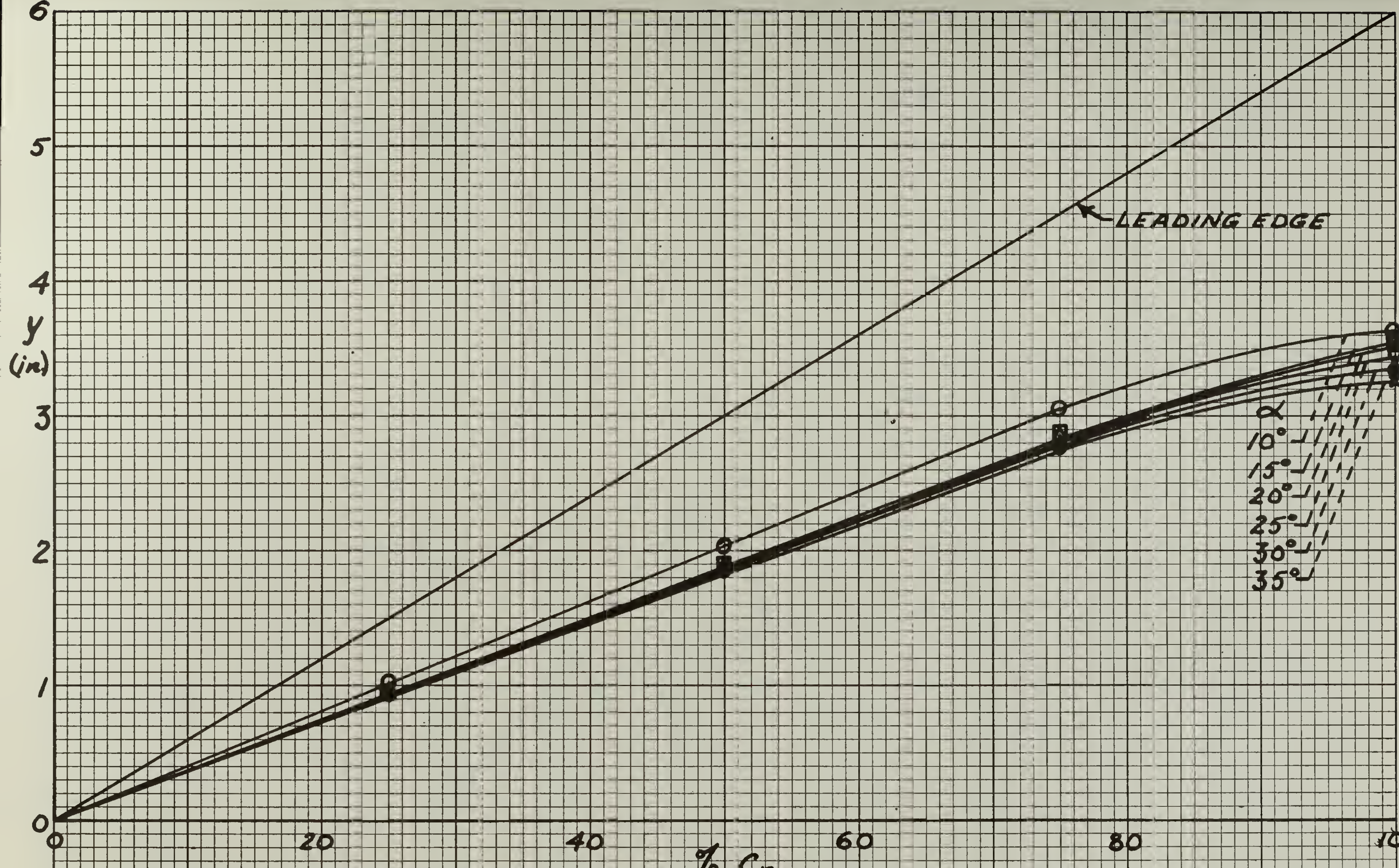

FLAT PLATE DELTA. SPANWISE POSITION OF VORTEX CORE VS % C_r

FIG. 34

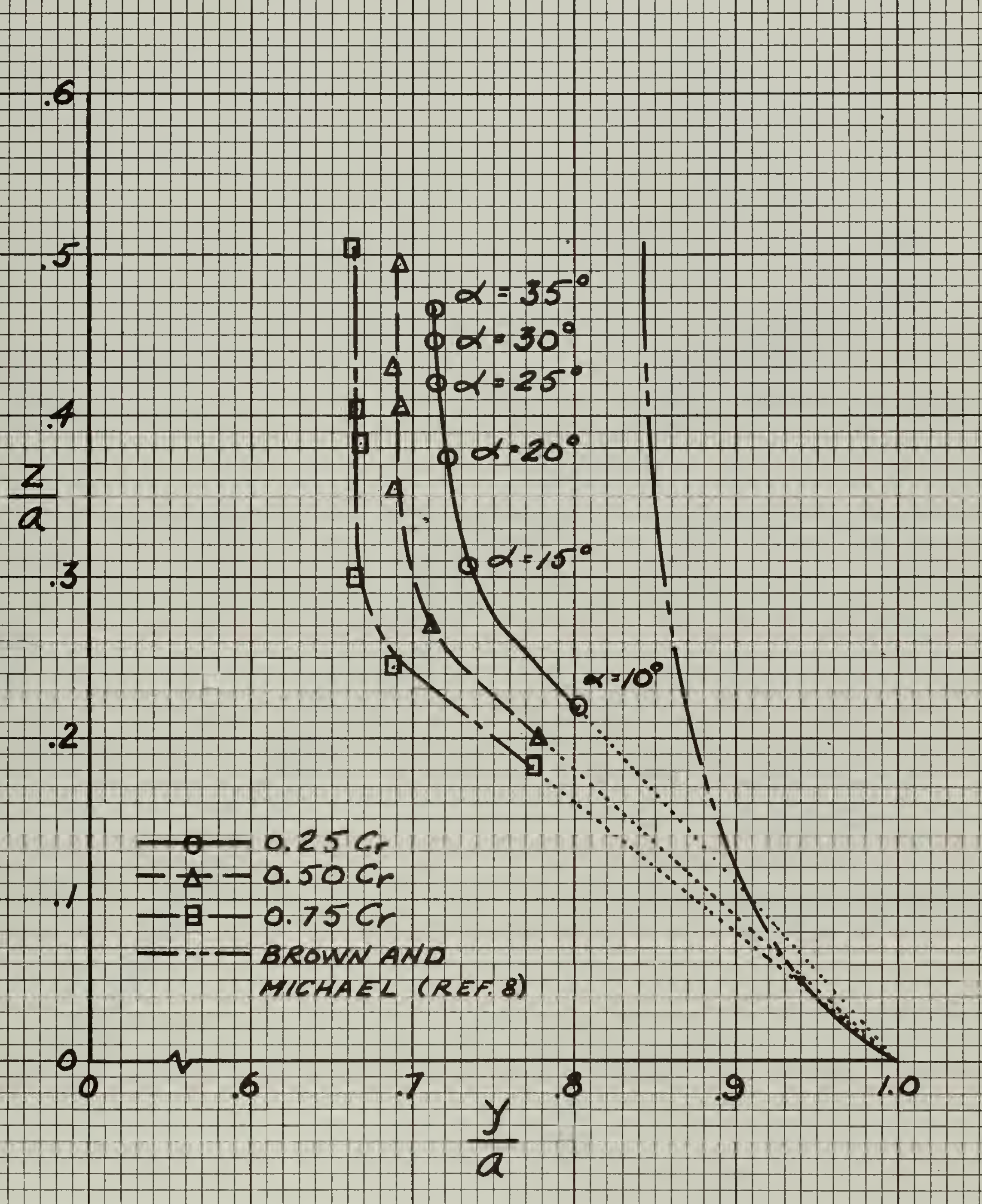

6 % DELTA. VORTEX POSITIONS

FIG. 35

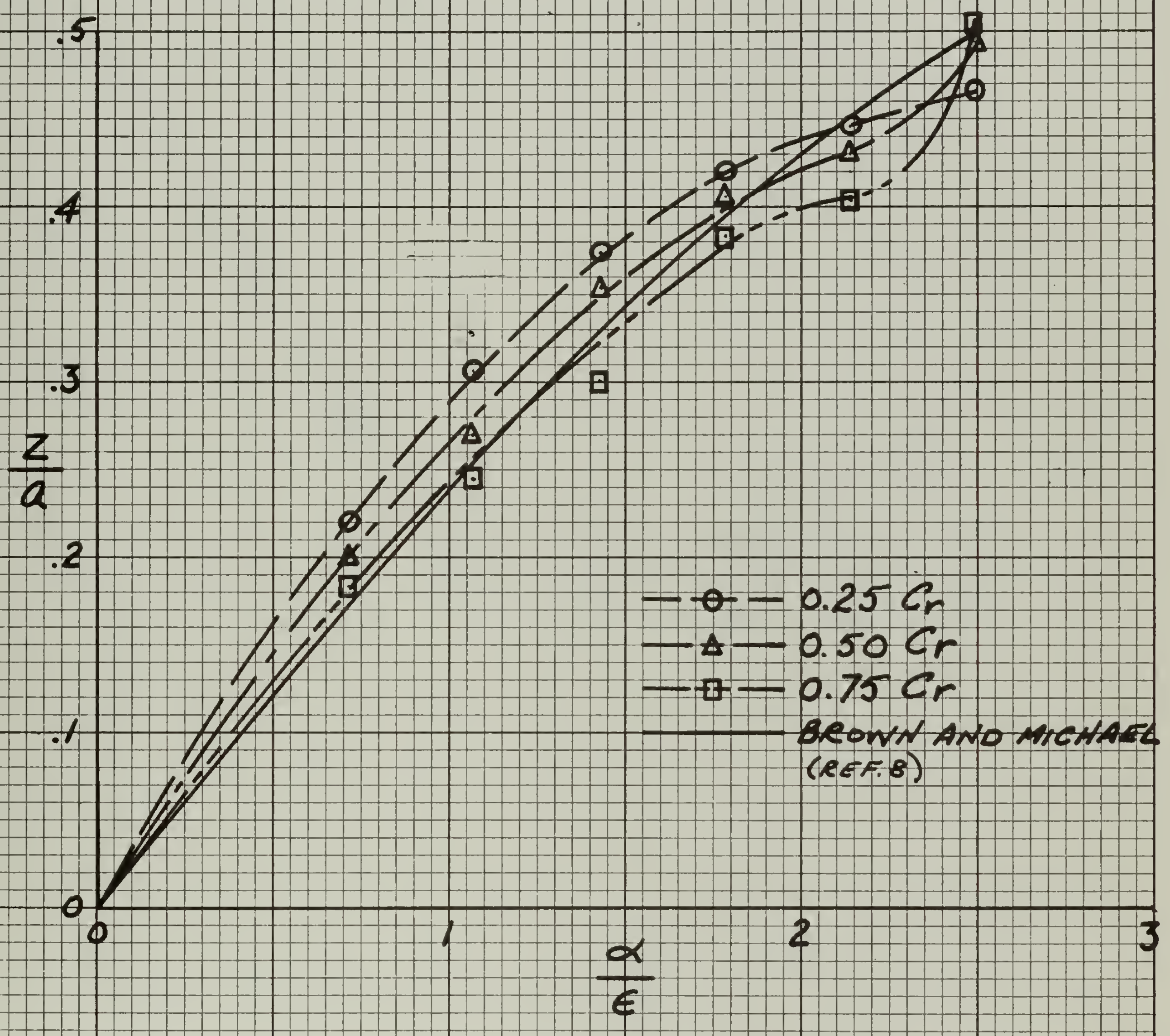

6% DELTA. VORTEX CORE HEIGHT
VERSUS α/ε

FIG. 36

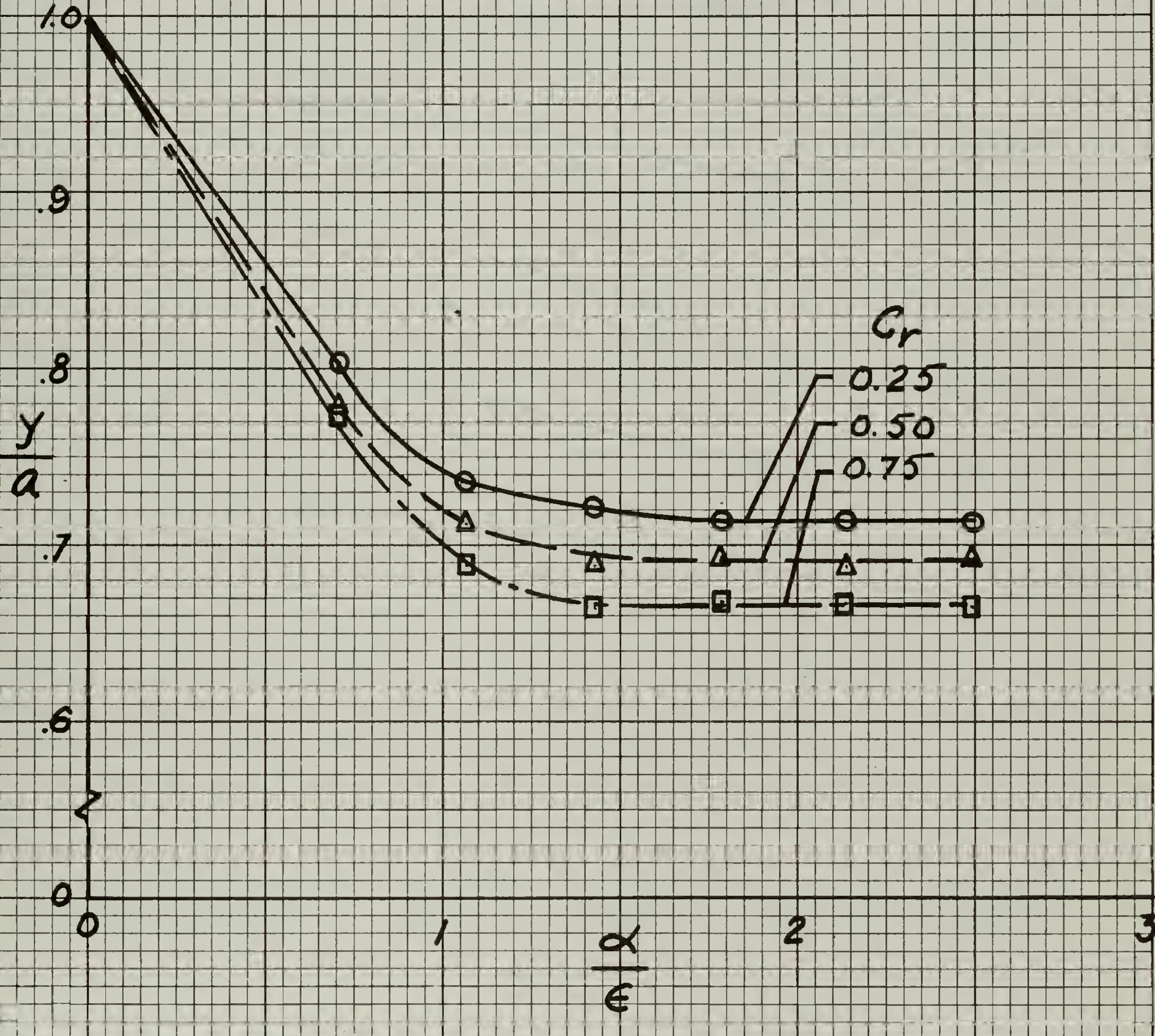

6% DELTA. SPANWISE POSITION OF VORTEX CORE VERSUS α/ε

FIG. 37

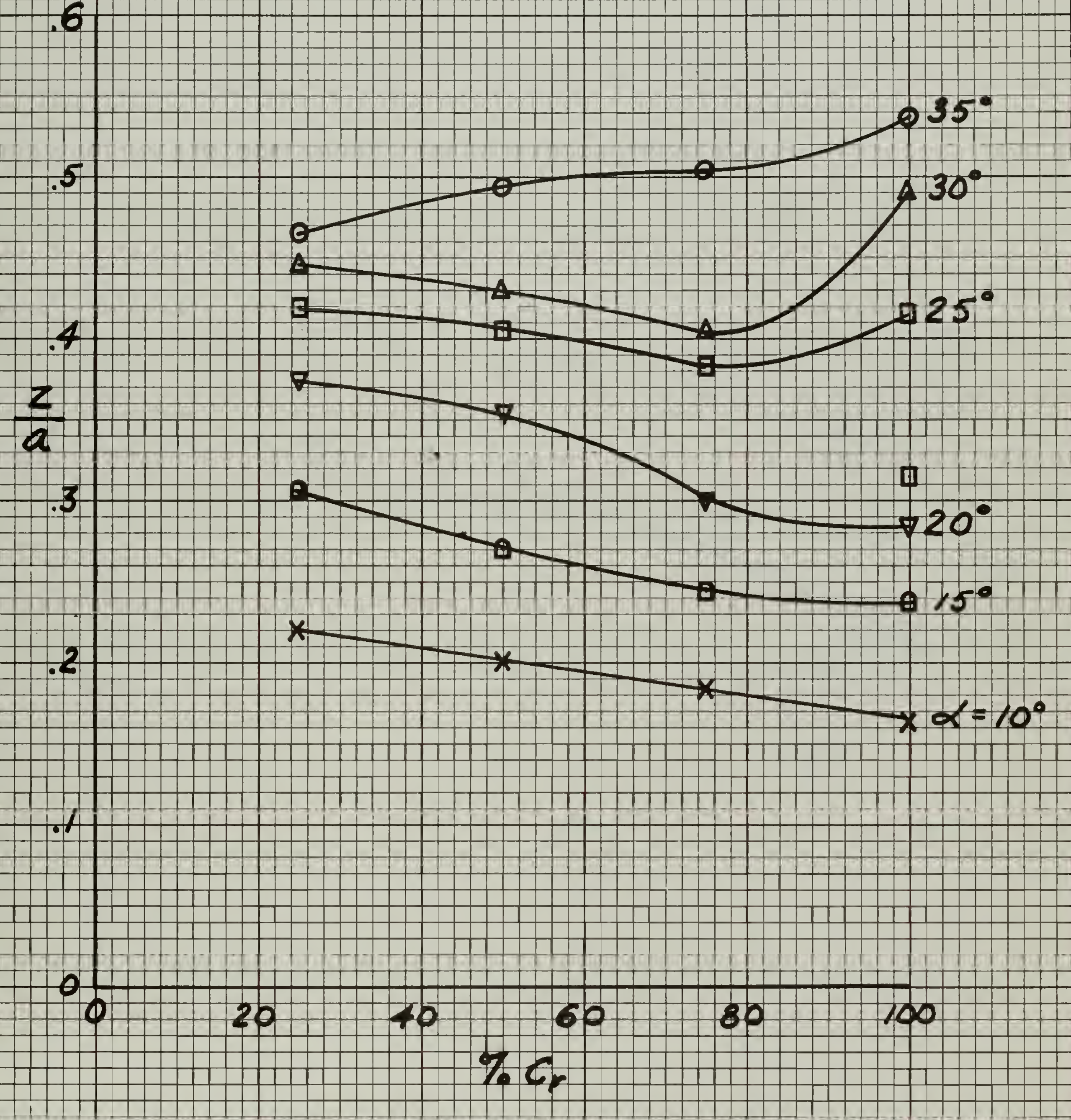

6% DELTA. VORTEX CORE HEIGHT VERSUS % C_r

FIG. 38

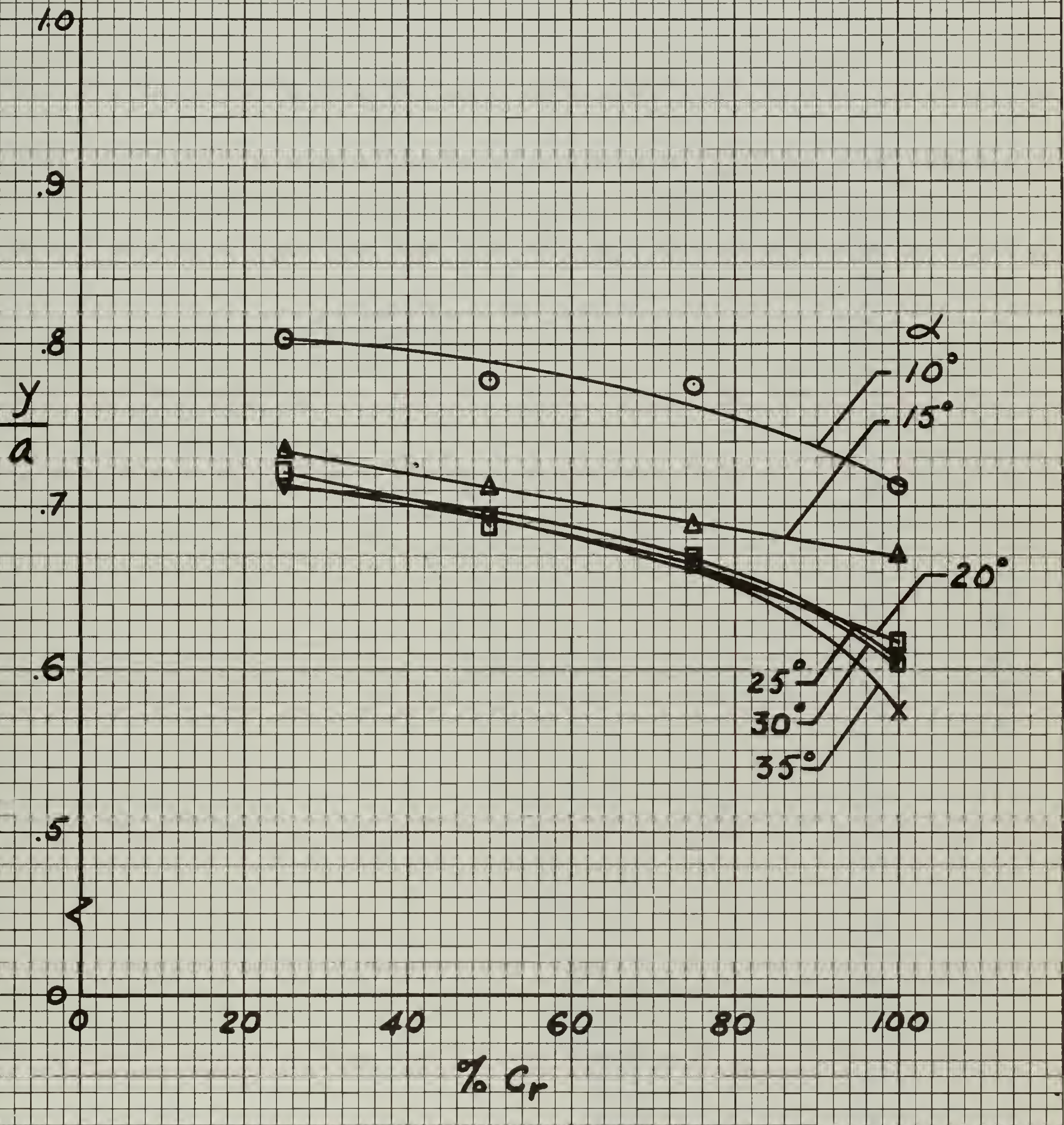

6% DELTA. SPANWISE POSITION OF VORTEX CORE VERSUS % C_r

FIG. 39

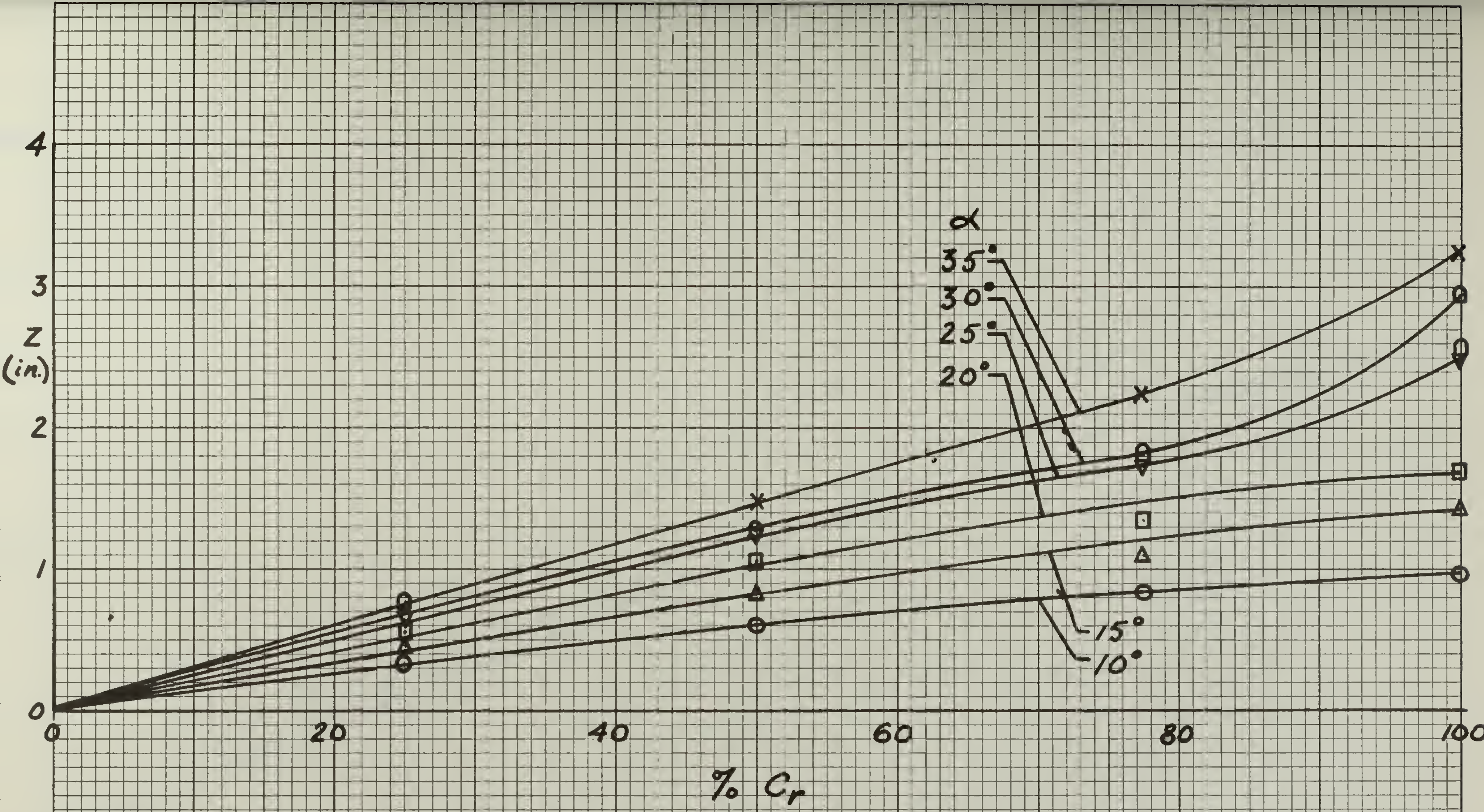

6% DELTA. VORTEX CORE HEIGHT VERSUS % C_r

FIG. 40

6% DELTA. SPANWISE POSITION OF VORTEX CORE VERSUS % C_r

FIG. 41

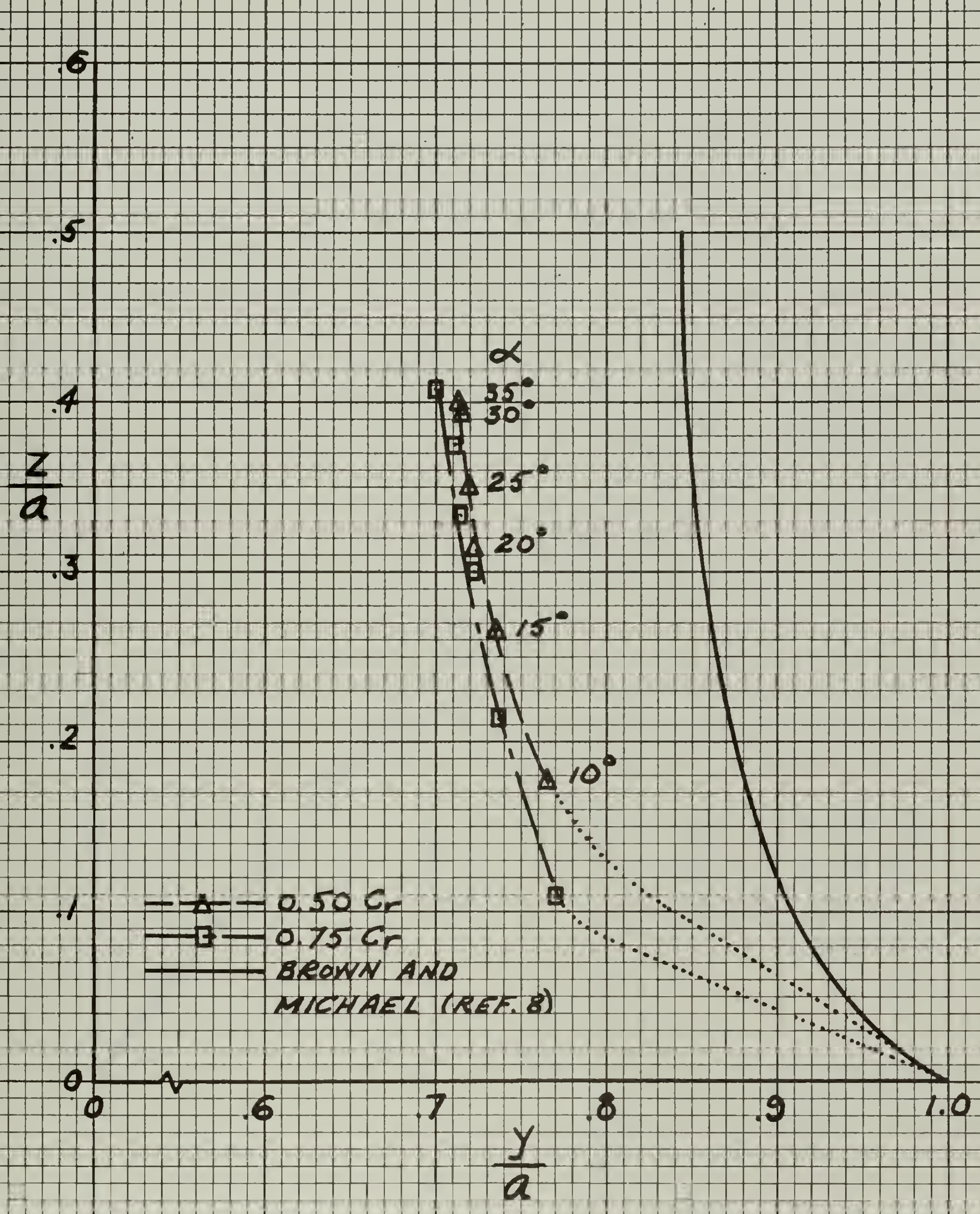

12 % DELTA. VORTEX POSITIONS

FIG. 42

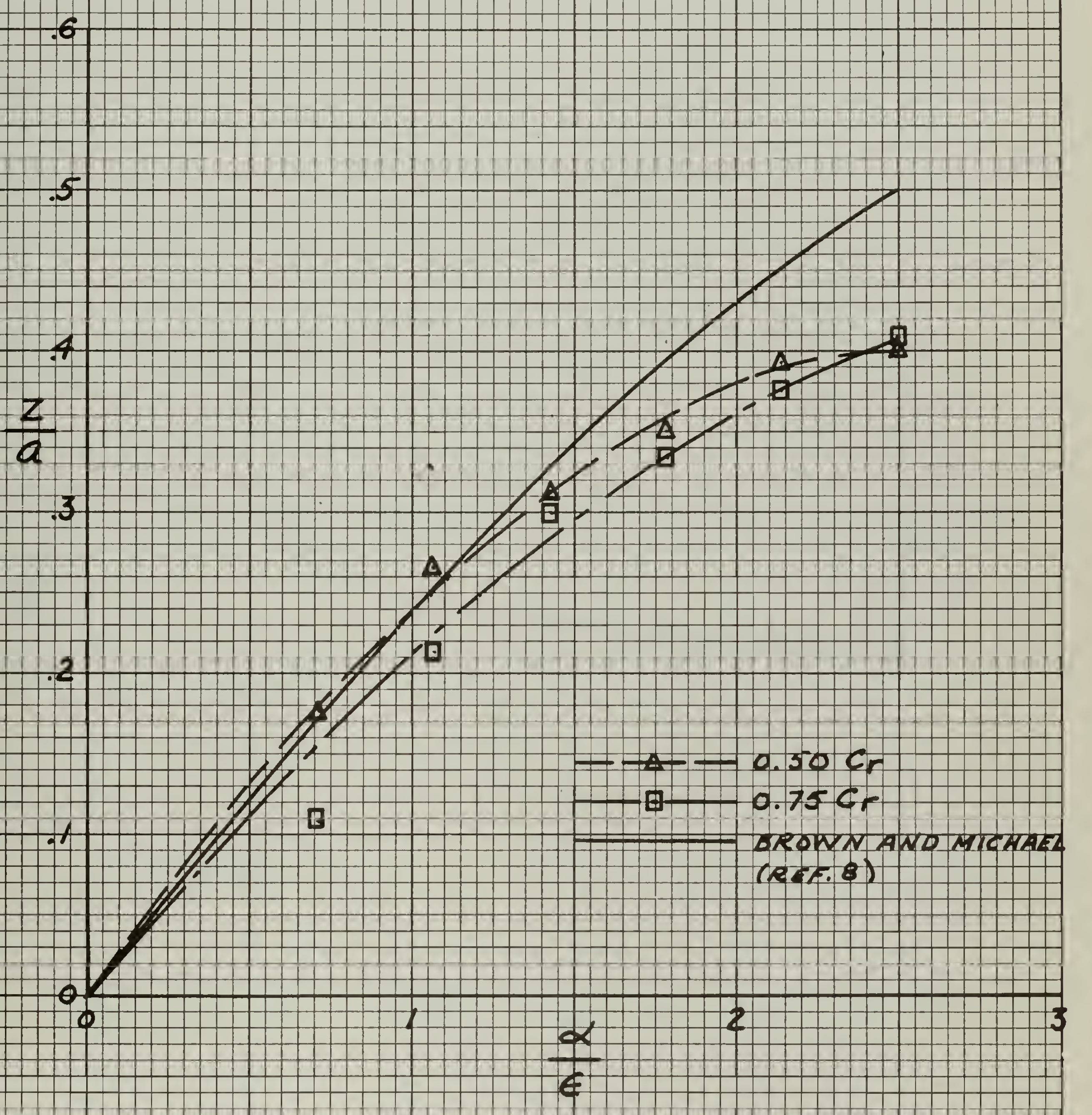

12% DELTA. VORTEX CORE HEIGHT VERSUS α/ε

FIG. 43

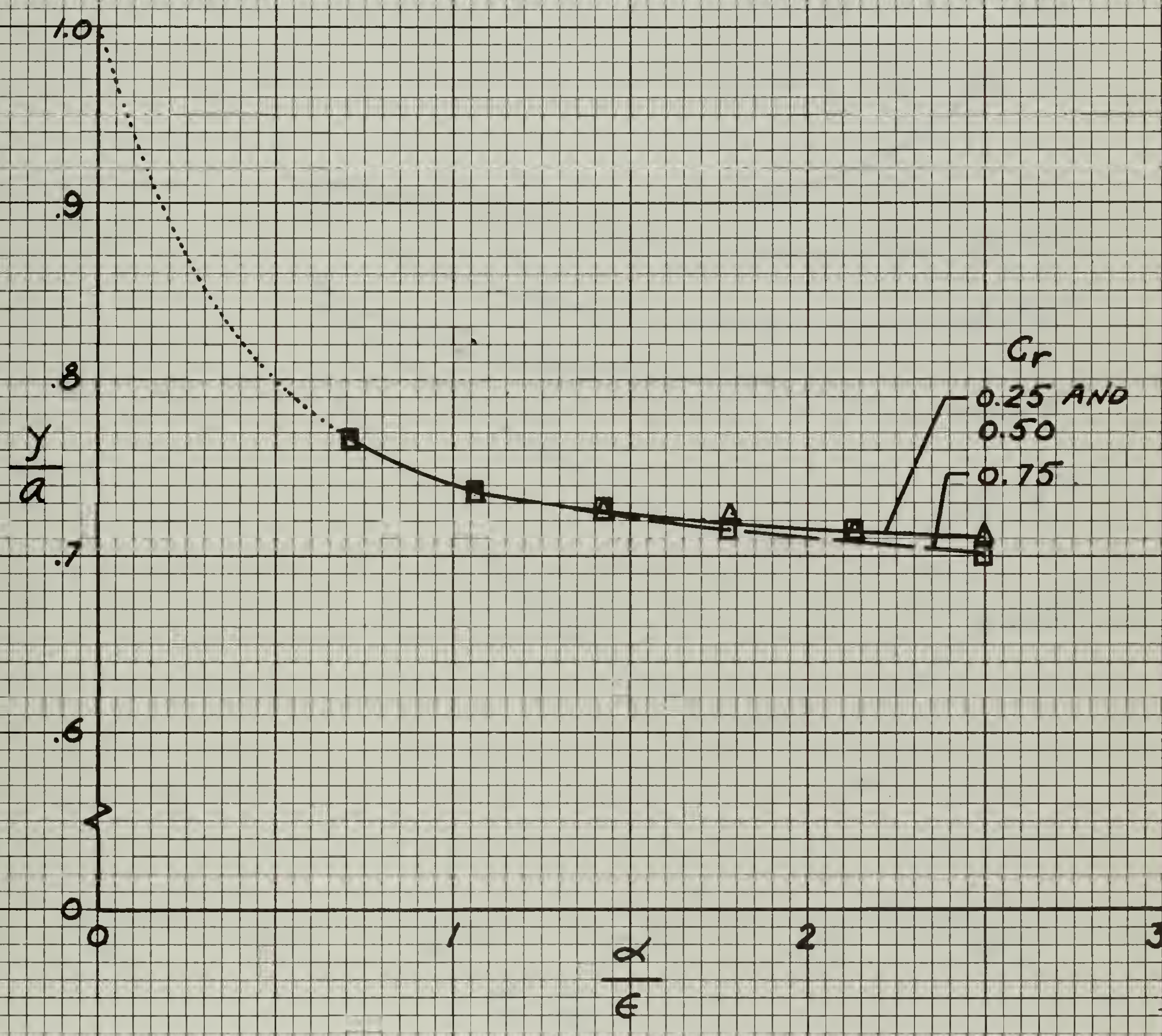

12% DELTA. SPANWISE POSITION OF VORTEX CORE VERSUS α/ϵ

FIG. 44

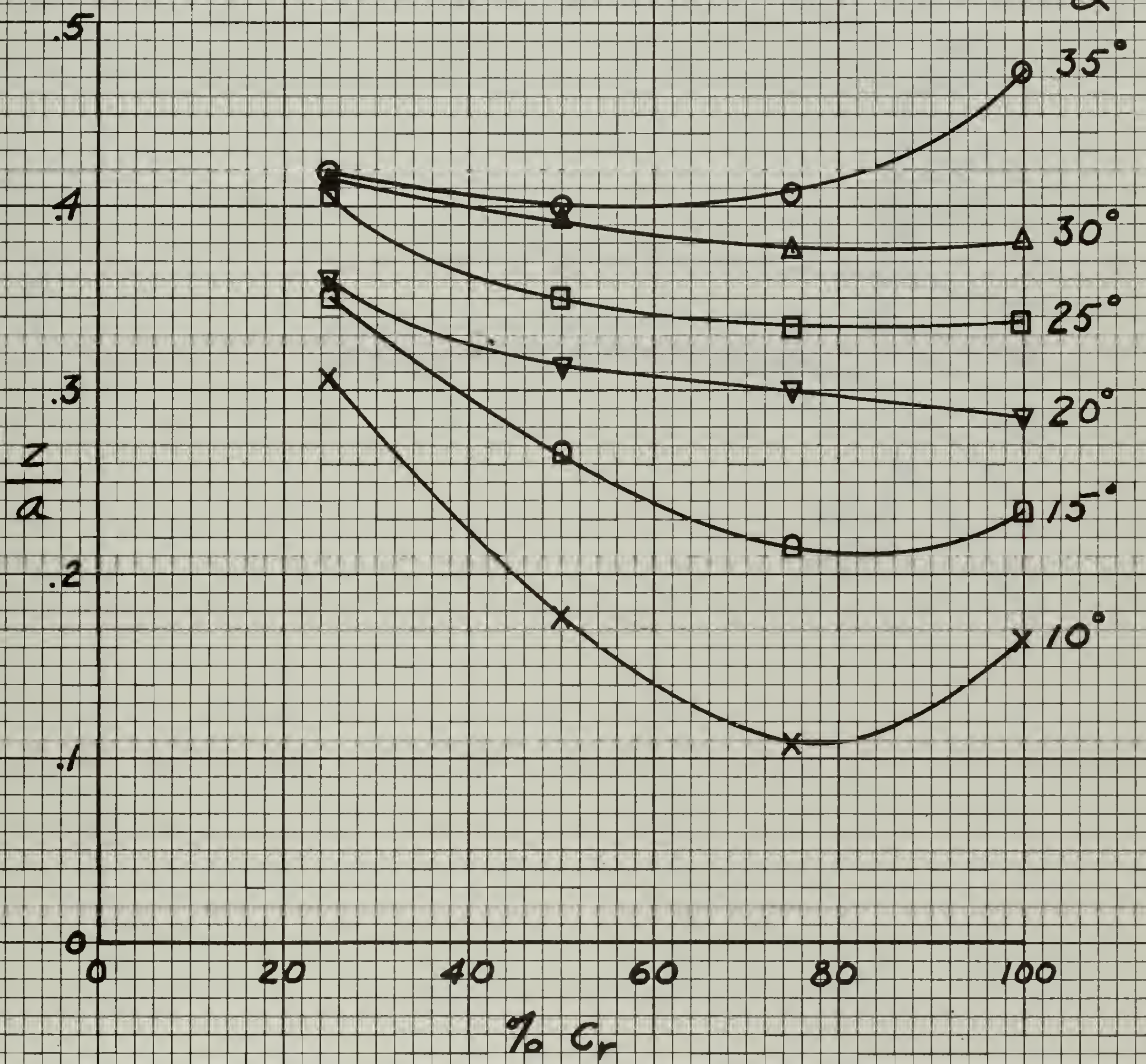

12% DELTA. VORTEX CORE HEIGHT VERSUS % C_r

FIG. 45

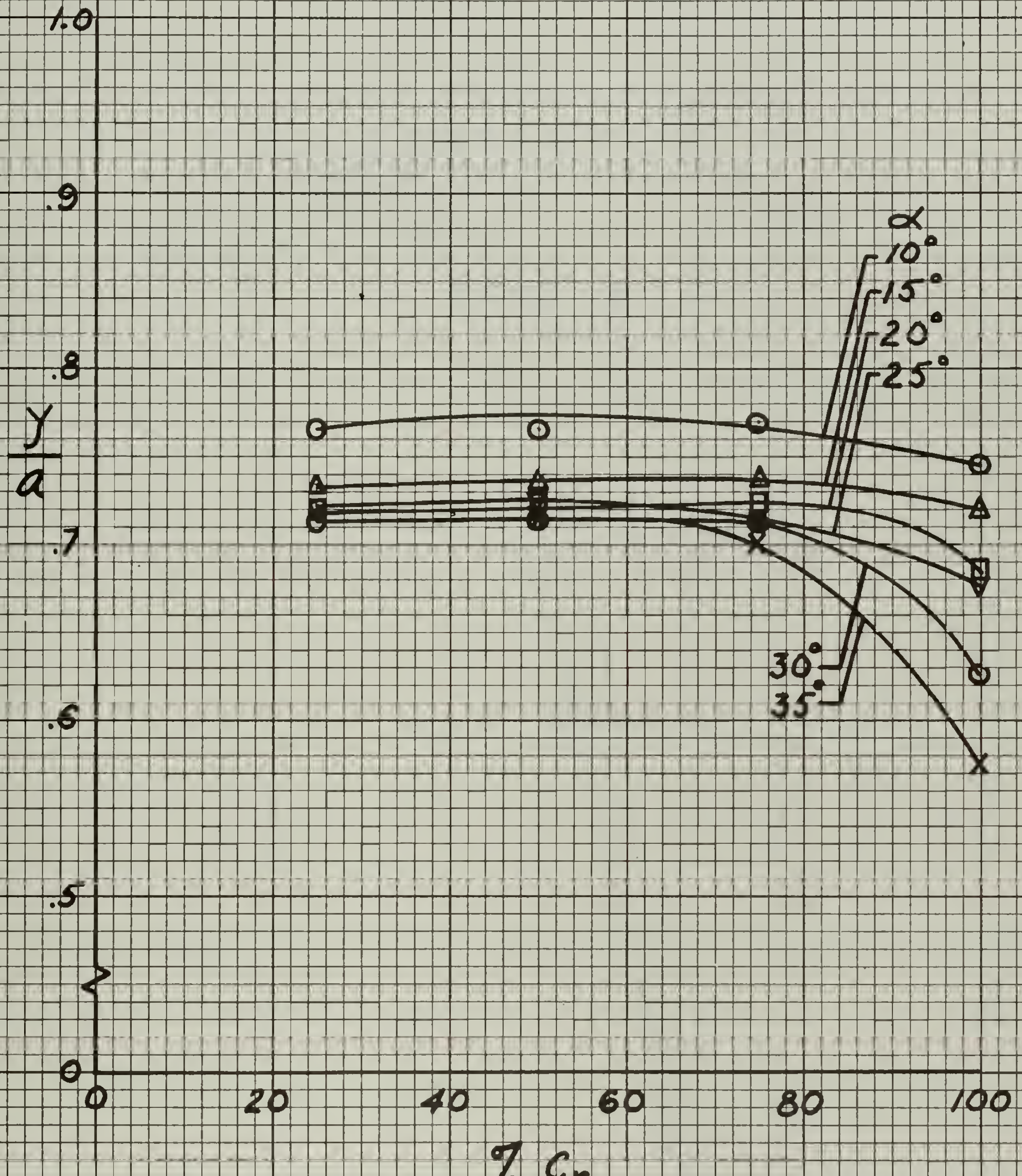

12% DELTA. SPANWISE POSITION OF VORTEX CORE VERSUS % C_r

FIG. 46

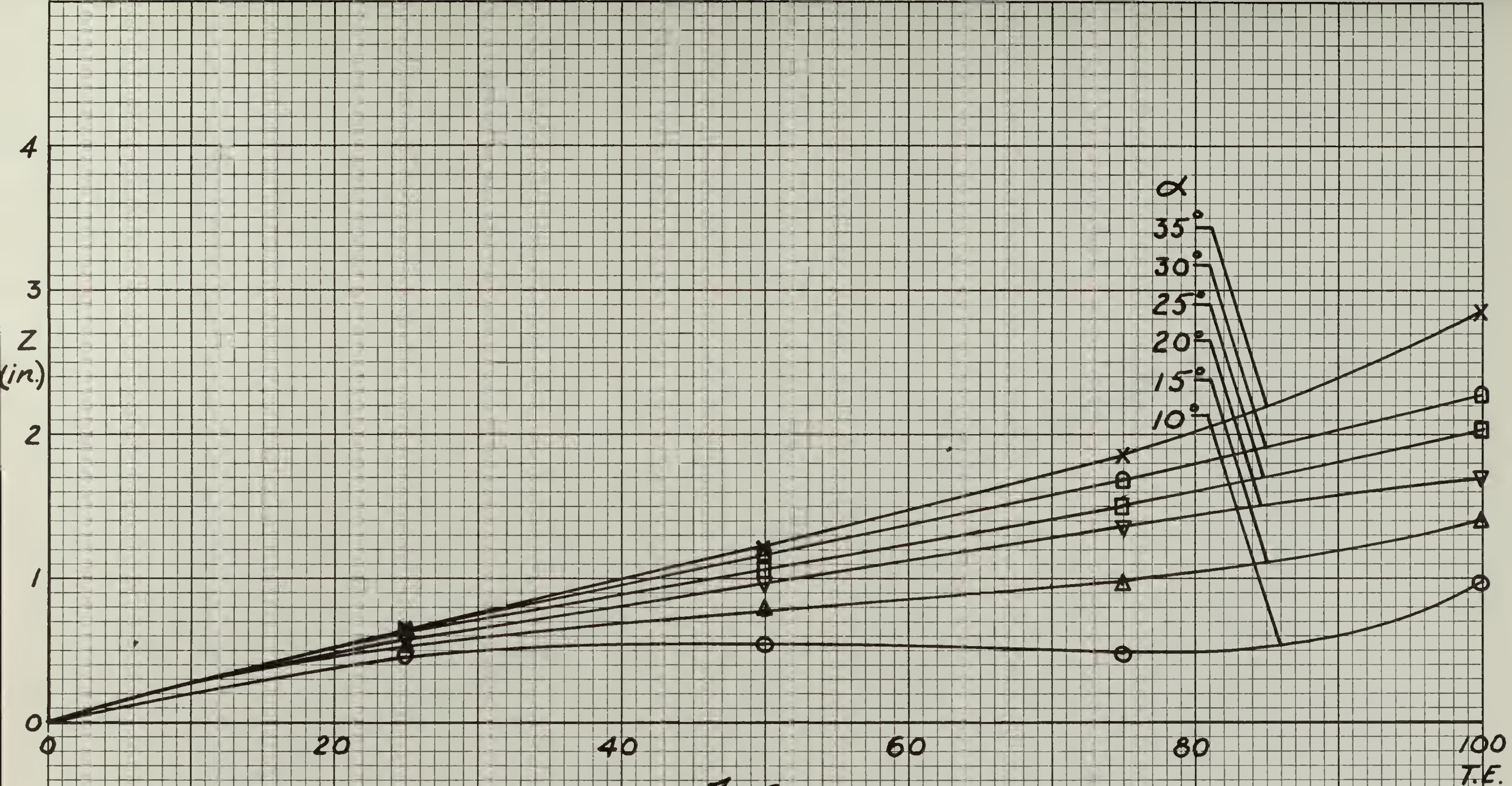

12% DELTA. VORTEX CORE HEIGHT VERSUS % C_r

FIG. 47

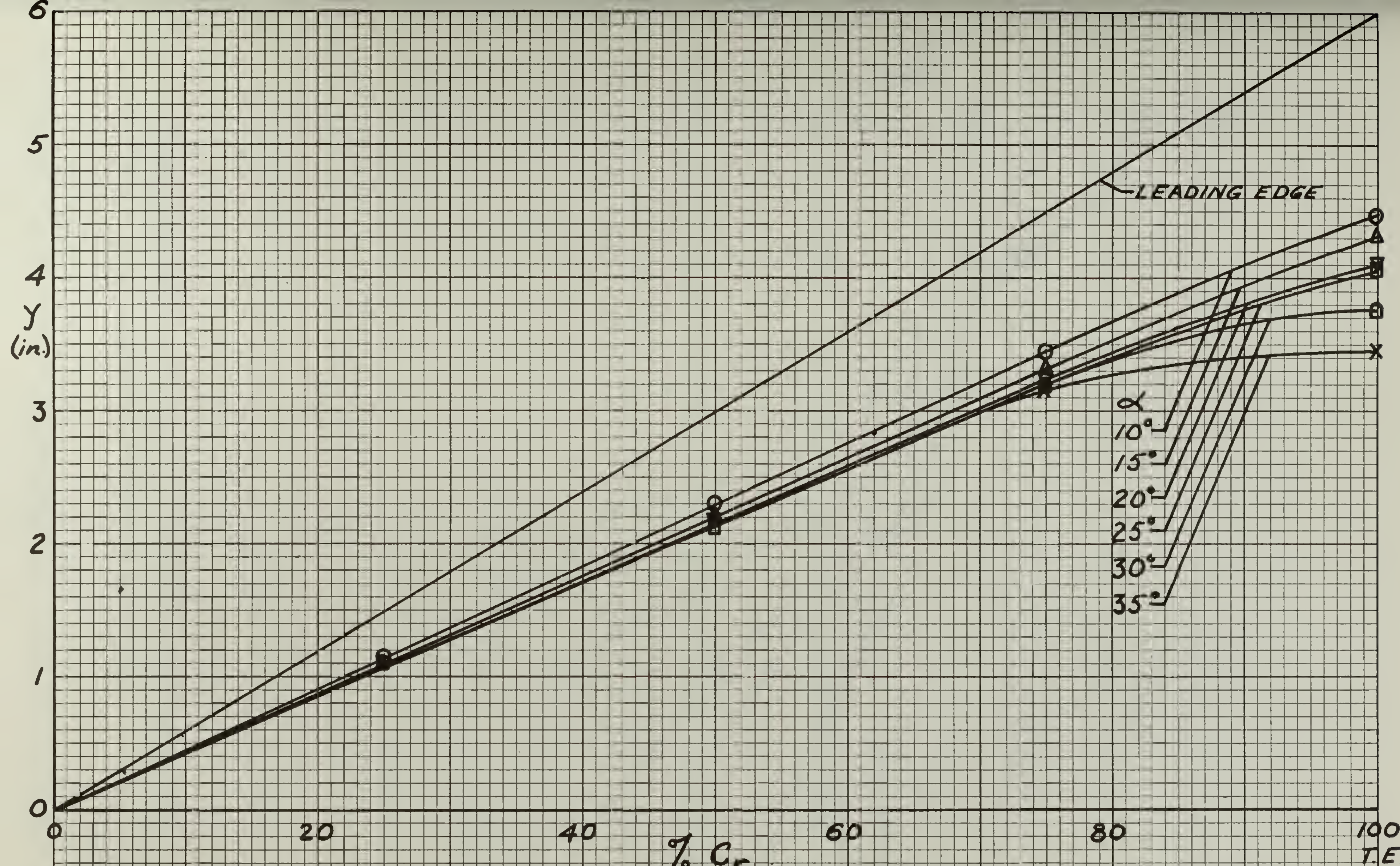

12% DELTA. SPANWISE POSITION OF VORTEX CORE VERSUS % C_r

FIG. 48

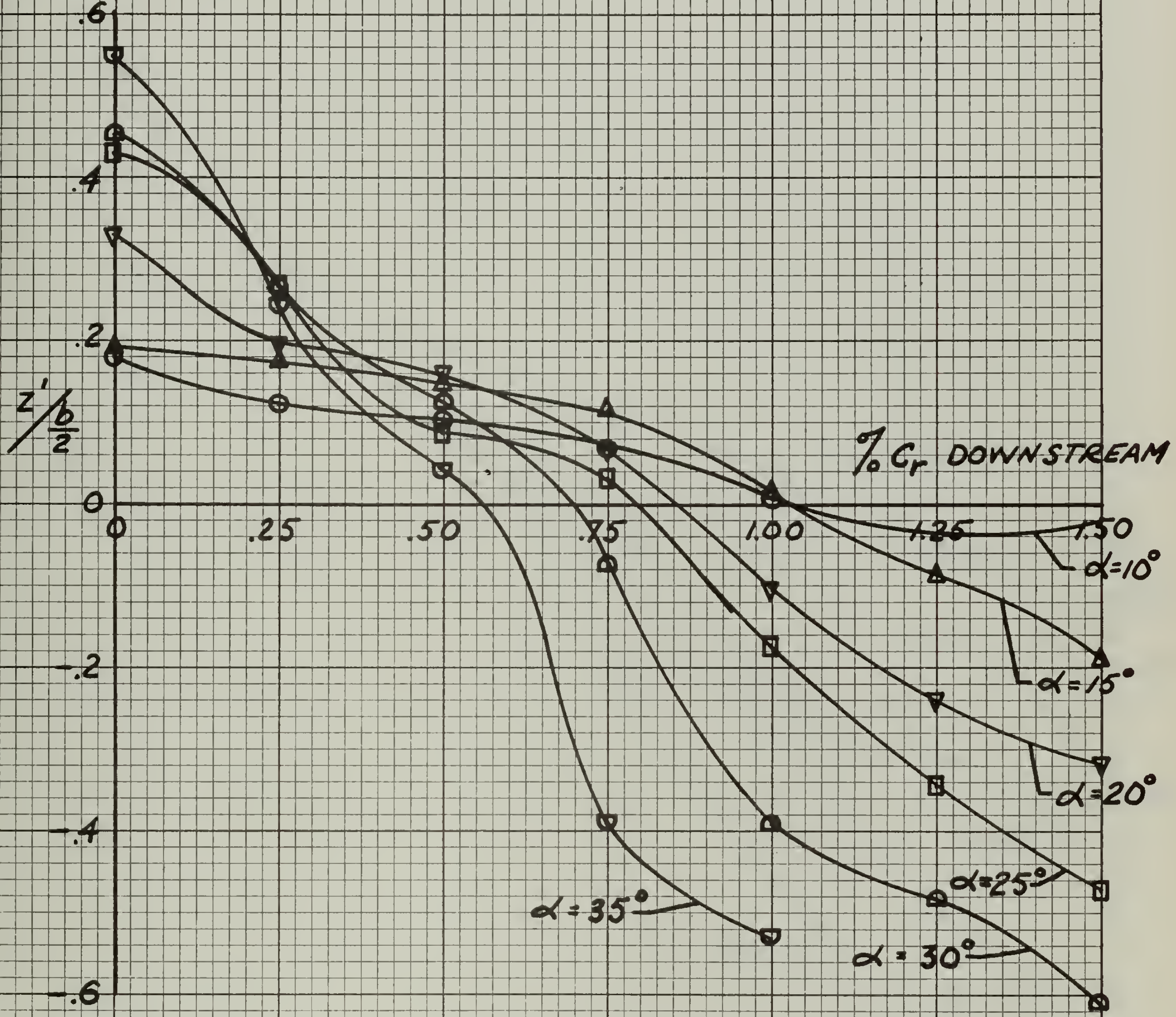

FLAT PLATE DELTA. VORTEX CORE LOCI
DOWNSTREAM OF T.E.

FIG. 49

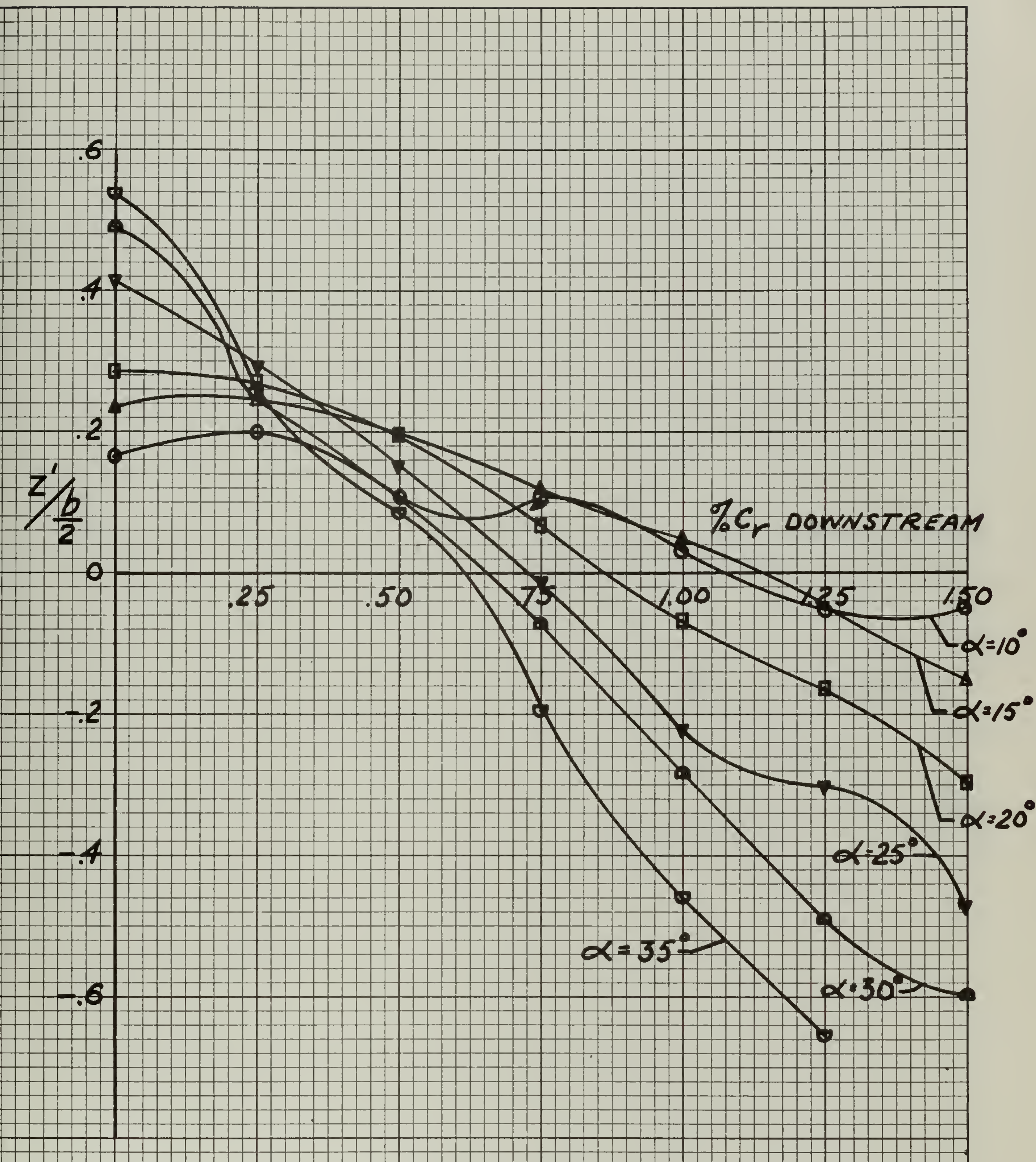

6% DELTA. VORTEX CORE LOCI DOWNSTREAM OF T.E.

FIG. 50

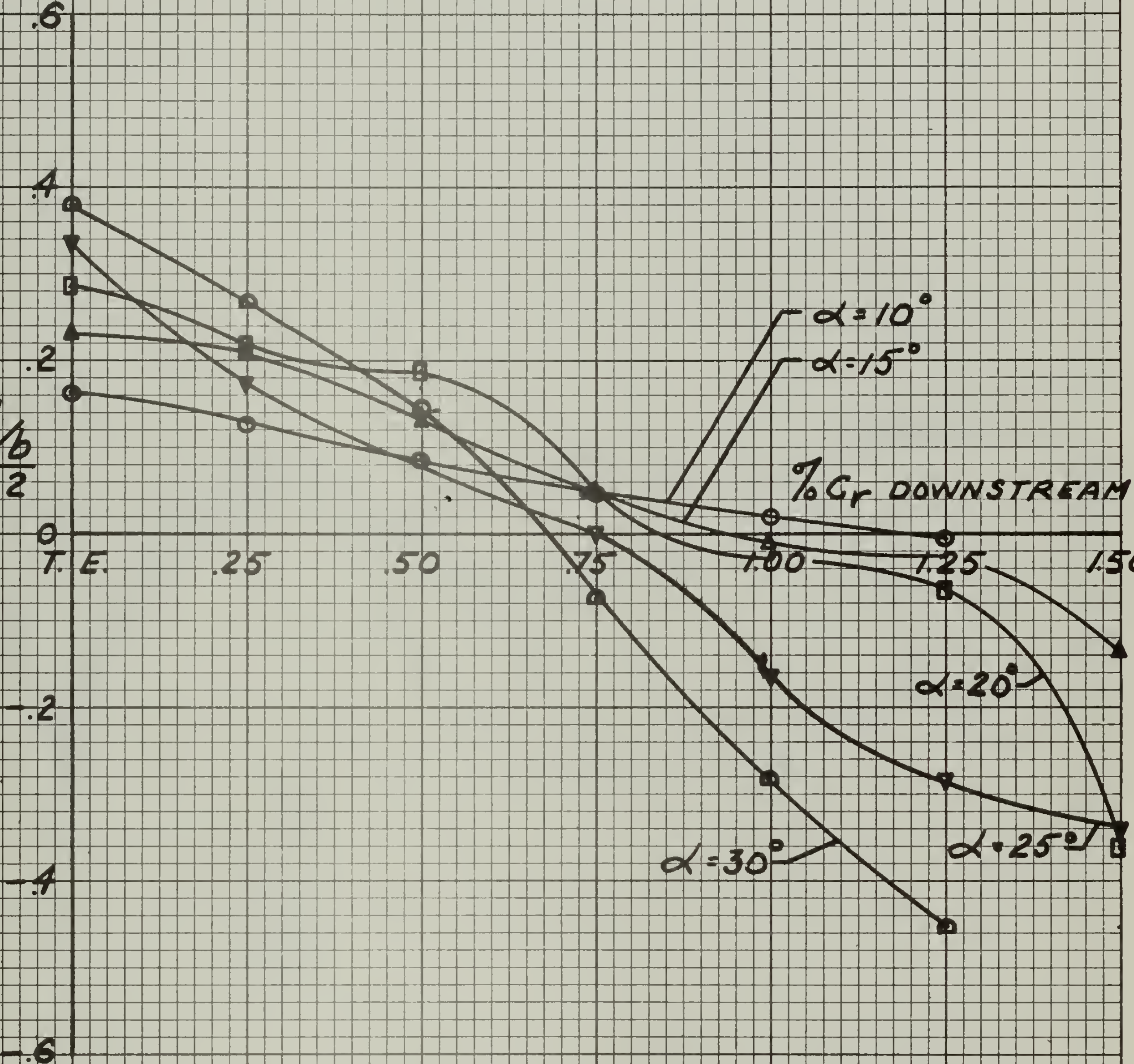

12% DELTA. VORTEX CORE LOCI DOWNSTREAM OF T.E.

FIG. 51

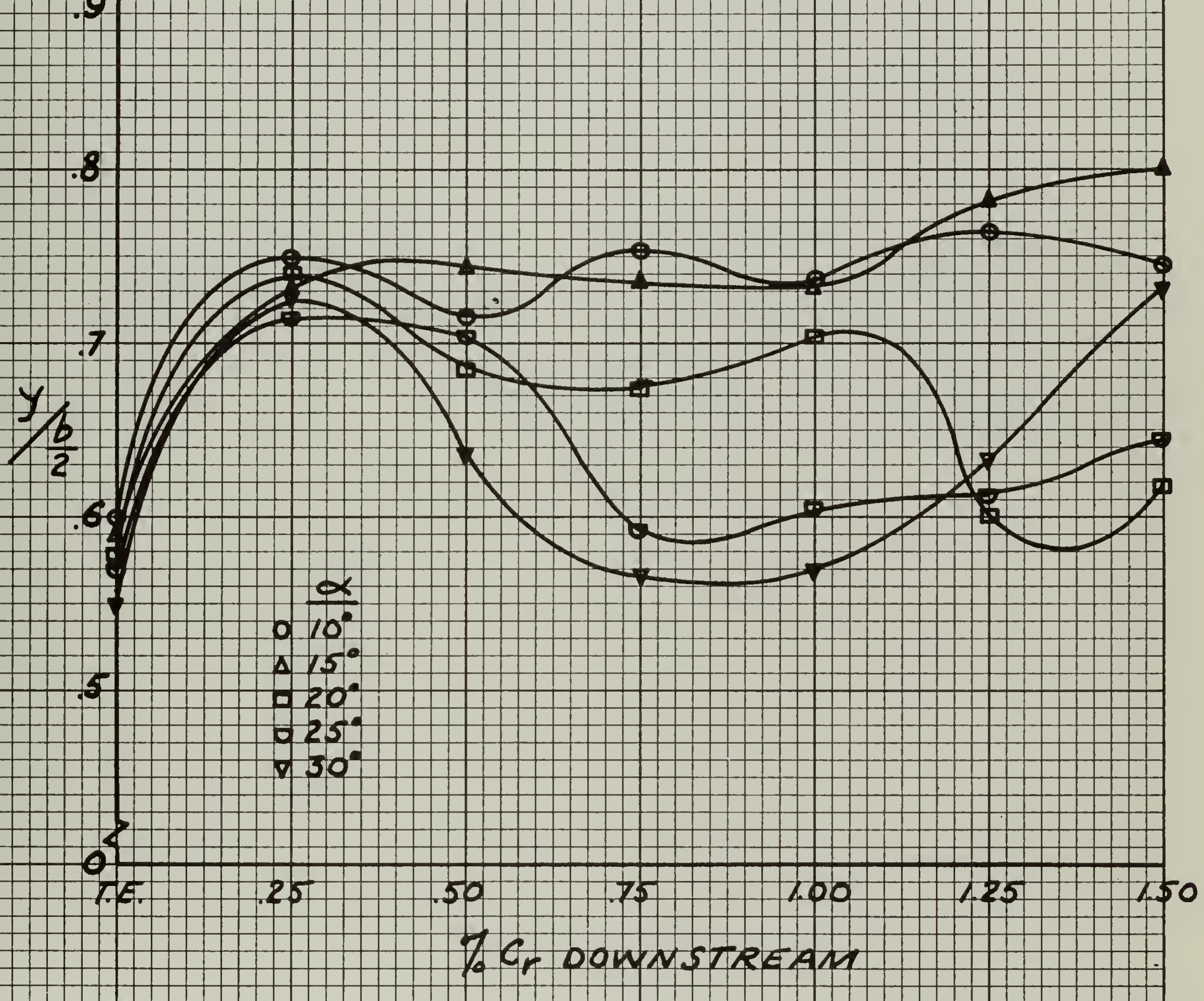

FLAT PLATE DELTA. VORTEX CORE LOCI
DOWNSTREAM OF T.E.

FIG. 52

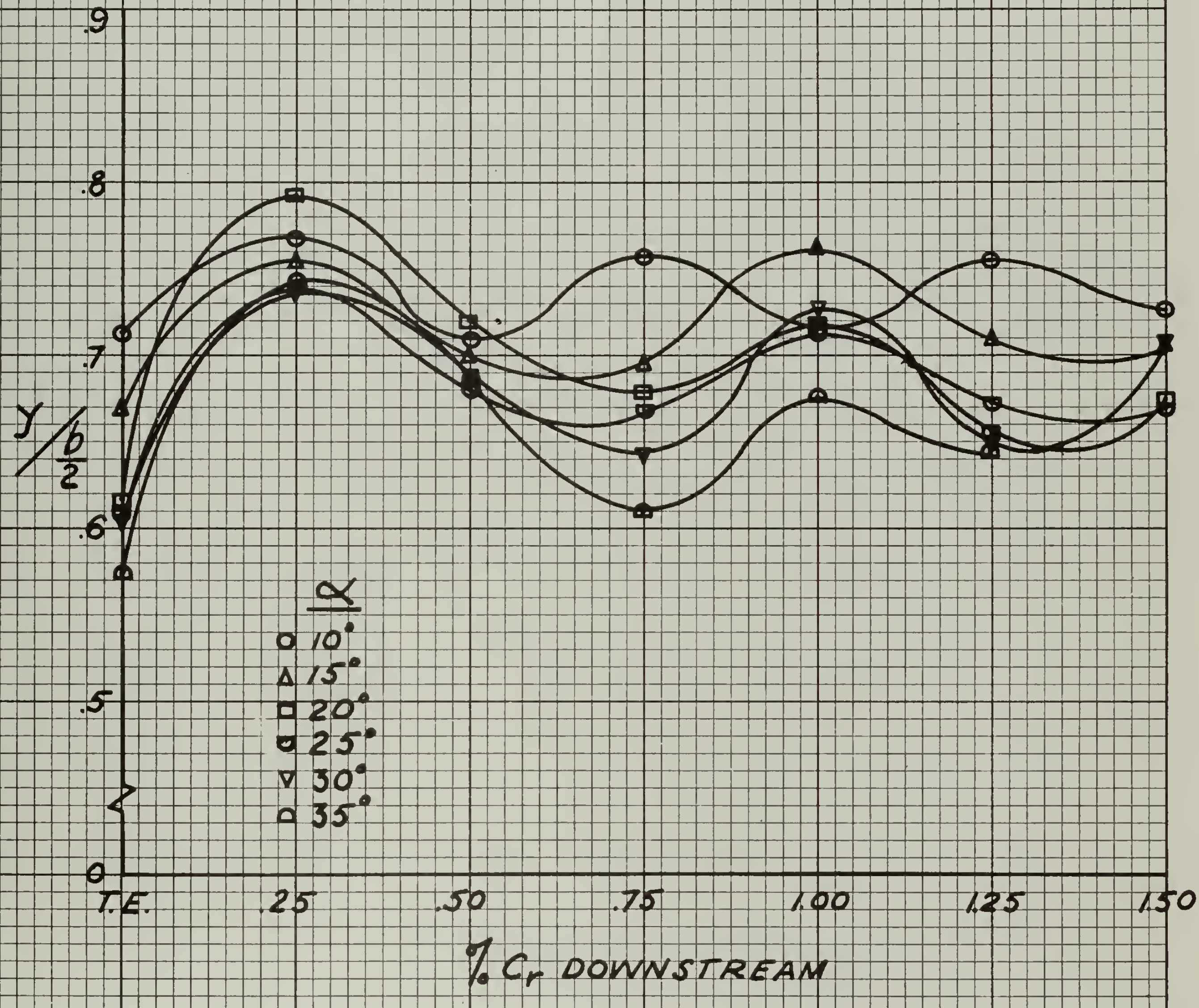

6% DELTA. VORTEX CORE LOCI DOWNSTREAM OF T.E.

FIG. 53

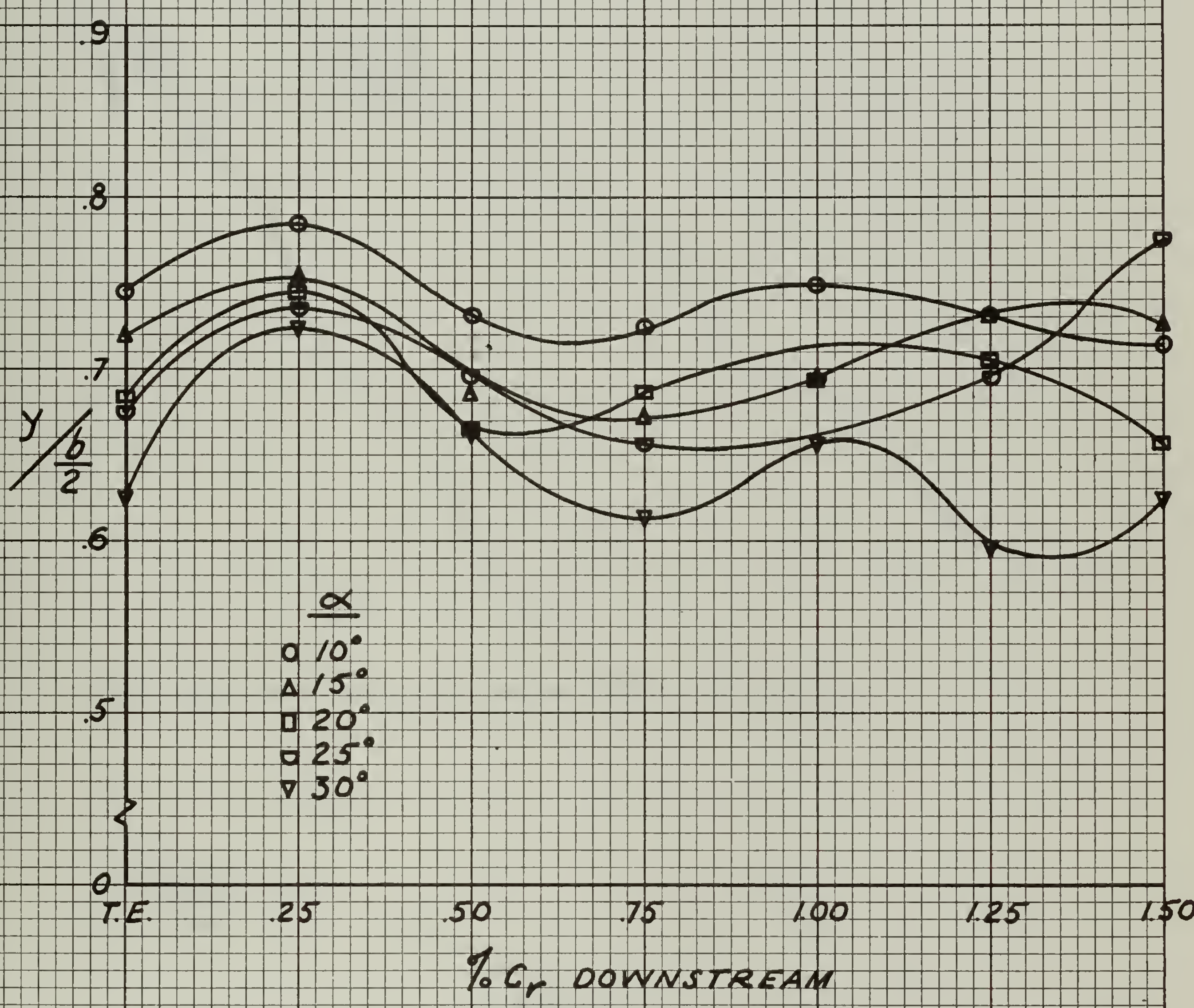

12% DELTA. VORTEX CORE LOCI DOWNSTREAM OF T.E.

FIG. 54

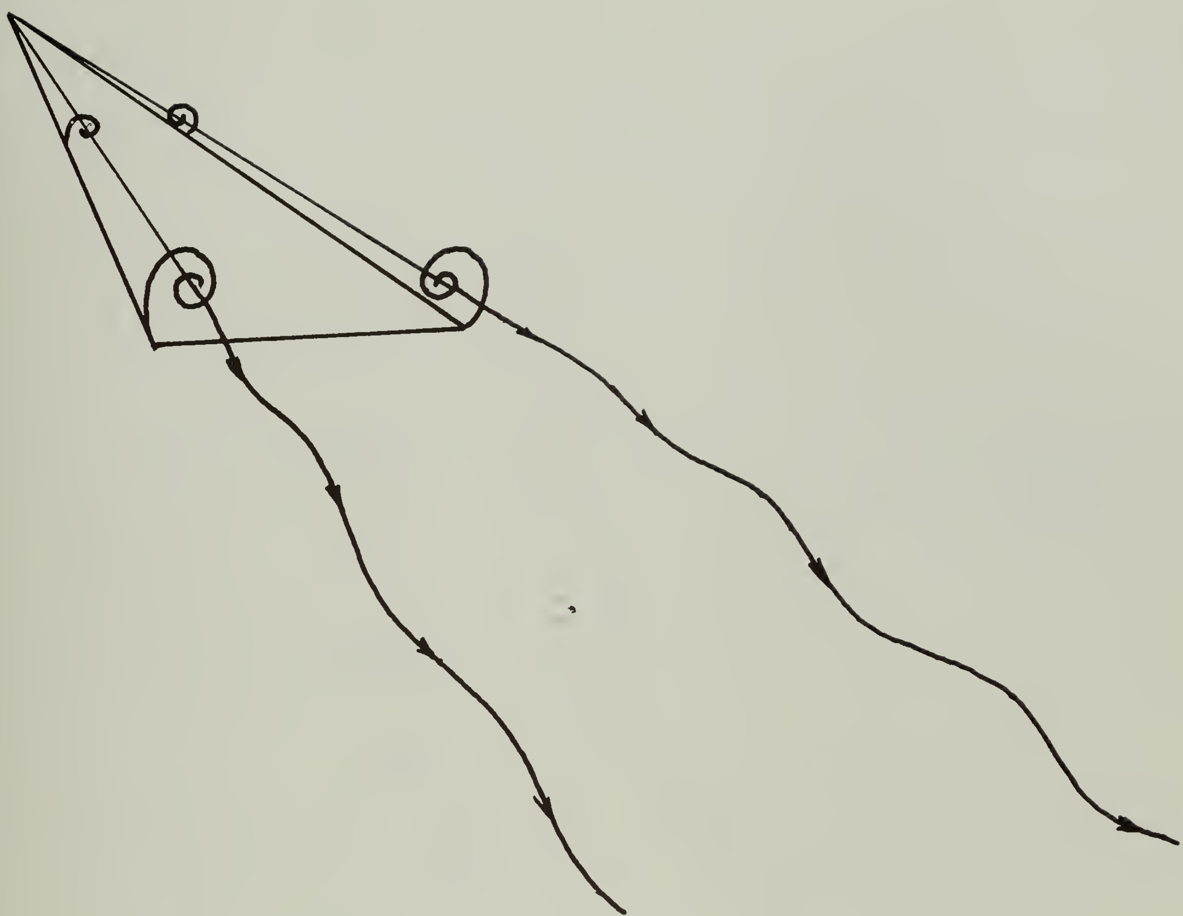

(a) Helical Downstream Path of Cores

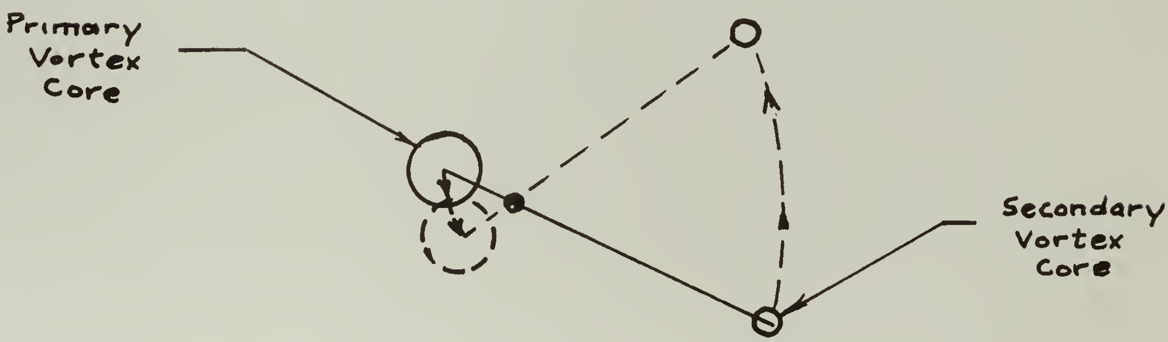

(b) Core Rotation in Cross-Flow Plane

Fig. 55 Downstream Core Movement

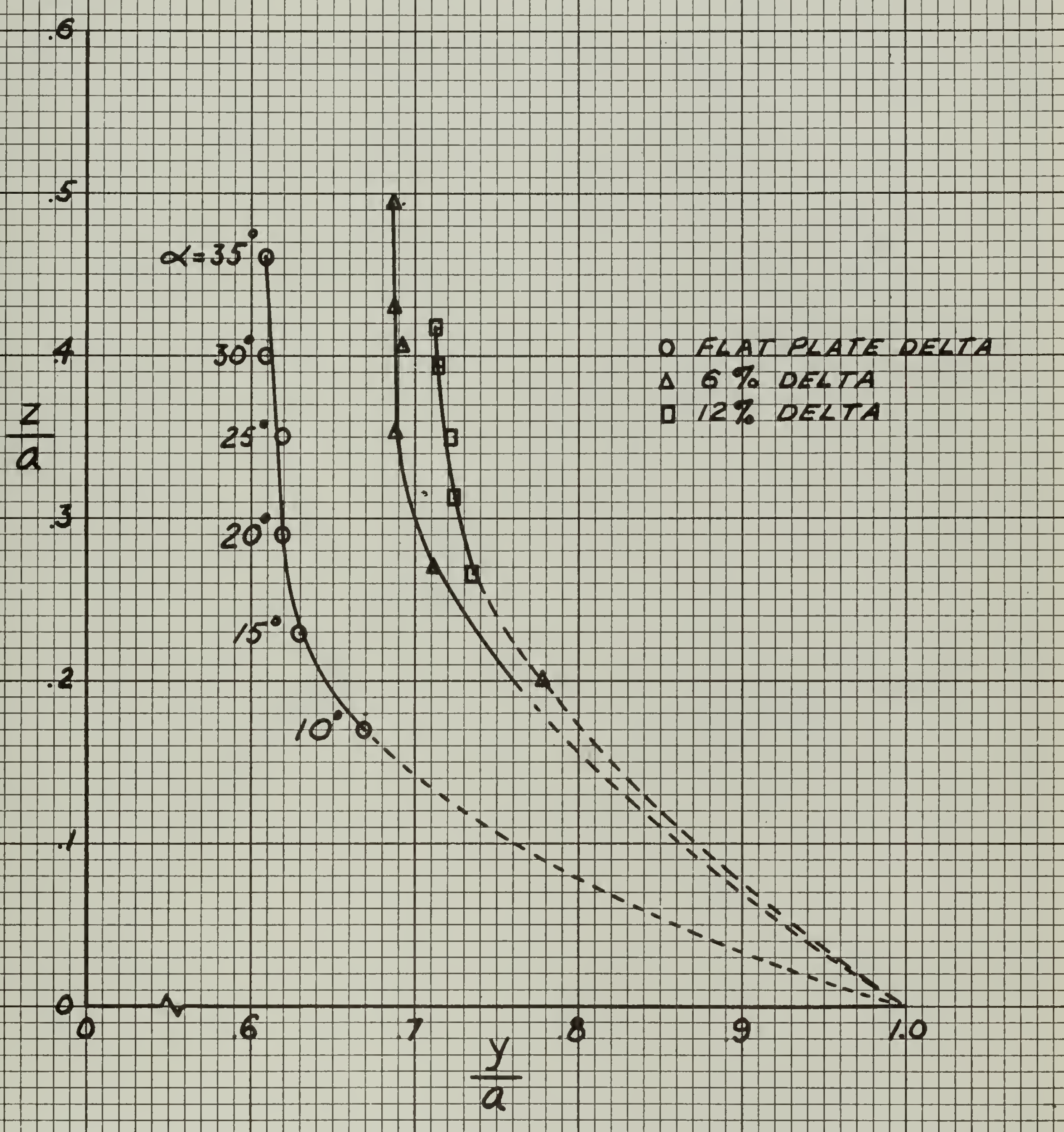

THICKNESS EFFECTS. VORTEX CORE POSITIONS

FIG. 56

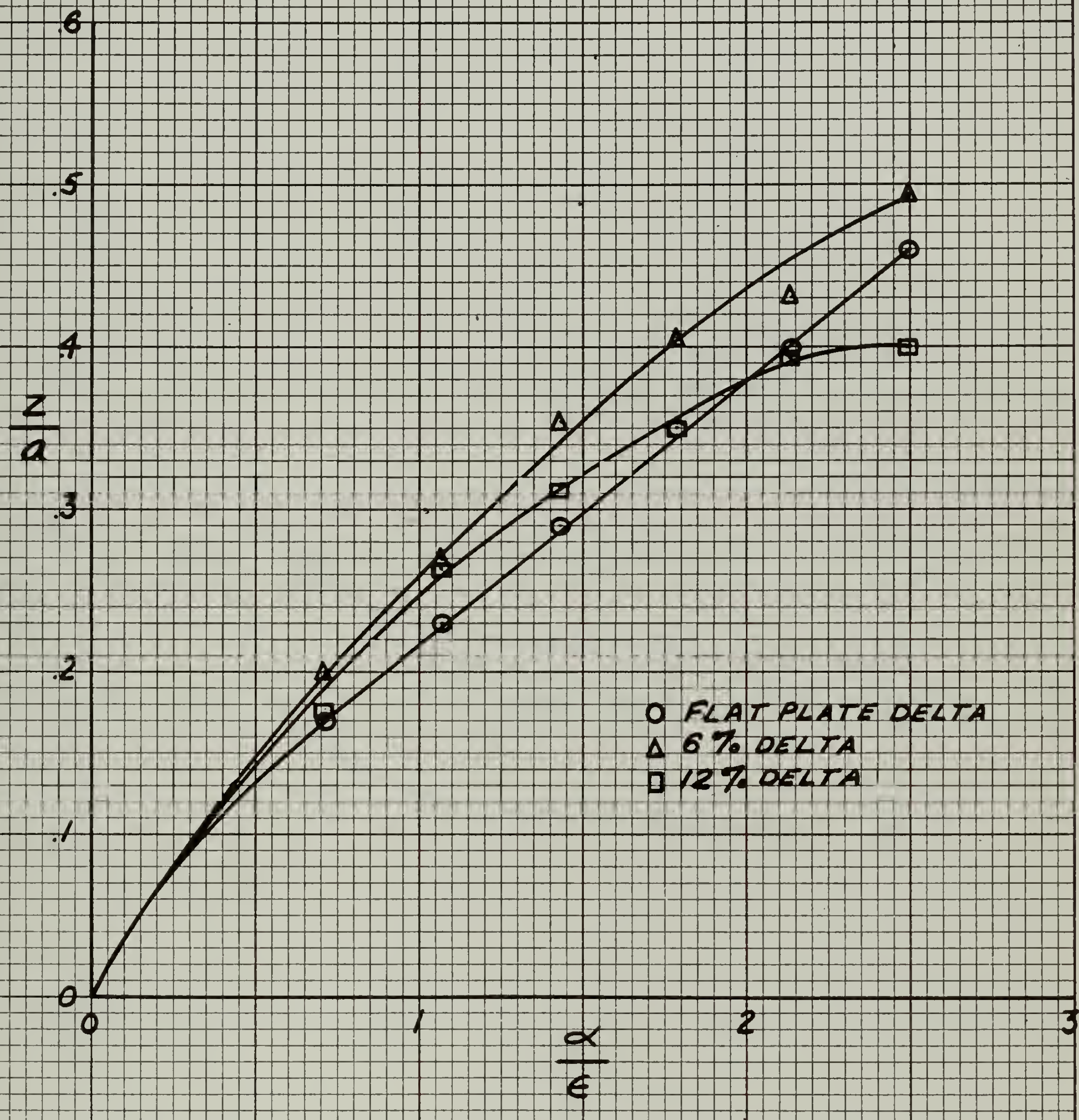

THICKNESS EFFECTS. VORTEX CORE HEIGHT VERSUS α/ε

FIG. 57

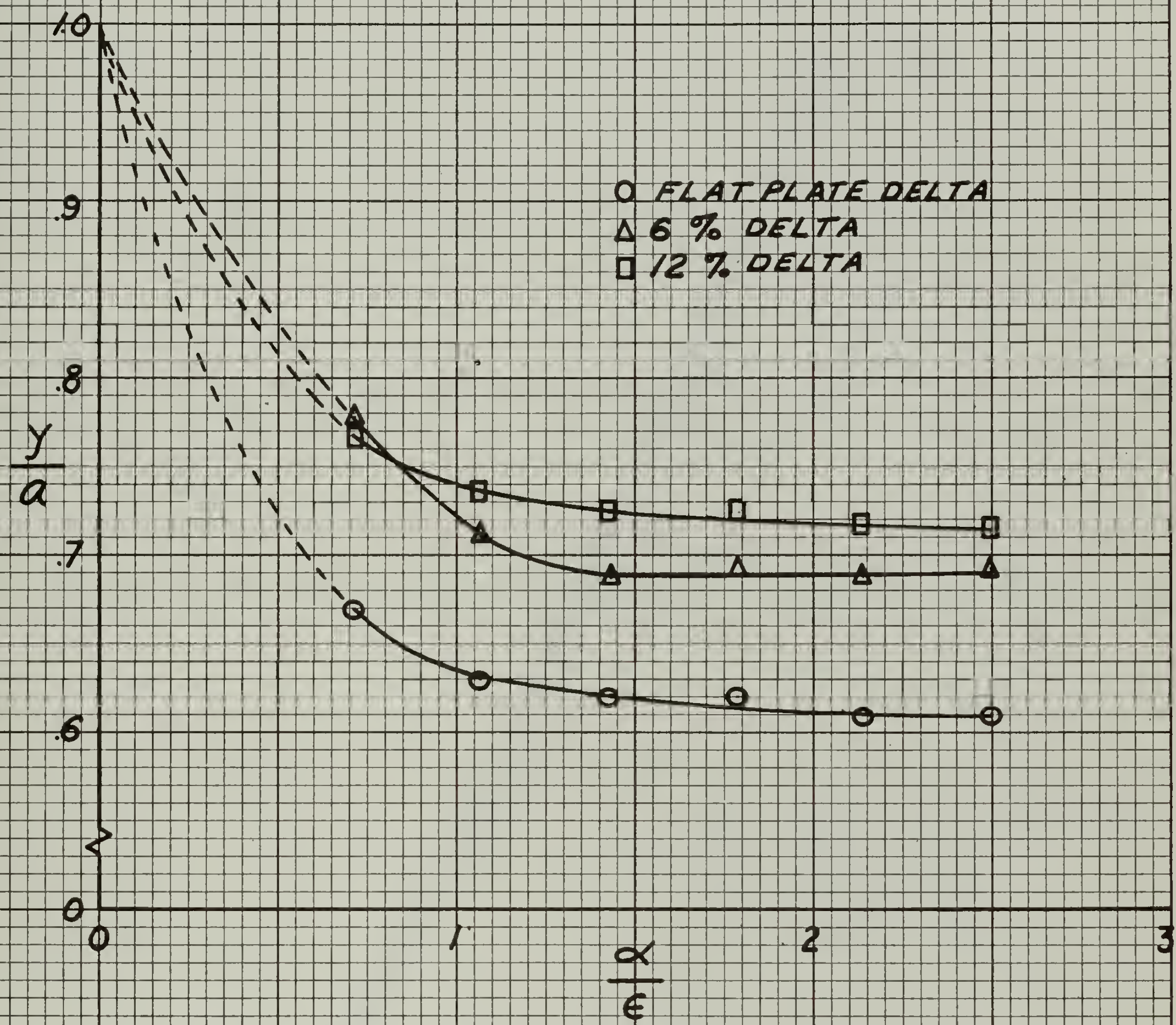

THICKNESS EFFECTS. SPANWISE POSITION OF VORTEX CORE VERSUS α/ε

FIG. 58

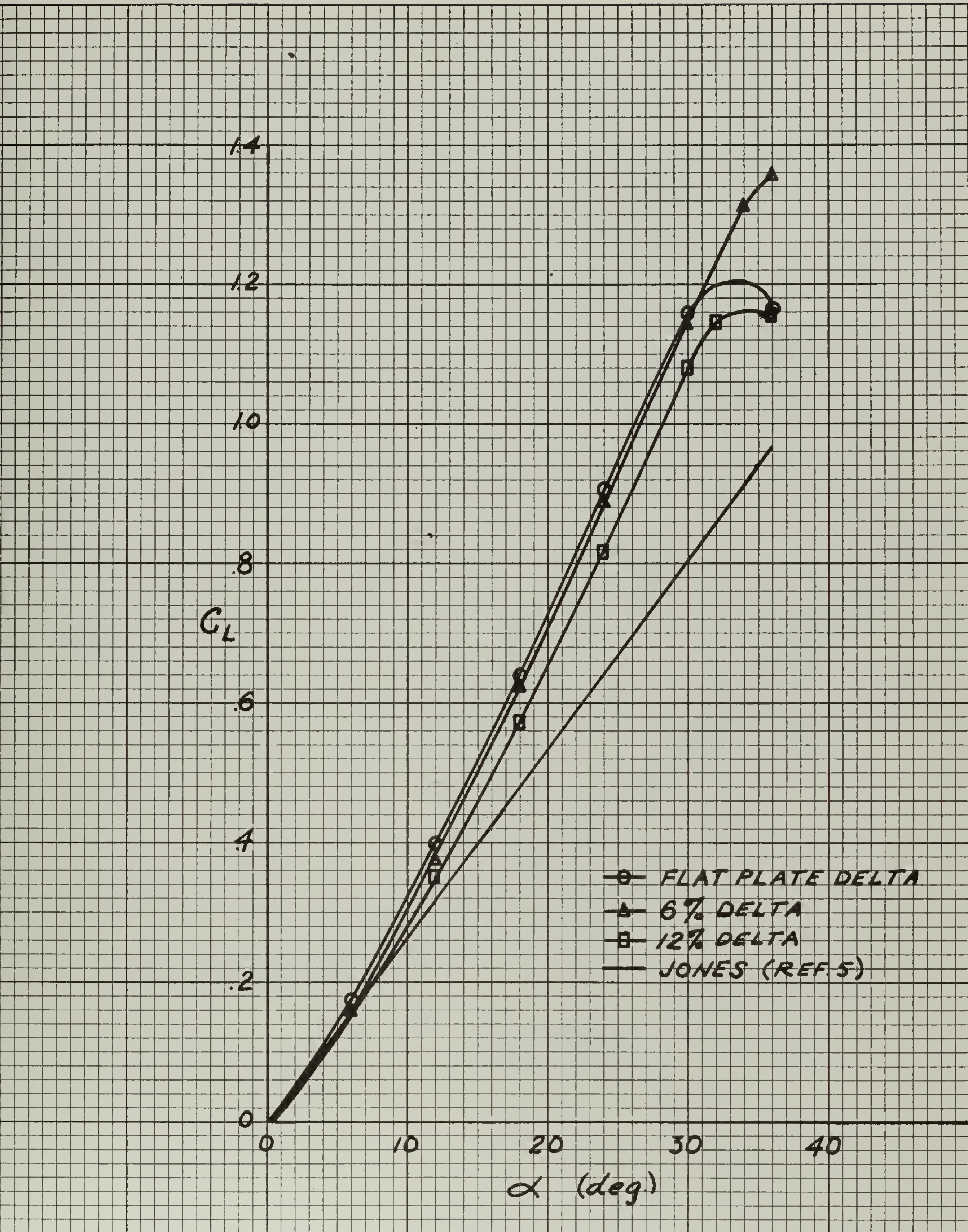

COMPARISON OF EXPERIMENTAL LIFT CURVES WITH POTENTIAL THEORY

FIG. 59

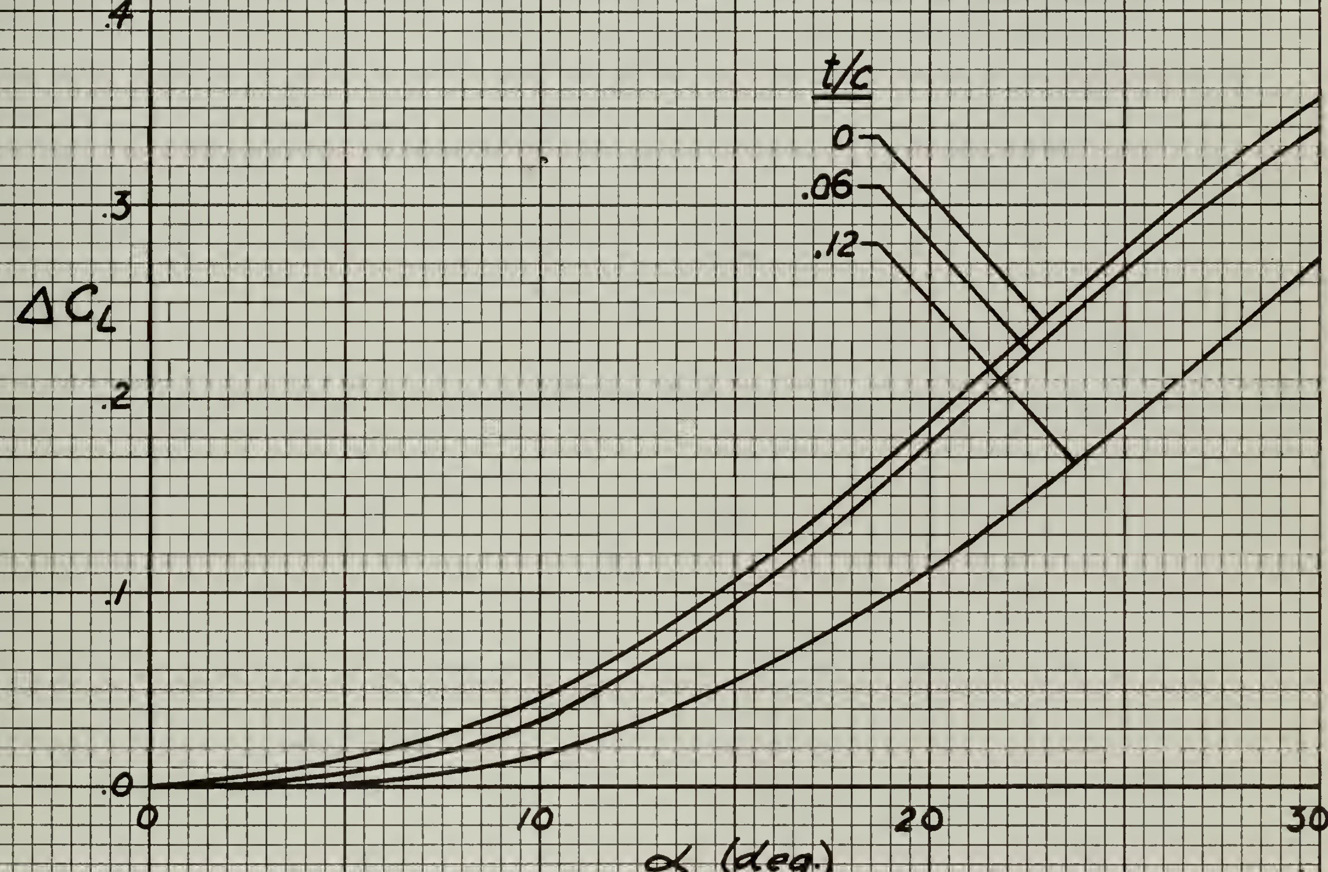

ΔC_L VERSUS α

FIG. 60

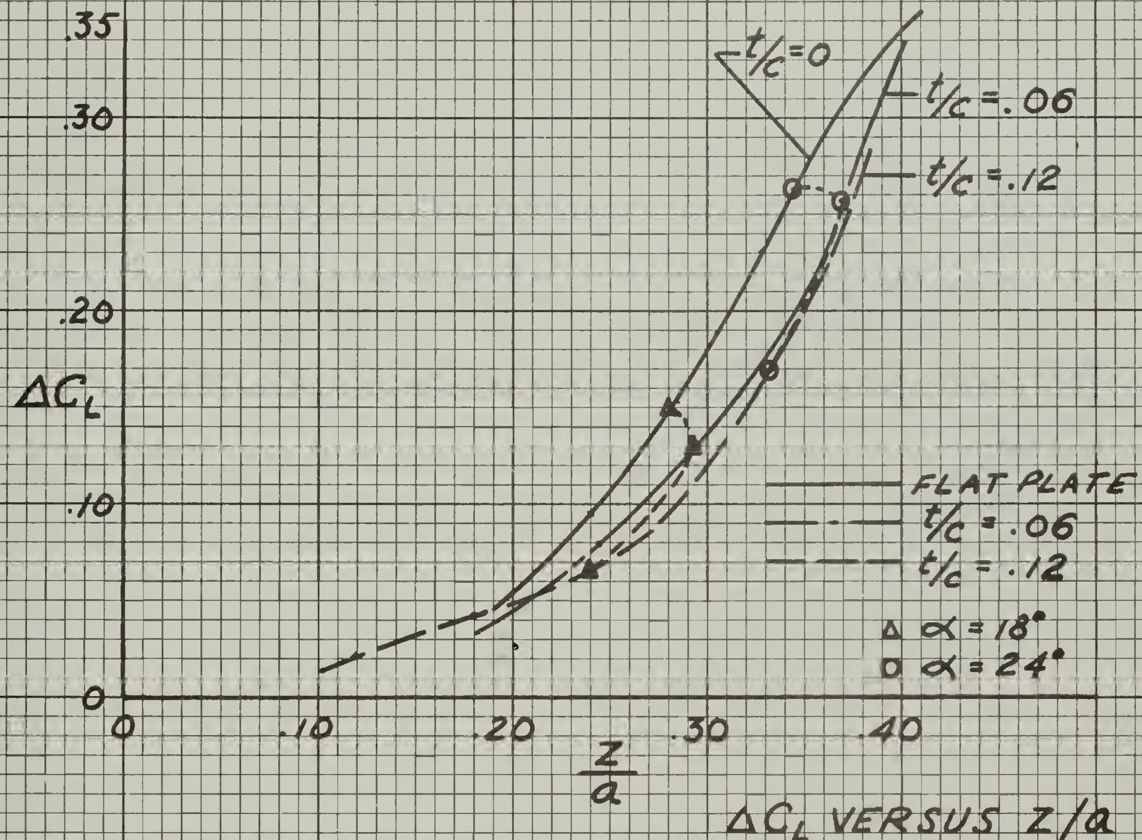
.35
.30
.20
.10
0
ΔC_L
t/c=0
t/c=.06
t/c=.12
FLAT PLATE
t/c = .06
t/c = .12
Δ α = 18°
O α = 24°
0
.10
.20
.30
.40
Z/a
ΔC_L VERSUS Z/a

FIG. 61

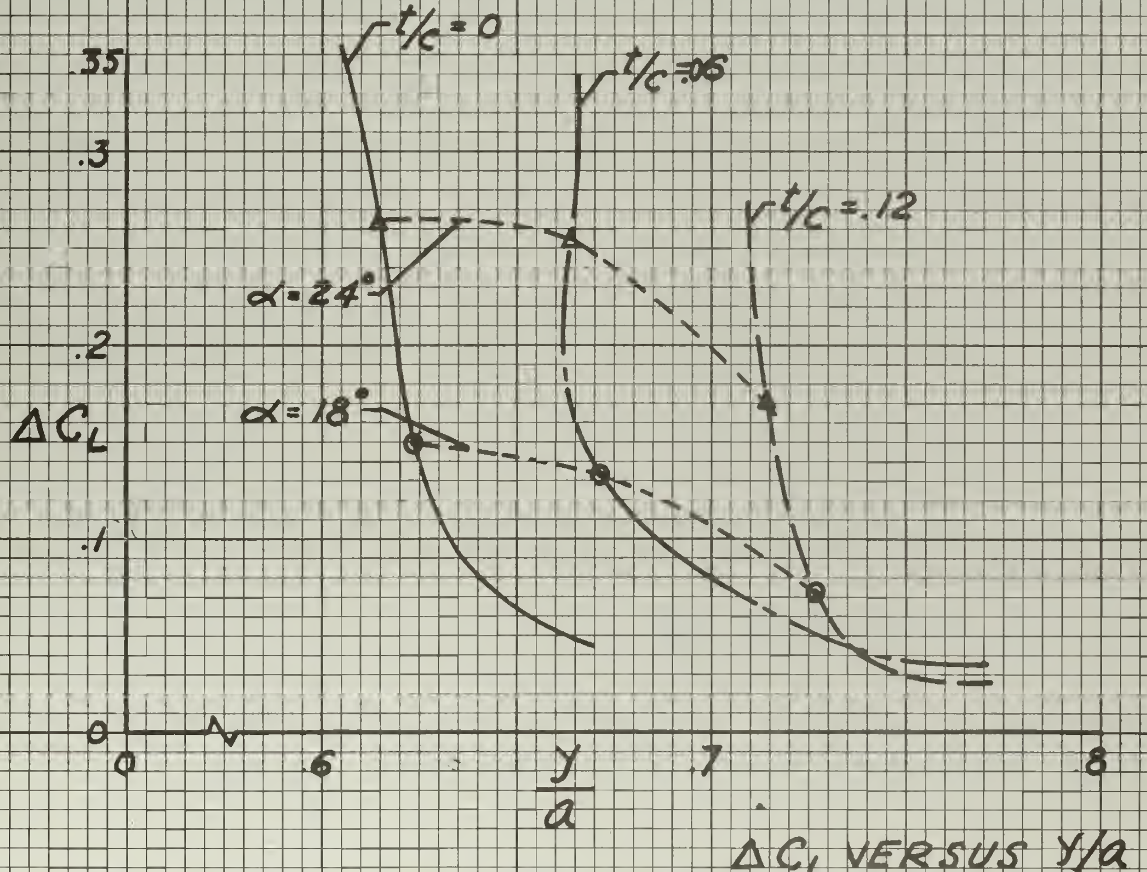
.35
.3
.2
.1
0
ΔC_L
t/c=0
t/c=.06
t/c=.12
α=24°
α=18°
0
.6
.7
.8
y/a
ΔC_L VERSUS y/a

FIG. 62

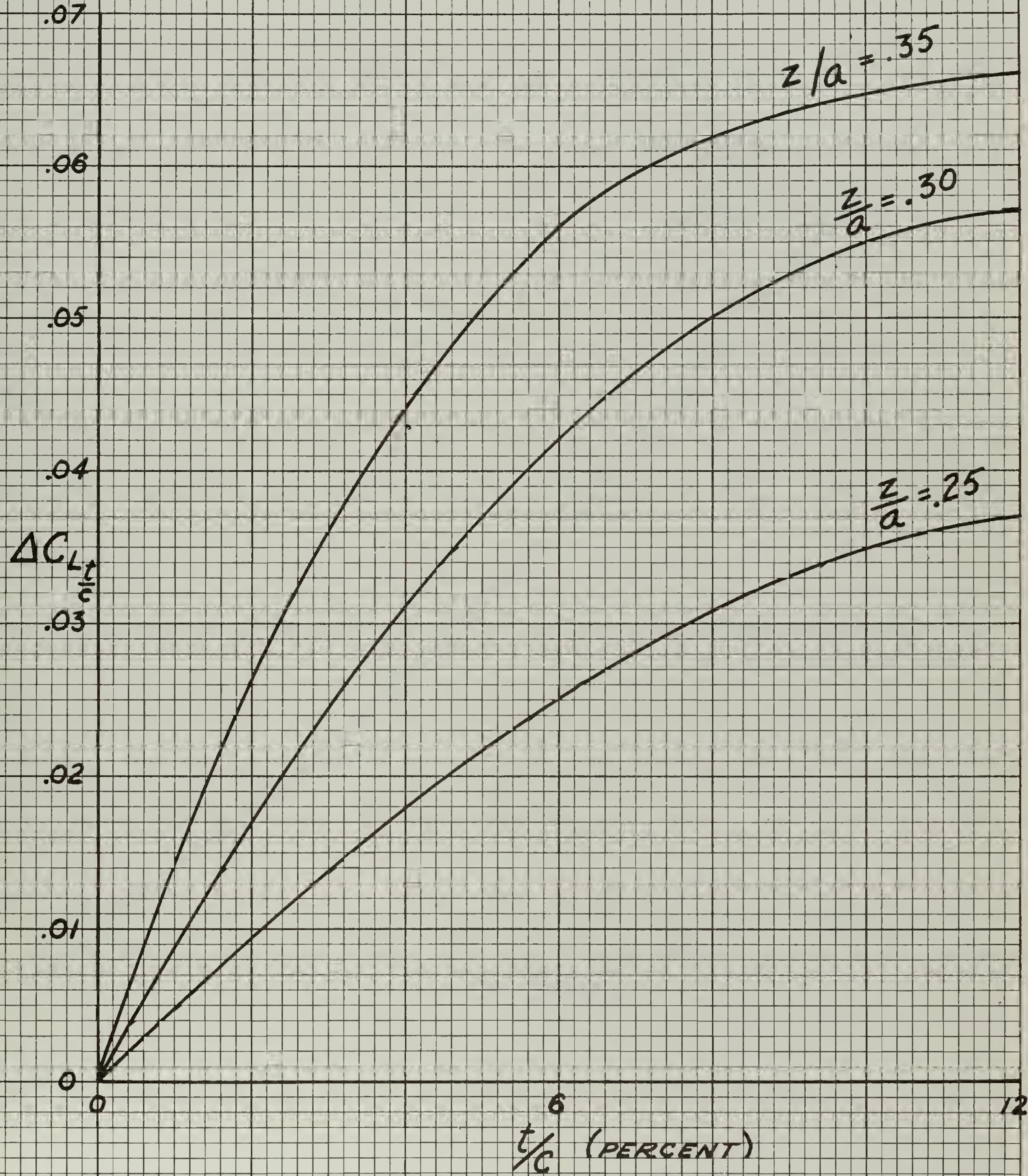

$\Delta C_{L_{\frac{t}{c}}}$ VERSUS t/c FOR VARIOUS z/a

FIG. 63

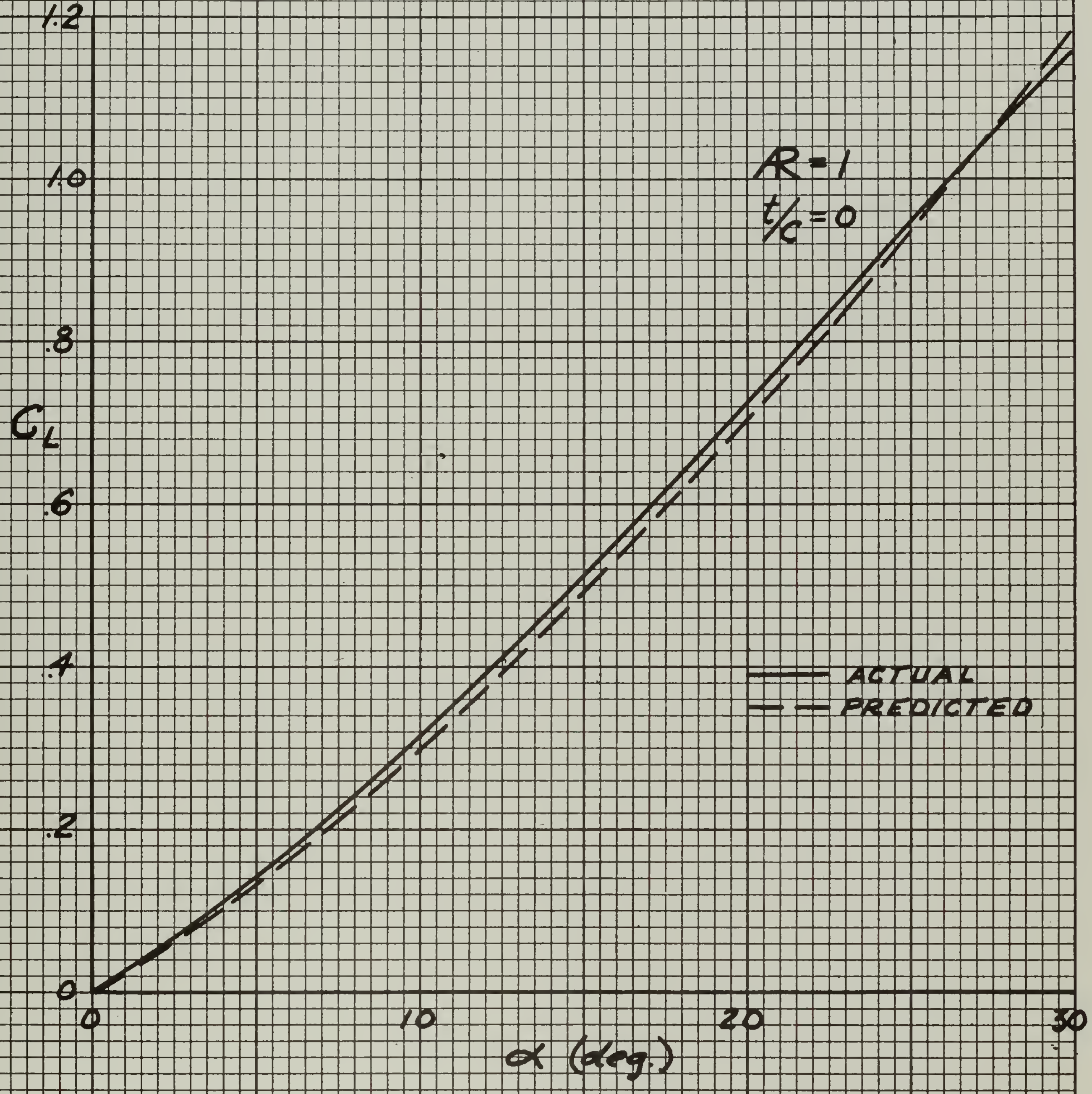

COMPARISON OF EXPERIMENTAL AND PREDICTED LIFT CURVES

FIG. 64

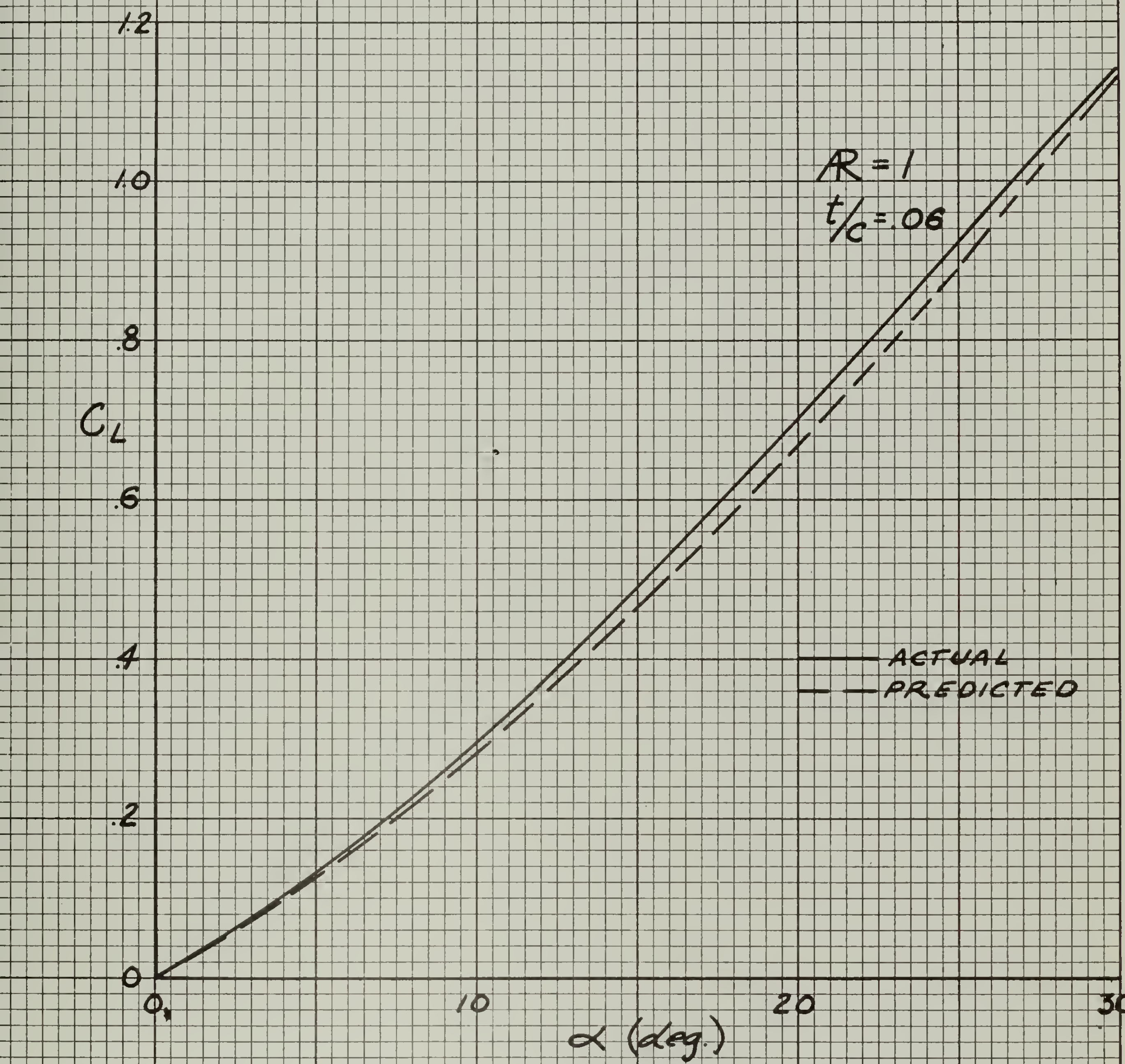

COMPARISON OF EXPERIMENTAL AND PREDICTED LIFT CURVES

FIG. 65

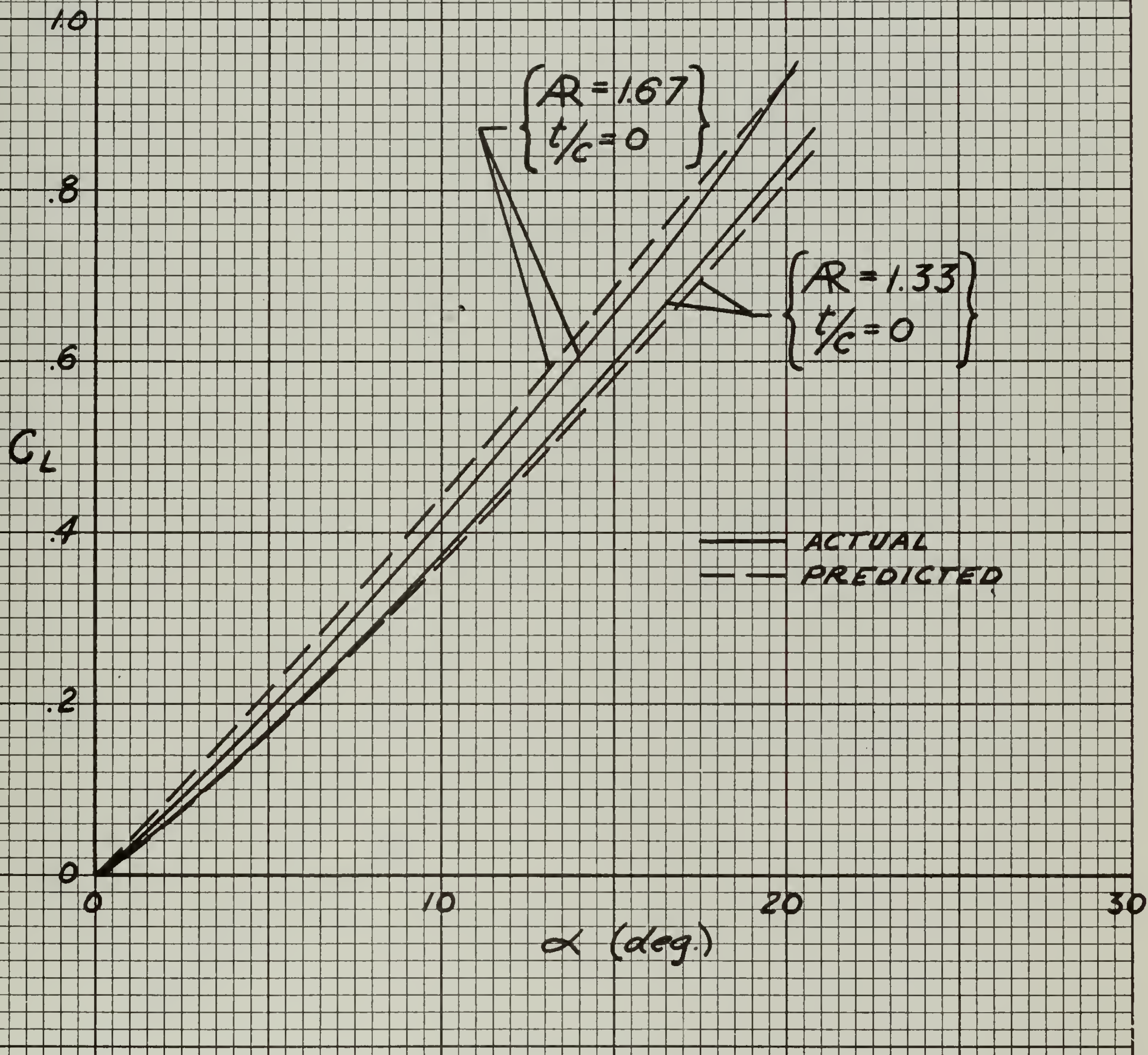

COMPARISON OF EXPERIMENTAL AND PREDICTED LIFT CURVES

FIG. 66

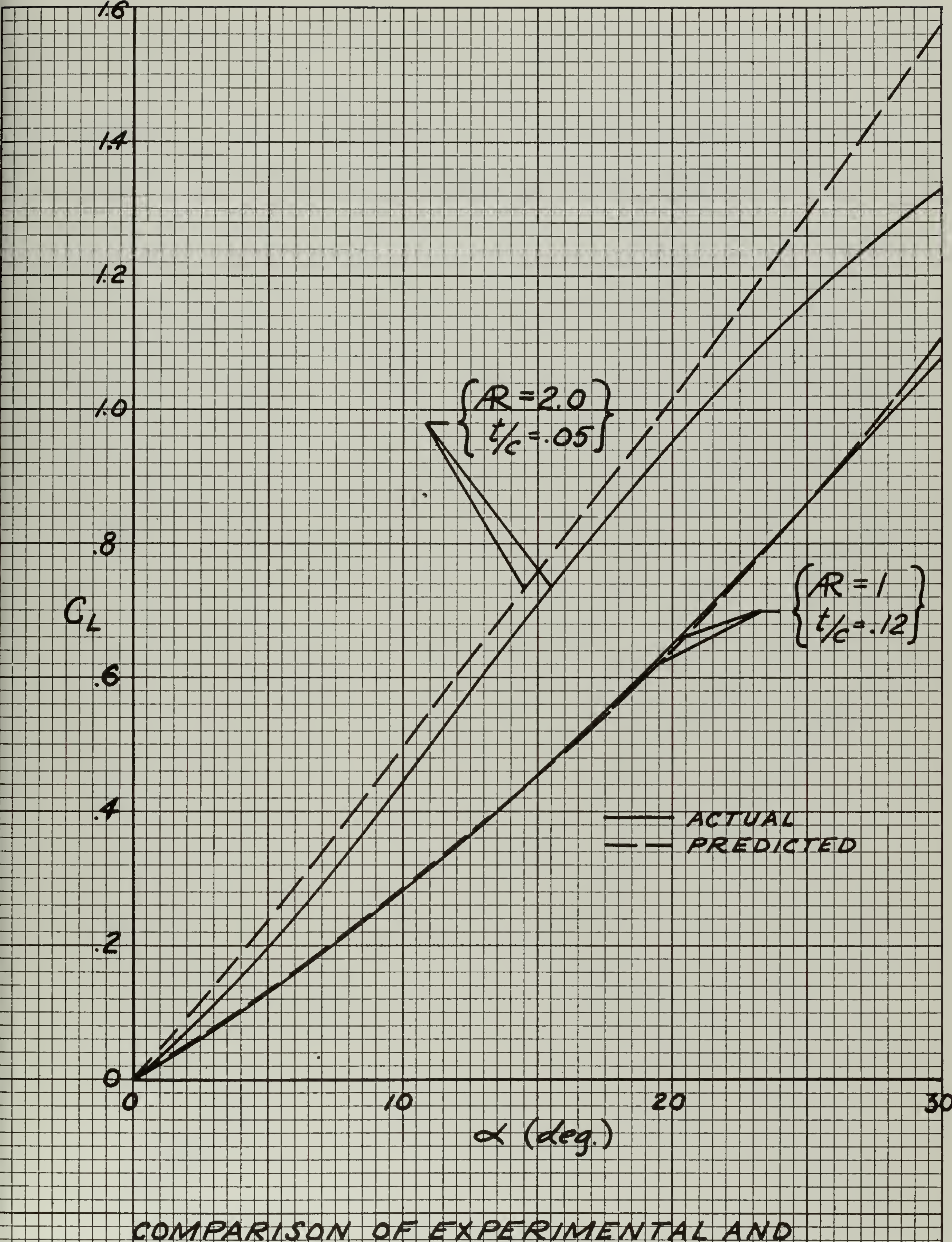

COMPARISON OF EXPERIMENTAL AND PREDICTED LIFT CURVES

FIG. 67

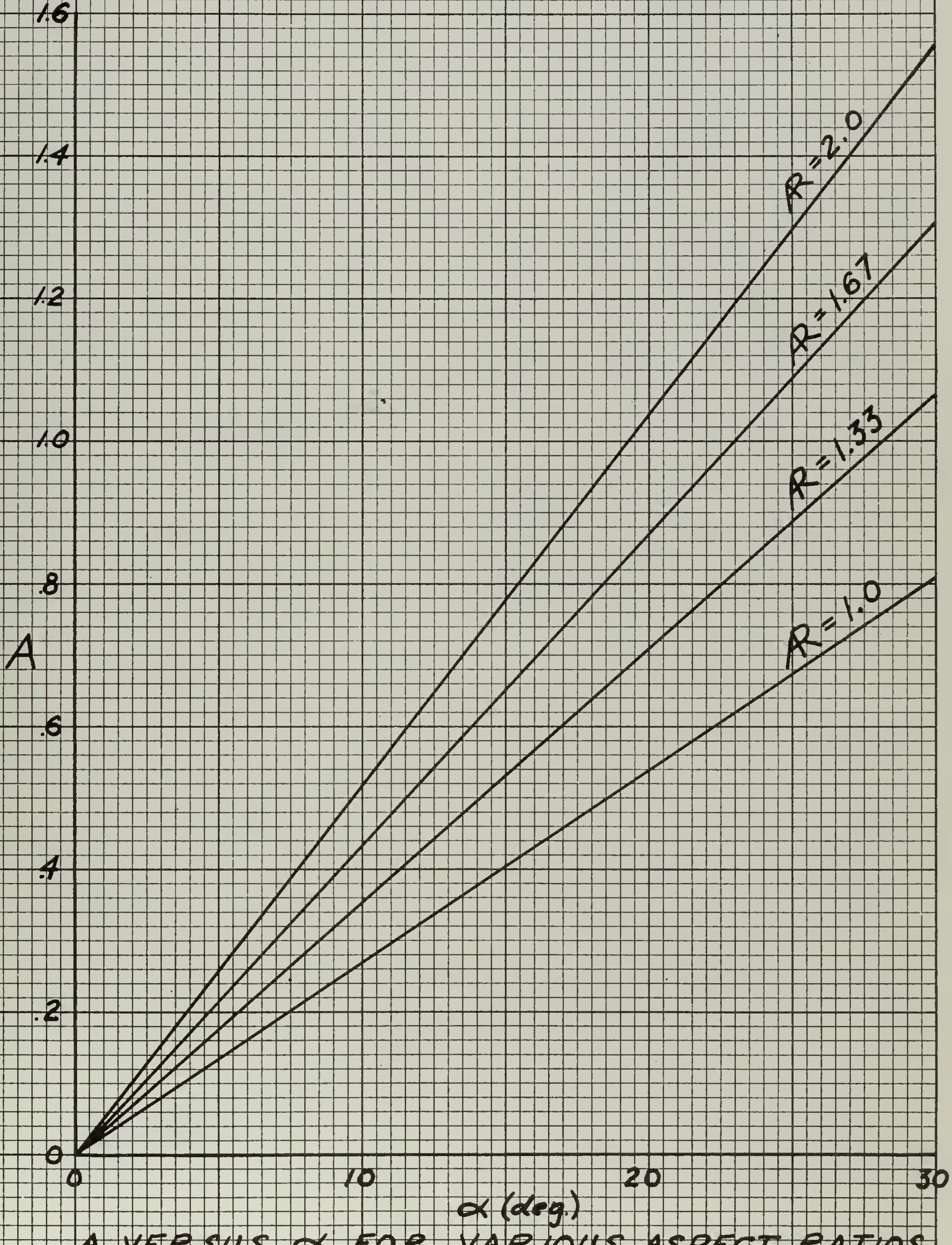

A VERSUS α FOR VARIOUS ASPECT RATIOS

FIG. 68

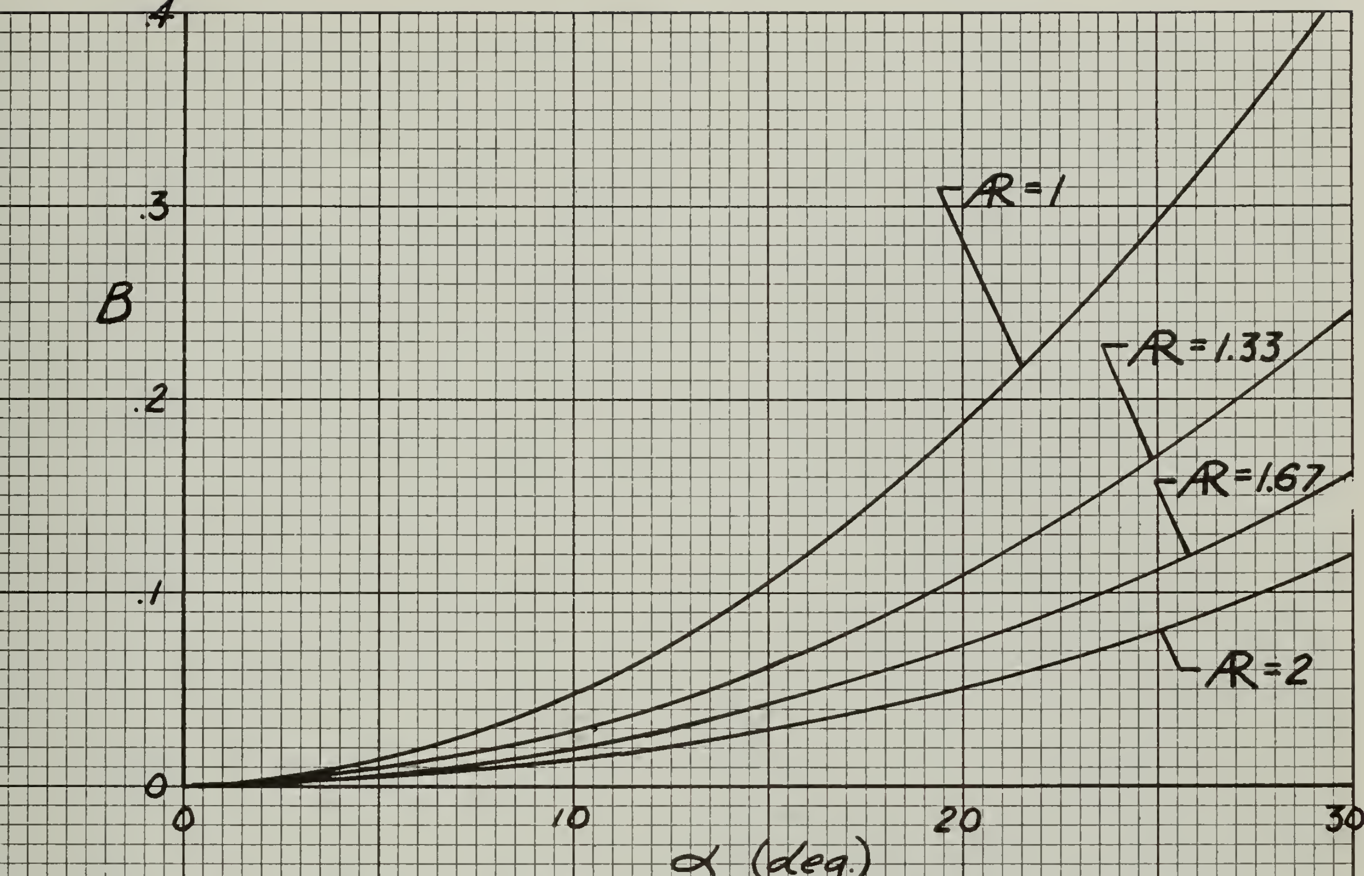

B VERSUS α FOR VARIOUS ASPECT RATIOS
FIG. 69

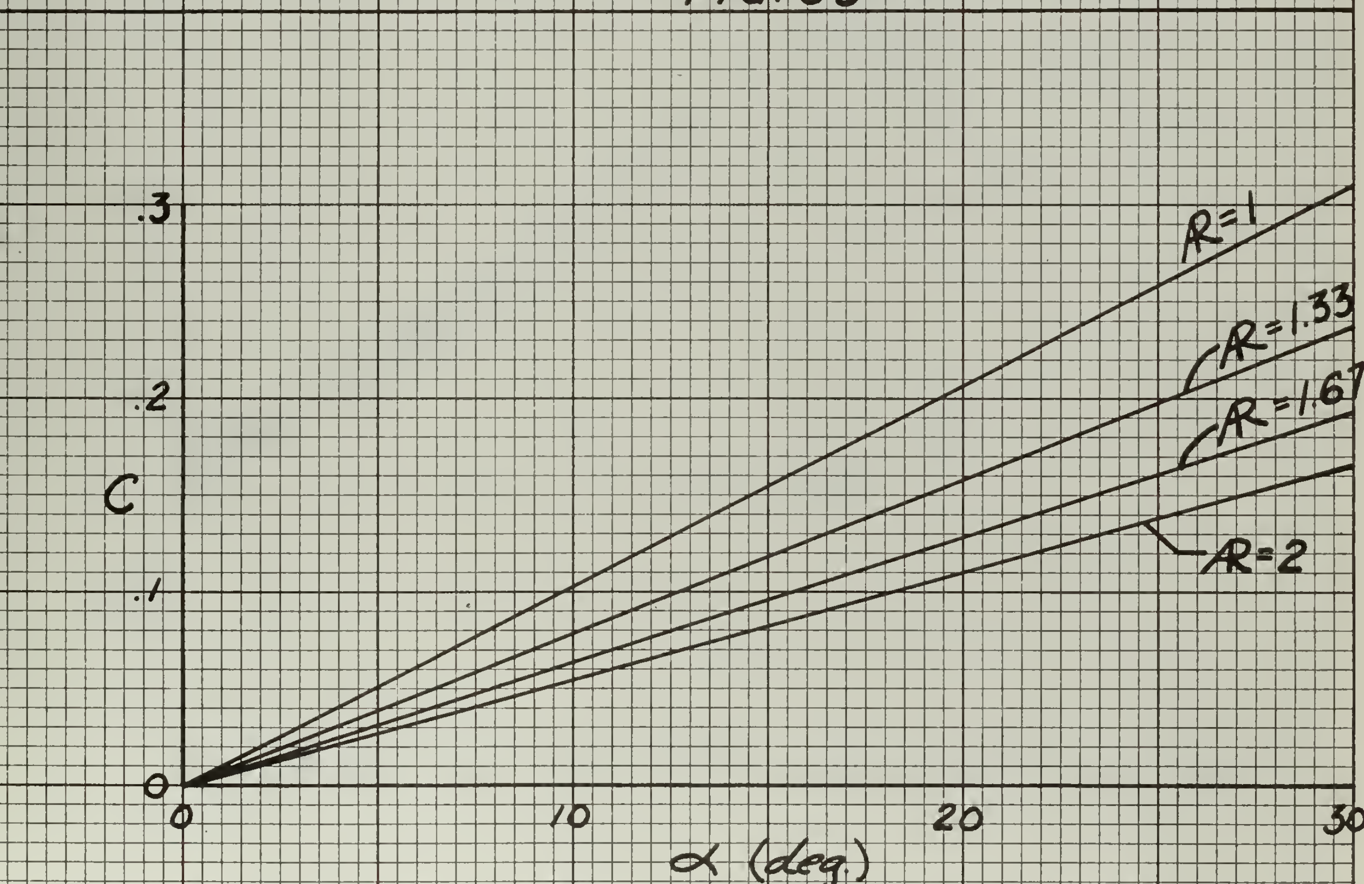

C VERSUS α FOR VARIOUS ASPECT RATIOS
FIG. 70

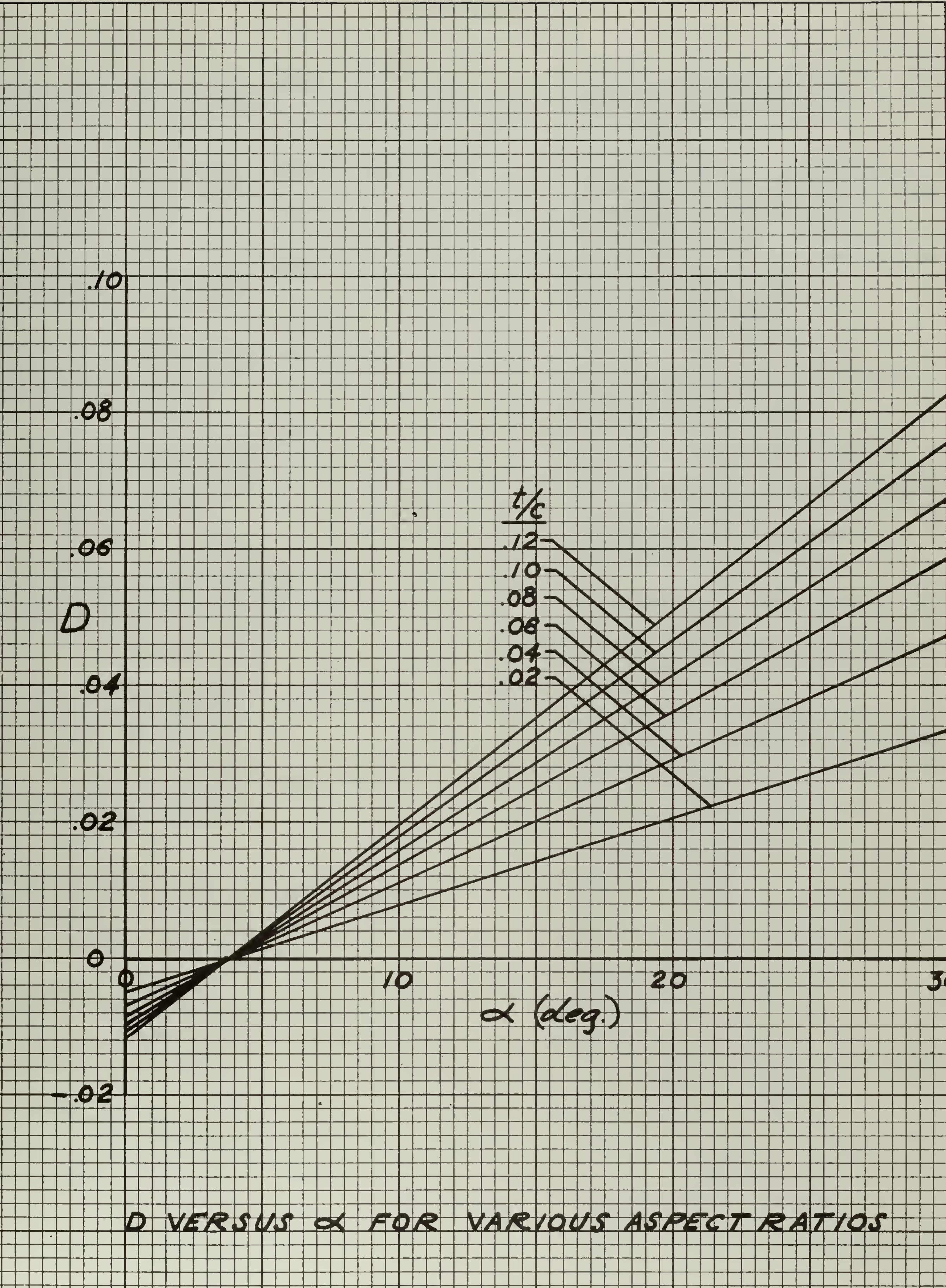

D VERSUS α FOR VARIOUS ASPECT RATIOS

FIG. 71

DISTRIBUTION LIST

Chief, Bureau of Naval Weapons (RAAD-3)
Department of the Navy
Washington 25, D. C.

Chief, Bureau of Naval Weapons (RRSY-13)
Department of the Navy
Washington 25, D. C.

Chief, Bureau of Naval Weapons (RRSY-5)
Department of the Navy
Washington 25, D. C.

Chief, Bureau of Naval Weapons (RM)
Department of the Navy
Washington 25, D. C.

Commanding Officer & Director
David Taylor Model Basin
Aerodynamics Laboratory
Washington 7, D. C.

Commander
U. S. Naval Ordnance Laboratory
Aeronautical Mechanics Division
Silver Spring 19, Maryland
Attn: Dr. Kurzweg

Chief of Naval Research (Code 461)
Department of the Navy
Washington 25, D. C.

Chief of Naval Research (Code 438)
Department of the Navy
Washington 25, D. C,

Commanding Officer
Office of Naval Research Branch Office
Navy #100 Fleet Post Office
New York, New York

Commanding Officer
Office of Naval Research Branch Office
1030 E. Green Street
Pasadena, California

Director
Naval Research Laboratory
Technical Information Office
Washington 25, D. C.

Chief, Bureau of Ships (Code 421)
Department of the Navy
Washington 25, D. C.

Naval Supersonic Laboratory
Massachusetts Institute of Technology
Cambridge, Massachusetts

Marine Corps Development Center
Marine Corps Schools
Quantico, Virginia
Attn: Air Section

Marine Corps Equipment Board
Marine Corps Schools
Quantico, Virginia
Attn: Aviation Section

Air Research & Development Command
U. S. Air Force
Andrews Air Force Base
Washington 25, D. C.

Air Research & Development Command
U. S. Air Force
Office of Scientific Research
Washington 25, D. C.

Wright Air Development Division
Aeronautical Research Laboratory
Wright-Patterson Air Force Base, Ohio

Wright Air Development Division
Aircraft Laboratory
Wright-Patterson Air Force Base, Ohio
Attn: WCLS-2

Office of Chief of Transportation
(TC-RES)
Department of the Army
Washington 25, D. C.

Commanding Officer
U. S. Army Transportation Research
Command (TCREC-AD)
Fort Eustis, Virginia

Office, Chief of Research &
Development
Department of the Army
Washington 25, D. C.
Attn: Aircraft & Electronics Divisior
Attn: R. L. Ballard

Commander
Armed Services Technical Information Agency
Document Service Center
Arlington Hall Station
Arlington 12, Virginia

National Aeronautical & Space Administration
Headquarters
1512 H Street, N. W.
Washington 25, D. C.
Attn: Mr. R. May

National Aeronautics & Space Administration
Ames Research Center
Moffett Field, California
Attn: Mr. C. W. Harper

National Aeronautics & Space Administration
Langley Research Center
Langley Air Force Base, Virginia
Attn: Mr. Donnelly

National Bureau of Standards
Department of Commerce
Washington 25, D. C.
Attn: Mr. G. B. Schubauer

Office of Technical Services
Department of Commerce
Washington 25, D. C.

Brooklyn Polytechnic Institute
Aerodynamics Laboratory
527 Atlantic Avenue
Freeport, L. I., New York

Brown University
Division of Engineering
Providence 12, Rhode Island
Attn: Dr. Paul Meeder

California Institute of Technology
Aeronautics Department
Pasadena, California
Attn: Dr. Clark Millikan

University of Colorado
Aeronautical Engineering Department
Boulder, Colorado
Attn: Dr. K. D. Wood

Cornell University
Graduate School of Aeronautics
Ithaca, New York
Attn: Dr. W. R. Sears

Georgia Institute of Technology
Guggenheim School of Aeronautics
Atlanta, Georgia
Attn: D. W. Dutton
W. Castles

University of Illinois
Aeronautical Engineering Department
Urbana, Illinois
Attn: Dr. H. S. Stillwell

The Johns Hopkins University
Applied Physics Laboratory
Baltimore 18, Maryland
Attn: Dr. F. H. Clauser
Mr. D. W. Rabenhorst

The Johns Hopkins University
Mechanical Engineering Department
Baltimore 18, Maryland
Attn: Dr. Stanley Corrsin

University of Maryland
Institute for Fluid Dynamics and
Applied Mathematics
College Park, Maryland
Attn: Prof. Shin-I Pai
Prof. W. Sherwood

Massachusetts Institute of Technology
Aeronautical Engineering Department
Cambridge 30, Massachusetts
Attn: Dr. R. H. Miller

University of Michigan
Department of Aeronautical Engineering
Ann Arbor, Michigan
Attn: Dr. W. Nelson

University of Minnesota
Aeronautical Engineering Department
Minneapolis 14, Minnesota
Attn: Prof. J. A. Akerman

Naval Postgraduate School
Aeronautical Engineering Department
Monterey, California
Attn: Dr. R. Head

New York University
Aeronautical Engineering Department
New York, New York
Attn: Dr. Lee Arnold

Technological Institute
Northwestern University
Mechanical Engineering Department
Evanston, Illinois
Attn: Prof. A. B. Cambel

The Ohio State University
Department of Aeronautical Engineering
Columbus 10, Ohio
Attn: Prof. G. L. vonEschen

Purdue University
Aeronautical Engineering Department
Lafayette, Indiana

Rensselaer Polytechnic Institute
Aeronautical Engineering Department
Troy, New York

University of Southern California
Engineering Center
Los Angeles 7, California
Attn: H. R. Saffell, Director

Stanford University
Guggenheim School of Aeronautics
Stanford, California
Attn: Prof. E. G. Reid

Stevens Institute of Technology
Fluid Dynamics Laboratory
Hoboken, New Jersey
Attn: Mr. L. H. Mott

Syracuse University
Mechanical Engineering Department
Syracuse, New York
Attn: Dr. S. Eskinasi

Agricultural & Mechanical College of Texas
Aeronautical Engineering Department
College Station, Texas
Attn: Prof. F. Weick

University of Washington
Department of Aeronautical Engineering
Seattle 5, Washington
Attn: Prof. F. S. Eastman

University of Wichita
Department of Engineering Research
Wichita 14, Kansas
Attn: Mr. R. K. Wattson

Aero Design & Engineering Corporation
Bethany, Oklahoma
Attn: Chief Engineer

Aerophysics Corporation
17 Dupont Circle
Washington 6, D. C.
Attn: Dr. G. Boehler

Santa Barbara Division of Curtiss Wright Corp
Santa Barbara, California
Attn: R. Voight

ARO, Incorporated
Tullahoma, Tennessee
Attn: Mr. J. M. Wild, Director

AVCO Manufacturing Corporation
Research & Advanced Development Division
201 Lowell Street
Wilmington, Massachusetts
Attn: Dr. C. J. Burton

Beech Aircraft Corporation
Wichita, Kansas
Attn: Mr. M. J. Gordon

Bell Aircraft Corporation
P. O. Box #1
Buffalo 5, New York
Attn: Advanced Design

Bell Helicopter Corporation
P. O. Box #482
Fort Worth 1, Texas
Attn: Mr. B. Kelley, V.P. Engineering

Boeing Airplane Company
Wichita, Kansas
Attn: Mr. H. Higgins

Chance Vought Aircraft
P. O. Box #5907
Dallas, Texas
Attn: Chief Engineer

Chrysler Corporation
Defense Engineering Division
Centerline, Michigan
Attn: Mr. Leonard Hamel

Collins Radio Company
Cedar Rapids, Iowa
Attn: Dr. A. Lippisch

Convair Division
General Dynamics Corporation
Fort Worth 1, Texas
Attn: Chief Engineer

Convair Division
General Dynamics Corporation
Pomona, California

Convair Division
General Dynamics Corporation
Military Relations Dept. 2-3
Mail Zone 2-31
P. O. Box #1950
San Diego 12, California

Cornell Aeronautical Laboratory, Inc.
4455 Genesee Street
Buffalo 21, New York
Attn: Mr. H. A. Cheilek

Curtiss-Wright Corporation
Research Division
Quehannas, Pennsylvania
Attn: Manager, Special Development Dept.

Douglas Aircraft Company, Inc.
El Segundo Division
El Segundo, California
Attn: Chief Engineer

Douglas Aircraft Company, Inc.
Long Beach, California
Attn: Chief Engineer

Douglas Aircraft Company, Inc.
Engineering Department
Santa Monica, California
Attn: Mr. E. Lapin

Fairchild Aircraft & Missiles Division
Research Department
Hagerstown, Maryland
Attn: Mr. R. Darby

Goodyear Aircraft Corporation
1210 Massillon Road
Akron 15, Ohio
Attn: Dr. R. Ross

Grumman Aircraft Engineering Corp.
Bethpage, L. I., New York
Attn: Dr. C. E. Mack, Chief of Research
Mr. F. T. Kurt

Hiller Aircraft Corporation
1350 Willow Road
Palo Alto, California
Attn: Mr. S. S. Sherby

Hiller Aircraft Corporation
Advanced Research Division
1350 Willow Road
Palo Alto, California
Attn: Dr. J. Sissingh

Kaman Aircraft Corporation
Old Windsor Road
Bloomfield, Connecticut
Attn: Mr. J. Thomas

Lockheed Aircraft Corporation
Burbank, California
Attn: Chief Engineer

Lockheed Missile Systems Division
Flight Sciences Department
Palo Alto, California
Attn: Dr. W. C. Griffith

Lockheed Aircraft Corporation
Georgia Division
86 S. Cobb Drive
Marietta, Georgia

The Martin Company
Baltimore 3, Maryland
Attn: Chief Engineer

The Martin Company
Baltimore 3, Maryland
Attn: Chief, Preliminary Design

McDonnell Aircraft Corporation
St. Louis, Missouri
Attn: Chief Engineer

North American Aviation, Inc.
Columbus Division
Columbus 16, Ohio
Attn: Chief Engineer

North American Aviation, Inc.
Inglewood, California
Attn: Chief Engineer

Northrop Aircraft, Incorporated
Hawthrone, California
Attn: Dr. W. Pfenninger

Piasecki Aircraft Corporation
Island Road, International Airport
Philadelphia 42, Pennsylvania
Attn: Chief Engineer

The Rand Corporation
Santa Monica, California
Attn: Mr. F. R. Collbohm

Republic Aviation Corporation
Farmingdale, L. I., New York
Attn: Chief Engineer

Ryan Aeronautical Company
Lindbergh Field
San Diego, California
Attn: Mr. W. L. Wheeler

Southern California Co-op Wind Tunnel
Pasadena, California
Attn: Mr. J. E. Smith

Sikorsky Aircraft Division
United Aircraft Corp.
Stratford, Conn.
Attn: Chief of Research

Temco Aircraft Corporation
P.O. Box 6191
Dallas, Texas
Attn: Engineering Library, Dept. 413D

Therm-Electric Company
Ithaca, New York
Attn: Dr. A. Ritter

United Aircraft Corporation
Hamilton Standard Division
Windsor Locks, Connecticut
Attn: Mr. G. Rosen

Vehicle Research Corporation
587 Drexel Place
Pasadena, California
Attn: Dr. S. Rethorst

Vertol Aircraft Corporation
Woodland Avenue
Morton, Pennsylvania
Attn: L. L. Douglas

Wiancko Engineering Company
Aeronautics Division
255 N. Halstead Avenue
Pasadena, California
Attn: C. L. Dailey

Pratt and Whitney Division
United Aircraft Corporation
400 Main Street
East Hartford, Conn.

Carnegie Institute of Technology
Mechanical Engineering Department
Pittsburgh 13, Pennsylvania
Attn: Prof. F. Osterle

Harvard University
Department of Engineering Sciences
Cambridge 38, Massachusetts

University of Texas
Defense Research Laboratory
P. O. Box #8029
Austin 12, Texas

Hughes Aircraft Company
Research & Development Laboratories
Culver City, California
Attn: Dr. A. E. Puckett

Library
Institute of the Aeronautical Sciences
2 East 64th Street
New York 21, New York

Marquardt Aircraft Company
7801 Havenhurst
Van Nuys, California

Solar Aircraft
2200 Pacific Highway
San Diego 12, California
Attn: Mr. L. H. Cherry

ABSTRACT

A low speed investigation of the flow over aspect ratio one delta wings of varying thickness has been made to better understand the relation between the vortices produced by leading edge separation and the non-linearity of the lift curve. The formation of the leading edge vortices is shown in smoke photographs. The vortex core loci over the wing and downstream are plotted. An empirical expression was developed for the lift curve.

ABSTRACT

A low speed investigation of the flow over aspect ratio one delta wings of varying thickness has been made to better understand the relation between the vortices produced by leading edge separation and the non-linearity of the lift curve. The formation of the leading edge vortices is shown in smoke photographs. The vortex core loci over the wing and downstream are plotted. An empirical expression was developed for the lift curve.

ABSTRACT

A low speed investigation of the flow over aspect ratio one delta wings of varying thickness has been made to better understand the relation between the vortices produced by leading edge separation and the non-linearity of the lift curve. The formation of the leading edge vortices is shown in smoke photographs. The vortex core loci over the wing and downstream are plotted. An empirical expression was developed for the lift curve.

ABSTRACT

A low speed investigation of the flow over aspect ratio one delta wings of varying thickness has been made to better understand the relation between the vortices produced by leading edge separation and the non-linearity of the lift curve. The formation of the leading edge vortices is shown in smoke photographs. The vortex core loci over the wing and downstream are plotted. An empirical expression was developed for the lift curve.

Bergesen, Andrew J. and Porter, James D.

An Investigation of the Flow Around Slender Delta Wings with Leading Edge Separation. Princeton University, Department of Aeronautical Engineering, Report No. 510, May 1960 - pps. 22- Figs. 71.

1. Delta Wings; 2. Smoke Flow Visualization; 3. Lift Curve; I. Bergesen, Andrew J. and Porter, James D.; II. Princeton University, Department of Aeronautical Engineering, Report No. 510.

Bergesen, Andrew J. and Porter, James D.

An Investigation of the Flow Around Slender Delta Wings with Leading Edge Separation. Princeton University Department of Aeronautical Engineering, Report No. 510, May 1960 - pps. 22 - Figs. 71.

1. Delta Wings; 2. Smoke Flow Visualization; 3. Lift Curve; I. Bergesen, Andrew J. and Porter, James D.; II. Princeton University, Department of Aeronautical Engineering, Report No. 510.

Bergesen, Andrew J. and Porter, James D.

An Investigation of the Flow Around Slender Delta Wings with Leading Edge Separation. Princeton University, Department of Aeronautical Engineering, Report No. 510, May 1960 - pps. 22 - Figs. 71.

1. Delta Wings; 2. Smoke Flow Visualization; 3. Lift Curve; I. Bergesen, Andrew J. and Porter, James D.; II. Princeton University, Department of Aeronautical Engineering, Report No. 510.

Bergesen, Andrew J. and Porter, James D.

An Investigation of the Flow Around Slender Delta Wings with Leading Edge Separation. Princeton University Department of Aeronautical Engineering, Report No. 510, May 1960 - pps. 22 - Figs. 71.

1. Delta Wings; 2. Smoke Flow Visualization; 3. Lift Curve; I. Bergesen, Andrew J. and Porter, James D.; II. Princeton University, Department of Aeronautical Engineering, Report No. 510.